„Molecular biology, pharmacogenomics and pharmacoproteomics of shikonin for target oriented cancer therapy“

Dissertation
zur Erlangung des Grades

“Doktor der Naturwissenschaften”

im Promotionsfach Pharmazie

am Fachbereich Chemie, Pharmazie und Geowissenschaften
der Johannes Gutenberg-Universität in Mainz

vorgelegt von Dipl. Chemiker Benjamin Wiench
geboren am 27.06.1985 in Ludwigshafen

Mainz, November 2013

Datum der mündlichen Prüfung: 27.11.2013
D77 (Dissertation Universität Mainz)

Acknowledgement

Aus Gründen des Datenschutzes enthält die elektronische Fassung der Dissertation keine Danksagung.

Abstract

Chemotherapy is a mainstay of cancer treatment. Due to increased drug resistance and the severe side effects of currently used therapeutics, new candidate compounds are required for the improvement of therapy success. Shikonin, a natural naphthoquinone, was used in traditional Chinese medicine for the treatment of different inflammatory diseases and recent studies revealed the anticancer activities of shikonin. In this study, shikonin exhibited strong cytotoxic effects on various sensitive and multidrug-resistant cancer cell lines. Especially, leukemia and lymphoma cells were sensitive to shikonin. Transcriptome-wide mRNA expression studies showed that shikonin induced genetic pathways regulating cell cycle, mitochondrial function, levels of reactive oxygen species, and cytoskeletal formation. Taking advantage of the inherent fluorescence of shikonin, it was shown that the compound specifically accumulated in the mitochondria of cancer cells leading to an induction of ROS, a breakdown of the mitochondrial membrane potential, and ultimately induction of apoptosis. After elucidating the basal cellular mechanism of shikonin, its particular effect against leukemia cells was analyzed. Therefore, the data of different state-of-the-art quantitative *omics* technologies was integrated. The results indicated that the strongly cross-linked PI3K-Akt-mTOR axis was intensely affected by shikonin in leukemia cells. In addition, functional validation studies showed that shikonin inhibits the kinase activity of IGF1R, which is an important trigger of the PI3K-Akt-mTOR signaling cascade. Deregulations of the PI3K-Akt-mTOR pathway are frequently associated with hematological malignancies. An inhibition of this pathway by shikonin apparently coincides with its particular effect against leukemia cells. Besides the elucidation of the cellular mechanisms underlining shikonins activity, its effect against cancer stem cells was tested as well, revealing that CSCs exhibit a moderate resistance to shikonin. Nevertheless, in comparison to clinically established chemotherapeutics, shikonin was much more effective against this particular cell population. Ultimately, the direct targeting of mitochondria, inhibition of mTOR signaling and its effect against cancer stem cells make shikonin a promising candidate for the next generation of targeted chemotherapy.

During the studies it was examined that shikonin exhibits a strong intrinsic fluorescence that can be used for live drug-uptake kinetics measured by flow cytometry. In an additional project, this approach was enhanced to a general experimental procedure usable for most drugs exhibiting an inherent fluorescence. Ultimately, a protocol was established that links drug-uptake measurements with multi-dimensional cytotoxicity screenings and biochemical assays.

Zusammenfassung

Chemotherapie ist einer der wichtigsten Ansätze zur Behandlung von Krebserkrankungen. Da aktuelle Zytostatika oft schwere Nebenwirkungen hervorrufen und häufig Resistenzen auftreten, werden dringend neue Leitsubstanzen zur Verbesserung des Therapieerfolgs benötigt. Shikonin, ein substituiertes Naphthochinon, wurde in der traditionellen Chinesischen Medizin zur Behandlung verschiedener entzündlicher Erkrankungen genutzt und neuste Studien belegten, dass der Naturstoff auch Potential für die Krebstherapie aufweist. In der vorliegenden Arbeit wurde gezeigt, dass Shikonin verschiedene sensitive und resistente Krebszelllinien abtötet und besonders effektiv gegen Leukämie- und Lymphom-Zellen wirkt. Eine mRNA-Expressionsanalyse des gesamten Transkriptoms identifizierte Auswirkungen von Shikonin auf den Zellzyklus, die Funktion der Mitochondrien, den Gehalt an reaktiven Sauerstoffspezies und das Zytoskelett. Die Eigenfluoreszenz von Shikonin wurde genutzt, um eine Akkumulation der Substanz in den Mitochondrien zu zeigen, was zu einer Überproduktion von ROS, dem Zusammenbruch des mitochondrialen Membranpotentials und schließlich zum Einleiten der Apoptose führte. Nach der Aufklärung des primären zellulären Mechanismus von Shikonin wurde dessen besonderer Effekt gegen Leukämiezellen untersucht. Dafür wurden die Datensätze verschiedener quantitativer *omics* Versuche kombiniert und eine bioinformatische Auswertung zeigte, dass der PI3K-Akt-mTOR Signalweg stark von Shikonin beeinflusst wird. Validierungsexperimente ergaben, dass Shikonin den IGF1 Rezeptor, einen der wichtigsten Rezeptoren des Signalwegs, direkt inhibiert. Da der Signalweg häufig in hämatologischen Krebserkrankungen konstitutiv aktiviert ist, erklärt dies denn starken Effekt von Shikonin gegen Leukämiezellen. Neben der Aufklärung molekularer Mechanismen zeigten Tests mit Krebsstammzellen, dass diese eine geringe Resistenz gegen Shikonin besitzen. Diese war jedoch im Vergleich zu klinisch genutzten Zytostatika sehr schwach ausgeprägt. Zusammenfassend machen der Effekt gegen die Mitochondrien, die Inhibierung der mTOR Signaltransduktion und die Aktivität gegen Krebsstammzellen Shikonin zu einer vielversprechenden Leitstruktur für neue Zytostatika.

Die Eigenfluoreszenz von Shikonin wurde genutzt um die Aufnahmekinetik der Substanz in Krebszellen mittels Durchflusszytometrie zu messen. Dieses Vorgehen wurde in einem zusätzlichen Projekt zu einer Methode weiterentwickelt, die auf die meisten fluoreszierenden Medikamente angewandt werden kann. Abschließend wurde ein Protokoll entworfen, dass die Messung der zellulären Aufnahmekinetik an Zytotoxizitätsbestimmungen und weitere biochemische Endpunktmessungen koppelt.

Table of contents

1 Introduction

1.1 General aspects of cancer

According to the World Health Organization (WHO) cancer is a leading cause of death worldwide and accounted for 7.6 million deaths in 2008. The continuing growth and aging of the world's population mean that the burden of cancer will increase and deaths from cancer worldwide are projected to rise to over 11 million in 2030 (1). In general, cancer is a generic term for a broad group of various diseases, all involving the uncontrolled growth and spreading of cells. Defining features of cancer are that cells proliferate uncontrollably, form malignant tumors, invade nearby parts of the body and spread to other organs through the lymphatic system in a process referred to as metastasis. Hanahan and Weinberg defined six hallmarks of cancer that collectively dictate malignant growth (Figure 1): self-sufficiency in growth signals, insensitivity to growth-inhibitory signals, evasion of cell death, limitless replicative potential, sustained angiogenesis, and tissue invasion and metastasis (2). Recently, two additional hallmarks involved in the pathogenesis of cancer were suggested: deregulation of cellular energetics and avoidance of immune destruction (3).

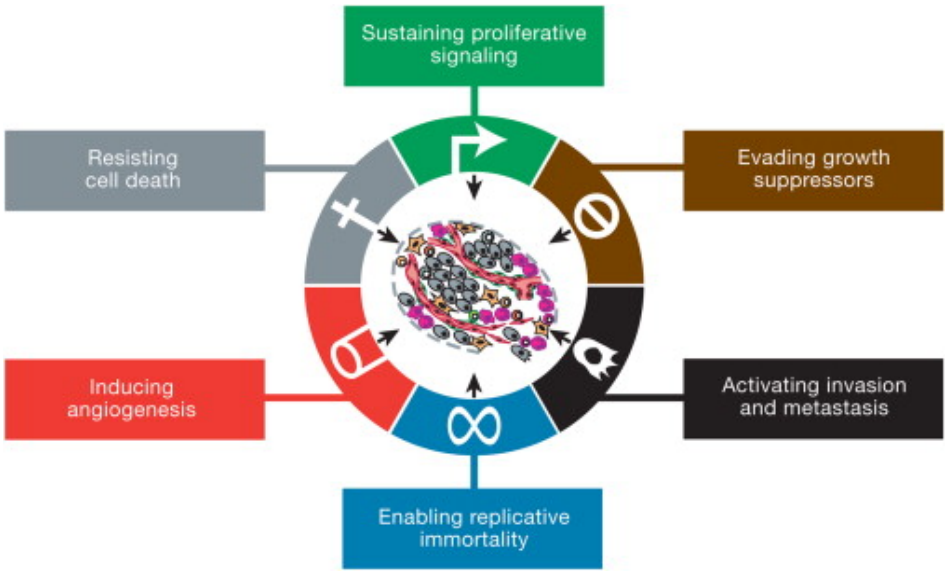

Figure 1: The hallmarks of cancer. Cancer cells have acquired a set of functional capabilities that enable tumor growth and metastatic dissemination. Image adapted from Hanahan and Weinberg (3).

Cancer is caused by mutations in oncogenes, tumor-suppressor genes, and miRNA genes and these genetic alterations are usually somatic events, although germ-line mutations can

predispose a person to cancer (4). Several lines of evidence indicate that tumorigenesis is a multistep process of sequential mutations in several, often many genes (2, 4). Only 5-10% of all cancer cases can be attributed to inherent genetic defects, whereas the remaining 90-95% have their roots in environmental and lifestyle factors including smoking, diet, alcohol, excessive sun exposure, environmental pollutants, infections, stress, obesity, and physical inactivity (5).

Current treatment strategies of cancer comprise surgery, radiotherapy, chemotherapy and palliative care. The choice of treatment depends on the type, grade and localization of the cancer as well as the general health constitution and wishes of the patient. The goal of cancer treatment is to cure the disease with a combination of treatment modalities directed at the primary tumor (surgery or radiation), and potential metastases (chemotherapy) or to prolong life while improving quality of life (6). In the following, this study will focus on special aspects of chemotherapy.

1.2 Chemotherapy and new treatment strategies

Cancer chemotherapy is defined as the treatment of cancer with cytostatic drugs. Classical chemotherapy comprises agents that target rapidly dividing cells. The majority of therapeutics can be divided into alkylating drugs (e.g. cyclophosphamide), platinum derivatives (e.g. cisplatin), antimetabolites (e.g. methotrexate), DNA-topoisomerase inhibitors (e.g. etoposide), microtubule inhibitors (e.g. vinblastine and docetaxel) and cytotoxic antibiotics (e.g. doxorubicin) (7). Since these agents target fast-dividing cells by affecting cell division or DNA synthesis, they also cause severe side effects by killing proliferating but non-malignant cells. Major side effects of classical chemotherapy are leukopenia, thrombocytopenia and a decrease of erythrocytes resulting in a depression of the immune system, tendency to bleed easily and anemia (8). Furthermore, cytostatic drugs damage mucous membranes and cause gastrointestinal distress. A temporary side effect is dramatic hair loss. Chemotherapeutics can also cause damage directly to specific organs (e.g. cardiotoxicity, hepatotoxicity, and nephrotoxicity).

A further fundamental problem of chemotherapy is that cancer cells - by virtue of their genomic instability - rapidly develop resistance to chemotherapeutics. Around 40% of human tumors develop resistance to chemotherapeutic drugs (9) and metastases resistant to therapy are the major cause of treatment failure and death from cancer (10). Drug resistance can occur

due to a variety of mechanisms, such as increased drug inactivation, drug efflux from cancer cells, enhanced repair of chemotherapy-induced damage, activation of pro-survival pathways and inactivation of cell death pathways (Figure 2) (9, 11).

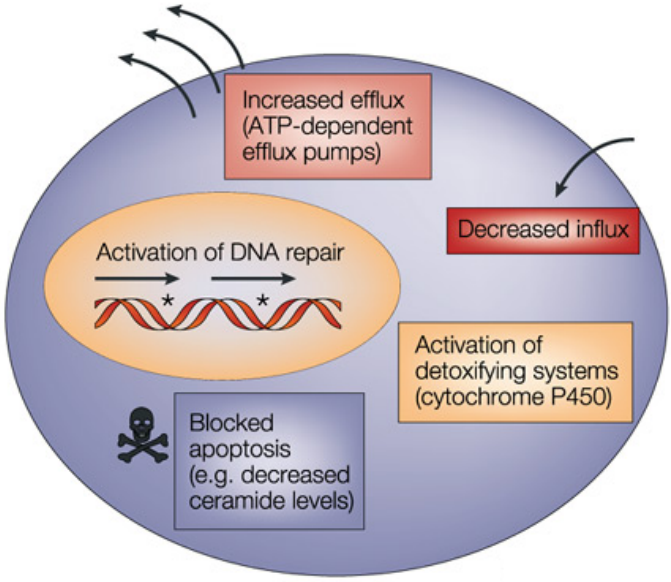

Figure 2: Cancer cell specific mechanisms of drug resistance. Overexpression of drug efflux pumps (e.g. ABC transporters), reduced drug influx, activation of detoxifying enzymes (e.g. cytochrome P450), repair of drug induced DNA-damage and inhibition of apoptotic signaling pathways (e.g. p53) are known mechanisms of cancer cells against chemotherapeutic drugs. Image adapted from Gottesman *et al.* (9).

Frequently, cancer cells simultaneous acquire resistance to many chemically unrelated cytotoxic molecules, a phenomenon referred to as multidrug resistance (MDR). The most important mediators of MDR are ATP-binding cassette (ABC) transporters (12). These transporters are multi-domain integral membrane proteins utilizing the energy of ATP hydrolysis to serve as drug efflux pumps. ABC transporters have been conserved across the three kingdoms of archaea, eubacteria, and eukarya and they form one of the largest of all protein families (13). The transporters have a broad specificity for a wide range of chemically unrelated molecules and an overexpression in cancer cells causes a reinforced resistance against chemotherapeutics (9). The multidrug resistance protein 1 (p-glycoprotein, ABCB1) is the best characterized of all ABC transporters and confers resistance of cancer cells to a variety of chemotherapeutics (e.g. doxorubicin, taxol, etoposide) (14). By now, several different ABC transporters were found to play key roles in MDR, for example the breast cancer resistance protein (BCRP, ABCG2) and the multidrug resistance-associated protein 1 (MRP1, ABCC1) (12).

To minimize side effects and circumvent drug resistance a new generation of chemotherapeutics was developed based on the principle of molecular targeted therapy. This new approach counters the growth of cancer cells by interfering with specific targeted molecules needed for carcinogenesis without causing general damage to non-malignant cells. Unfortunately, an acquisition of resistance appears not only to traditional chemotherapy but also to targeted therapies (15). A detailed introduction to the opportunities and limitations of molecular targeted therapy can be found in chapter 1.2.3. In summary, chemotherapy is a mainstay of cancer treatment, but due to increased drug resistance and the severe side effects of currently used therapeutics, new candidate compounds and treatment strategies are required for an improvement of therapy success.

1.2.1 Natural products for cancer therapy

Natural products are small molecules or substances produced by terrestrial plants, animals, marine organisms, microorganisms or even minerals that have a pharmacological activity. These compounds represent a valuable source for the development of novel anticancer drugs. Over a time frame from around the 1940s to 2010, 49% of the small molecules and 41% of all drugs used for cancer therapy were either natural products or directly derived therefrom (Figure 3) (16).

Especially the secondary metabolites of organisms, which are produced as a defense against competitors, herbivores and pathogens and as signaling compounds exert pharmacological features (17). Prominent examples for successfully employed natural products in cancer therapy are the *Vinca* alkaloids from *Catharanthus roseus* G. Don. (Apocynaceae), the DNA topoisomerase I inhibitor camptothecin from *Camptotheca acuminate* Decne. (Nyssaceae), and the terpene paclitaxel from *Taxus brevifolia* Nutt. (Taxaceae) (18). Since only a minor fraction of the estimated total of 250.000 – 300.000 plant species has been studied exhaustively for possible medical applications (19), it is most likely that plants even contain much more undiscovered compounds which could be useful for cancer therapy. However, it is very expensive and time consuming to screen plant species for active compounds and to identify and isolate specific entities useful for cancer treatment.

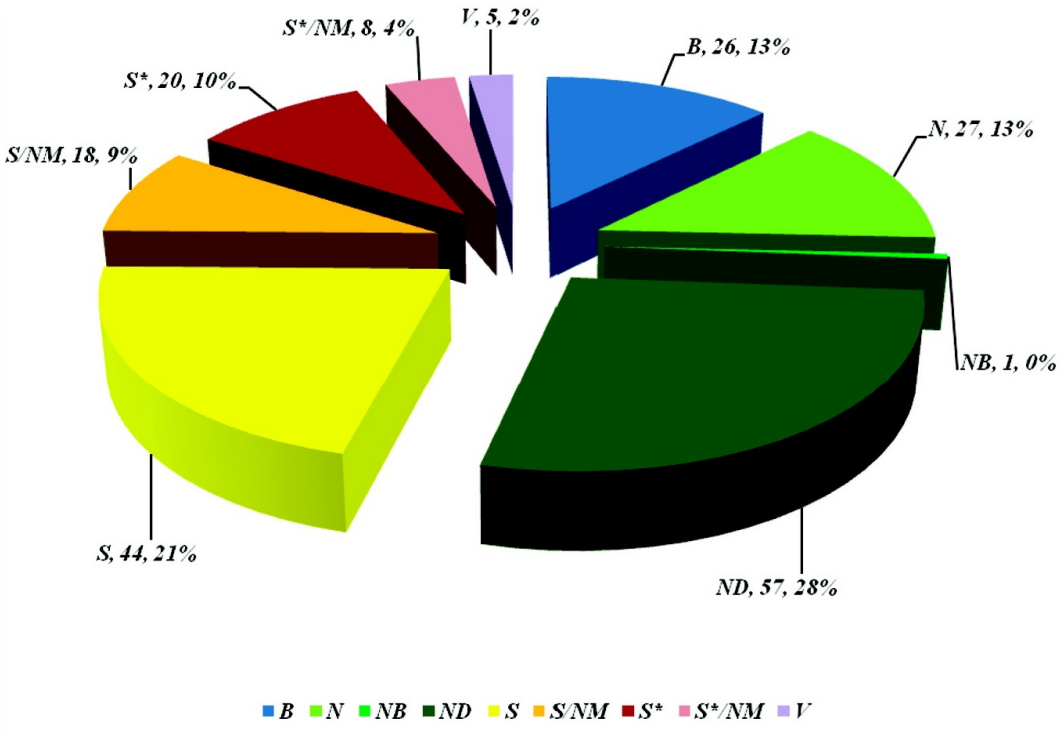

Figure 3: All anticancer drugs 1940s – 2010 by source. Image adapted from Newman and Cragg (16). (B: Biological; N: Natural product; NB: Natural product "Botanical"; ND: Derived from natural product; S: Total synthetic drug; S/NM: S/Natural product mimic; S*: Made by total synthesis, but the pharmacophor is a natural product; S*/NM: S*/Natural product mimic; V: Vaccine)

About three quarters of plant-derived drugs in clinical use today came to the attention of pharmaceutical companies because of their use in traditional medicines (19). According to the WHO, traditional medicine is the total sum of knowledge, skills and practices based on theories, beliefs and experiences indigenous to different cultures that are used to maintain health, as well as to prevent, diagnose, improve or treat physical and mental illnesses (20). Such traditional medicines frequently developed over thousands of years and they contain knowledge regarding application and efficacy that is usually useful for modern medicine. One can expect that the search for bioactive plant compounds is more successful among medicinal plants of traditional folk medicines than a random search across all plant species (18). One of the most powerful and matured folk medicines is traditional Chinese medicine (TCM). TCM has a 5.000 year-old tradition and many of the natural products used in tumor chemotherapy are derived from or have a direct relationship to TCM, speaking impressively for its power and potential (17). Increasing knowledge of the molecular mechanisms of TCM-derived drugs and recent developments in their applications demonstrate that the combination of TCM with modern cutting-edge technologies provides an attractive strategy for the development of novel

and improved cancer therapeutics (17). One promising anti-cancer agent derived from TCM and major subject of this study is the natural naphthoquinone shikonin.

1.2.2 Shikonin

The naphthoquinone pigment shikonin is the most important pharmacologically active substance in the dried root of *Lithospermum erythrorhizon* (Figure 4). In TCM, root extracts of *Lithospermum erythrorhizon* have been used to treat macular eruption, measles, sore-throat, carbuncles and burns (21).

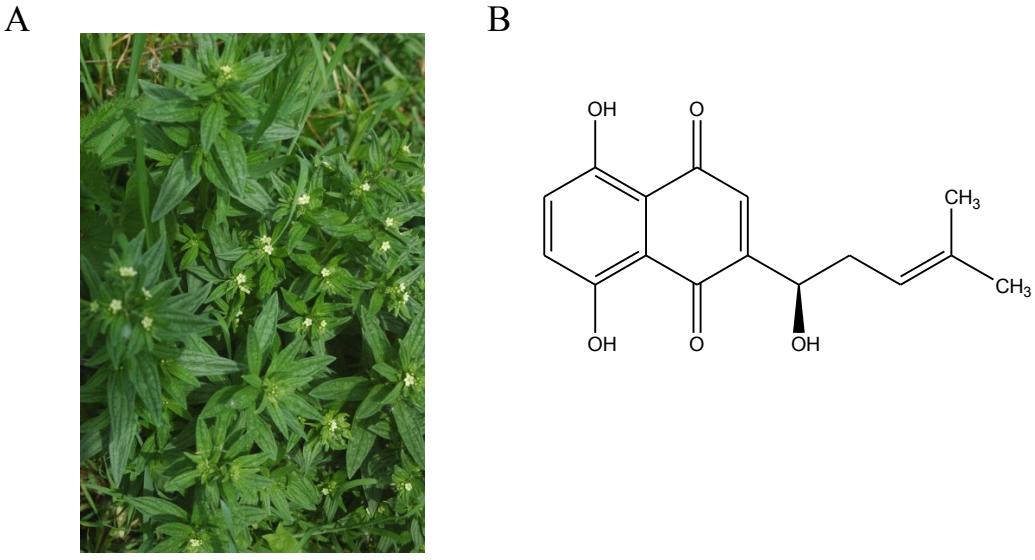

Figure 4: Picture of the plant *Lithospermum erythrorhizon* (ja.wikipedia.org) (A) and the chemical structure of shikonin (B).

The anti-tumorigenic effect of shikonin was first scientifically described by its activity against murine sarcoma-180 cells (22). A clinical trial using shikonin in 19 cases of late-stage lung cancer revealed that a shikonin-containing pharmacological mixture was safe for human consumption and effective for the treatment of late stage cancer (23). The mechanism by which shikonin triggers its cytotoxic effect against malignant cells is controversial. Recently, it was shown that shikonin induces ROS and apoptosis in cancer cells (24). Furthermore, induction of necroptosis (25), inhibition of topoisomerase II activity (26), down-regulation of NFκB signaling (27), cell cycle arrest through up-regulation of p53 and down-regulation of cyclin-dependent protein kinase 4 (28), inhibition of proteasome function (29), and inhibition

of tumor necrosis factor alpha (30) were suggested as possible cellular mechanisms of shikonin. A very recent study showed that shikonin inhibits cancer cell glycolysis by targeting tumor pyruvate kinase M2 (31). This plethora of suggested mechanisms leads to a diffuse picture of shikonin's mode of action and inhibits its application in a molecular target therapy. Since shikonin is a promising lead compound for the next generation of chemotherapeutics, it is essential to clearly define its basal mode of action in cancer cells.

1.2.3 Targeted cancer therapy

Contrary to traditional chemotherapy, which in most cases simply kills rapidly dividing cells, molecular targeted therapy refers to a new generation of anti-cancer drugs designed to interfere with cancer-specific molecules or cellular aberrations having a crucial role in tumor growth and progression (32). Molecular targeted drugs mostly comprise small molecules or antibodies with various molecular mechanisms. Figure 5 gives an overview of some molecular targeting drugs and their respective mechanisms in cancer cells.

The first breakthrough of molecular targeted therapy was the approval of imatinib (marketed by Novartis as Gleevec or Glivec) by the FDA (US Food and Drug Administration) for the treatment of chronic myelogenous leukemia (CML) in 2001. Imatinib kills cancer cells, by blocking the cancer specific BCR-Abl tyrosine kinase, that is present in 95% of patients with CML (33). The fusion protein BCR-Abl is the result of a chromosomal translocation, in which parts of chromosome 9 and 22 change places (Philadelphia chromosome) and create an oncogenic fusion gene of Abl1 (Abelson tyrosine protein kinase 1) and BCR (breakpoint cluster region) on chromosome 22. BCR-Abl has constitutively elevated tyrosine phosphokinase activity relative to wild-type Abl and excessively promotes cell division, which is the primary factor leading to CML (34). Before imatinib was available, CML patients were treated with traditional chemotherapeutics or bone marrow transplantation and only 30% of patients survived for five years after diagnosis. The development of imatinib has revolutionized the treatment of CML and recent studies showed that the estimated overall survival of patients who received imatinib as initial therapy was 89% after five years (35).

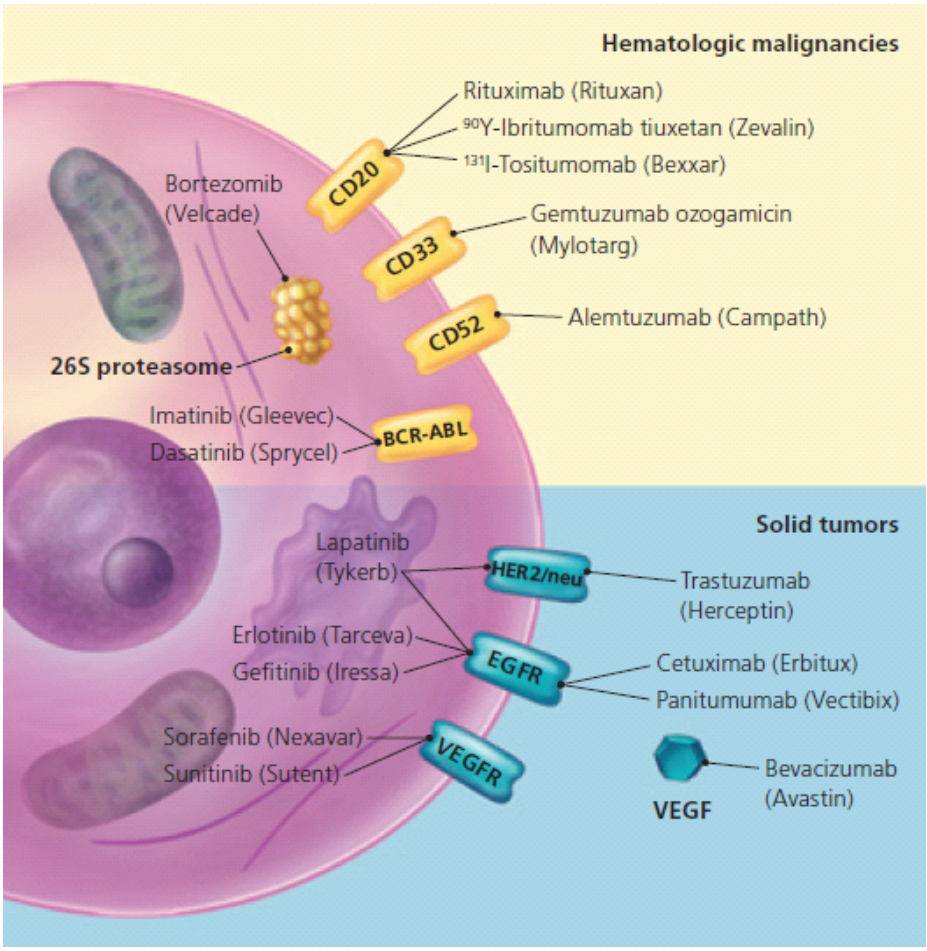

Figure 5: Drugs and cellular mechanisms of molecular targeted cancer therapy. The molecular targets in this figure are not overexpressed in a single cell type, but rather on various malignant and normal tissues. For example, CD20 is present on lymphoma and normal lymphoid cells, HER2/neu is present on 25 percent of breast cancer cells, and VEGFR is present on normal and tumor-associated vasculature. Image adapted from Gerber (36).

Another example for an approved molecular targeting drug is the monoclonal antibody trastuzumab, which targets the human epidermal growth factor receptor type 2 (HER2/neu). Overexpression of HER2/neu occurs in 20 to 30% of invasive breast carcinomas. Trastuzumab binds to the extracellular domain of HER2/neu and inhibits proliferation and survival of HER2/neu-dependent tumors. It is clinically used for the treatment of metastatic breast cancer with HER2/neu overexpression and for adjuvant therapy of early-stage breast cancer (37).

Despite the great success of targeted cancer therapy in the last 15 years, there are also drawbacks and limitations. The increased costs of targeted therapy are an economic problem. Especially, if targeted therapy includes monoclonal antibodies, costs can escalate exponentially (36). This is aggravated by the fact that many of the new drugs are efficient in

only a minority of patients (38). The most severe drawback is that similar to traditional chemotherapy, cancer cells can also develop resistance to targeted drugs. For example, the majority of patients with metastatic breast cancer who initially respond to trastuzumab, demonstrate disease progression within one year after treatment initiation (39).

Therefore, the future of targeted therapy lies in personalized treatment. This includes an individualized medicine that delivers the right care to the right cancer patient at the right time and results in measurable improvements in outcomes and a reduction of health care costs (38). The basis for this kind of treatments are predictive biomarkers, genetic testing and molecular diagnostics to identify individual cancer patients who are more likely to respond positively to targeted drugs. Furthermore, the identification of novel cancer specific targets and new lead compounds for molecular targeted therapy are urgently needed to improve therapy success. Natural products can serve as a source for new therapeutics and they have to be considered not only as a seminal source of cytotoxicity-inducing agents, but also for their use as molecularly targeted agents (40). For example, results of this study indicated that shikonin directly targets the mitochondria of cancer cells and in addition has a strong effect on the mammalian target of rapamycin (mTOR) signaling cascade. Both mechanisms play an important role in targeted cancer therapy.

1.2.4 Targeting mitochondria for cancer therapy

Resistance to cell death and reprogramming of metabolic pathways are two hallmarks of human cancer cells as well as major causes of chemotherapeutic inefficacy (3). Mitochondria are key structures for both traits: i) mitochondria are crucial for cellular energy production and cell survival, ii) mitochondria are major regulators of the intrinsic apoptotic pathway (41). Mitochondrial membrane permeabilization (MMP) and the subsequent release of mitochondrial death effectors (e.g. cytochrome c) are key events for caspase activation and apoptosis (42). The induction of mitochondrial apoptosis can be triggered by various intracellular stimuli such as Ca^{2+} overload or high levels of reactive oxygen species (ROS) (43). In addition, both stimuli reinforce each other leading to Ca^{2+}/ROS-mediated mitochondrial dysfunction (44).

In cancer cells, the structure and function of mitochondria differ significantly from normal eukaryotic cells (45). Cancer cells display decreased mitochondrial activity, and instead shift to aerobic glycolysis for ATP production, a phenomenon known as the Warburg effect (46).

Cancer cells are often more resistant to activation of the mitochondrial apoptotic pathway due to overexpression of anti-apoptotic Bcl-2 family proteins (47) or stabilization of the mitochondrial membrane against apoptosis-associated permeabilization (48). Another trait associated with cancer cells are elevated ROS levels, probably caused by mitochondrial dysfunction (49). Therefore, it is conceivable that cancer cells have a lower tolerance to further oxidative insults induced by ROS-generating drugs (47, 50). Furthermore, mutations in mitochondrial DNA were correlated with increased tumorigenicity in prostate and breast cancer (51, 52).

Because of the altered mitochondrial functions in neoplasia, direct targeting of mitochondria in cancer cells has become an attractive strategy in cancer chemotherapy over the last few years. A direct induction of apoptosis in cancer cells via the mitochondrial pathway allows one to circumvent upstream signal transduction steps frequently impaired in human cancers (50). Thus, cancer cell resistance mechanisms can be avoided. Several mechanisms were identified to target mitochondria: direct targeting of mitochondria based on altered mitochondrial transmembrane potential, targeting cancer mitochondrial respiration, effecting cancer mitochondrial membrane permeability, targeting mtDNA or targeting altered metabolisms associated with mitrochondrial dysfunction (53). Figure 6 presents an overview of possible target sites of chemotherapeutics directly targeting mitochondria. Recently, HSP90, which is only contained in the mitochondria of cancer cells but not in their normal counterparts, was suggested as an additional target to affect mitochondria in cancer cells (54).

One successful example of drugs targeting mitochondria is the small molecule menadione (2-methyl-1,4-naphthoquinone, vitamin K3). Menadione undergoes futile redox cycles on the respiratory chain of mitochondria and causes an overproduction of ROS, ultimately inducing apoptosis (43). A clinical trial demonstrated that this compound can induce objective clinical responses in patients with advanced hepatocellular carcinoma (55).

Ultimately, compounds targeting mitochondria may help to improve the poor results of traditional therapies and furthermore represent a promising approach for the treatment of cancer cells resistant to standard chemotherapy (43).

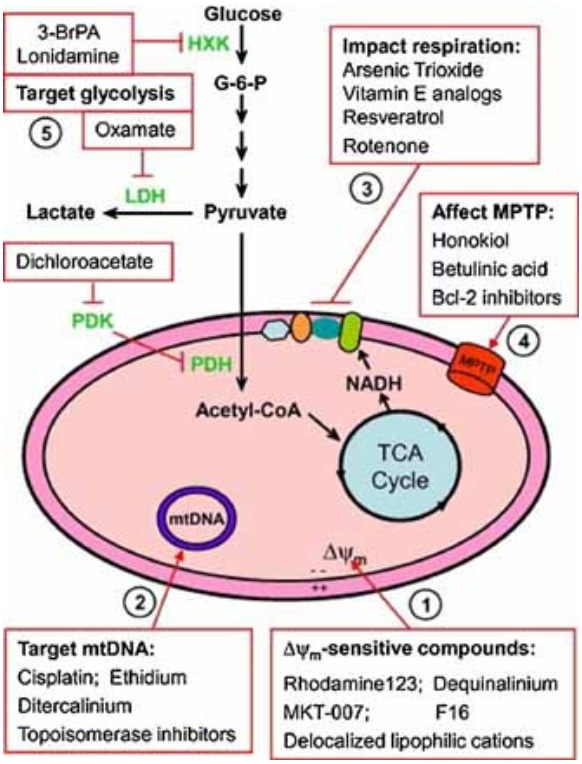

Figure 6: Overview of possible sites and functions of mitochondria as potential targets for anti-cancer therapy. (1) The elevated transmembrane potential of cancer cell mitochondria causes an accumulation of certain compounds. (2) Mitochondrial DNA (mtDNA) posses a unique structure and represents a potential target for therapy. (3) Inhibition of mitochondrial respiration has been shown to elevate ROS production, deplete ATP, and induce apoptosis. (4) Targeting the mitochondrial permeability transition pore (mPTP) alters transmembrane potential and triggers apoptosis. (5) Enzymes of the glycolytic pathway are often found elevated in cancer cells. Image adapted from Wenner (56) and Wang *et al.* (53).

1.2.5 Targeting mTOR signaling for cancer therapy

Targeting the mammalian target of rapamycin (mTOR) signaling became an attractive therapeutic strategy for cancer chemotherapy over the last few years (57, 58). The signaling pathway plays a central role in cellular growth control and survival through the regulation of protein synthesis and ribosomal protein translation (59). Deregulations of mTOR signaling are associated with tumorigenesis, angiogenesis, tumor growth, and metastasis (57, 60). The mTOR signaling pathway has been found to be frequently deregulated, especially in a wide range of hematological malignancies (61). The signaling cascade is activated by receptor tyrosine kinases (RTKs), e.g. insulin-like growth factor 1 receptor (IGF1R) and epidermal growth factor receptor (EGFR), integrins and cytokine receptors coupling external signals from growth factors, cytokines and the availability of nutrients to cell growth and proliferation (62). After binding of the corresponding ligands, the RTKs activate the phosphoinositide 3-kinase (PI3K), which in turn causes the phosphorylation of Akt.

Phosphorylated Akt inhibits the heterodimeric complex of tuberous sclerosis proteins 1 and 2 (TSC1/2) that negatively regulates the mammalian target of rapamycin complex 1 (mTORC1) by converting the Ras homolog enriched in brain (Rheb) into its inactive GDP-bound state. The GTP-bound form of Rheb directly interacts with mTORC1 and strongly stimulates its kinase activity (63, 64). mTORC1 is composed of six known protein components and the functional most important parts are the mammalian lethal with sec-13 protein 8 (mLST8), the regulatory-associated protein of mammalian target of rapamycin (raptor) and the catalytic mTOR subunit. The mTOR1 complex is a centerpiece of the signaling cascade that controls protein synthesis by phosphorylation of different effector proteins, e.g. the S6 kinase 1 (S6K1) and the 4E-binding protein 1 (4E-BP1) (64). Much less is known about the second mTOR complex mTORC2, that is composed of seven protein components. Besides mLST8 and the catalytic subunit mTOR, which are present in both mTOR complexes, a further important functional part of mTORC2 is the rapamycin-insensitive companion of mTOR (rictor). The mTOR2 complex responds to growth factors and regulates cell survival and metabolism, as well as the cytoskeleton (64). A simplified overview of the mTOR signaling cascade is displayed in Figure 7.

Currently used drugs targeting this pathway are rapamycin and its derivatives (rapalogs), which directly target the mTORC1 complex (65, 66). One weak point of these drugs is a resistance mechanism of cancer cells, which leads to an up-regulation of IGF1R after mTORC1 inhibition (67-69). This feedback mechanism causes an activation of the PIK3K-Akt-mTOR signaling cascade after initial inhibition resulting in only modest anti-cancer effects of rapalogs (61). Thus, there is an unmet need for compounds, which bypass or inhibit this feedback mechanism in order to optimize the therapy success of mTOR targeting drugs.

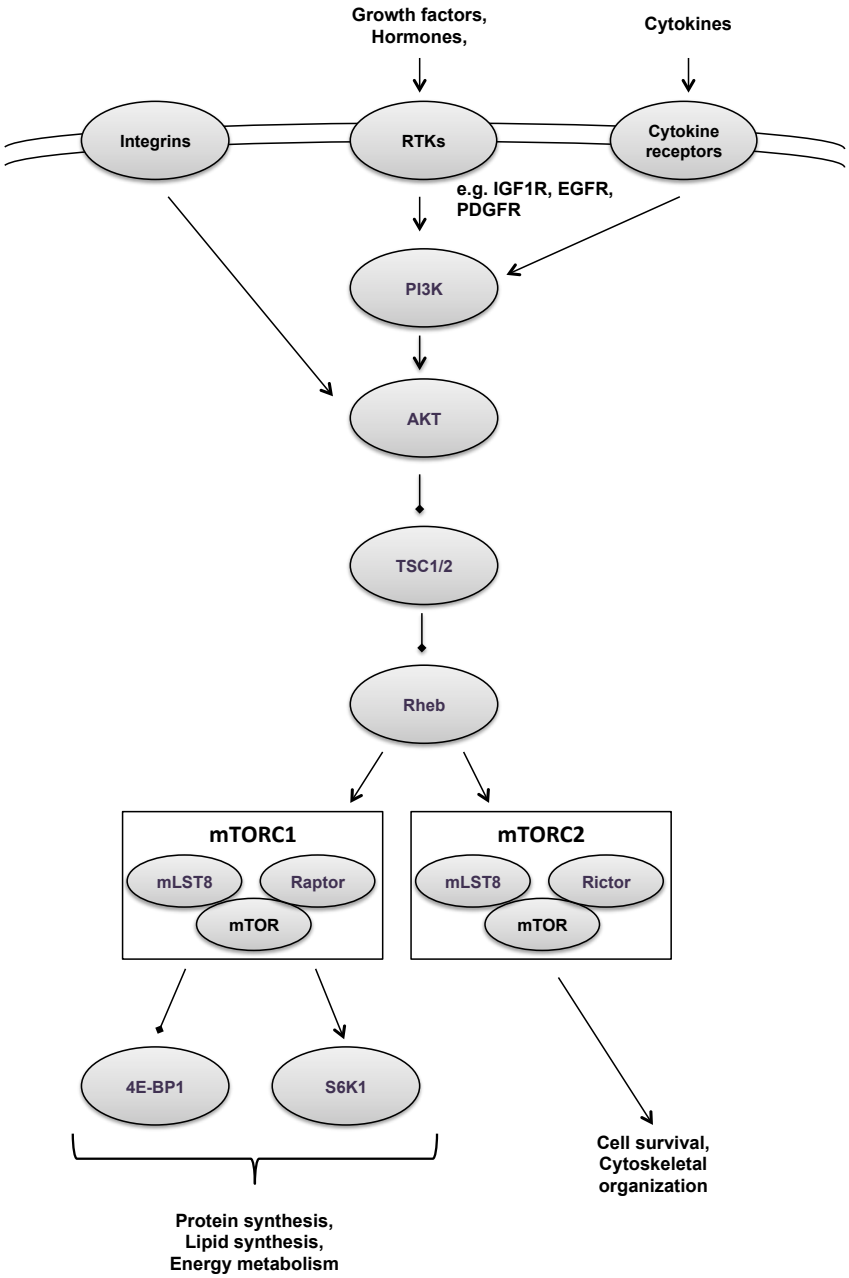

Figure 7: The mTOR signaling pathway. Key signaling nodes of the pathway are displayed in a simplified cascade. Arrows indicate an activation and blunt lines an inhibition of the following signaling node.

1.3 Cancer stem cells

Ten years ago, Al-Haji *et al*. proved that only a minority of isolated breast cancer cells had the ability to form new tumors (70). They gained evidence that this tumor initiating subpopulation of cancer cells differ from other cells within the tumor by exhibiting a $CD44^{+}/CD24^{-/low}$ phenotype. Since then, tumor initiating subpopulations of cancer cells were found in various malignant diseases, like pancreatic cancer (71), brain tumors (72), prostate cancer (73), leukemia (74), and many others [reviewed in (75)]. This subpopulations of cells

showed various phenotypes and expressed different surface markers (e.g. CD44, CD90 or CD133, reviewed in (76)), but they had the common feature to be highly tumorigenic. Furthermore, they all had the capacity to self-renew and to differentiate into heterogeneous lineages that comprise tumors (77). Because of the features they share with somatic stem cells, the tumorigenic cells were defined as cancer stem cells (CSCs) leading to the cancer stem cell hypothesis (78). The model assumes that the CSCs represent a small subset of cancer cells with the exclusive abilities to self-renew and maintain the tumor by dividing into further CSCs or differentiate into the heterogeneous non-tumorigenic cancer cell types, which in most cases appear to constitute the bulk of cancer cells within a tumor (77). The origin of CSCs is still a matter of discussion and it is unclear whether they are derived from tissue stem cells with malignant changes (79) or from differentiated cells by malignant transformation and recovering of stemness characteristics (80). Recent findings showed that CSCs play a crucial role in tumor invasion and metastasis (81, 82), angiogenesis (83) and the interplay with the tumor microenvironment (84).

In cancer therapy, CSCs represent a major obstacle, because they are resistant to standard chemo- and radiotherapy (85, 86). They are able to enter a non-proliferative or dormant state and thereby avoid common cancer therapy, which basically targets dividing cells (87). Furthermore, CSCs reside in a specialized microenvironment called the CSC niche (88). The CSC niche is composed of blood vessels, stromal cells and extracellular matrix components that retain the abilities of CSCs to self-renew or differentiate and that shelter the CSCs from genotoxic insults, contributing to their enhanced resistance (78). In addition to this protection by the microenvironment, cancer stem cells possess an own line of defense composed of ABC-transporters, which shield them from chemotherapeutic insult (89). The ABC transporters serve as drug efflux pumps and it was shown that MDR1, BCRP1 and ATP-binding cassette sub-family B member 5 (ABCB5) play a major role in the resistance of CSCs against chemotherapy [reviewed in (90)]. The survival of CSCs in a dormant state, the protection provided by the CSC niche, and the expression of ABC efflux pumps may be responsible for tumor recurrence after a primarily successful therapy. Hence, effective tumor eradication requires not only chemotherapeutics that kill the differentiated and fast dividing bulk cells of a tumor, but it also requires agents that target the small and protected CSC population to prevent relapse (77, 91) (Figure 8).

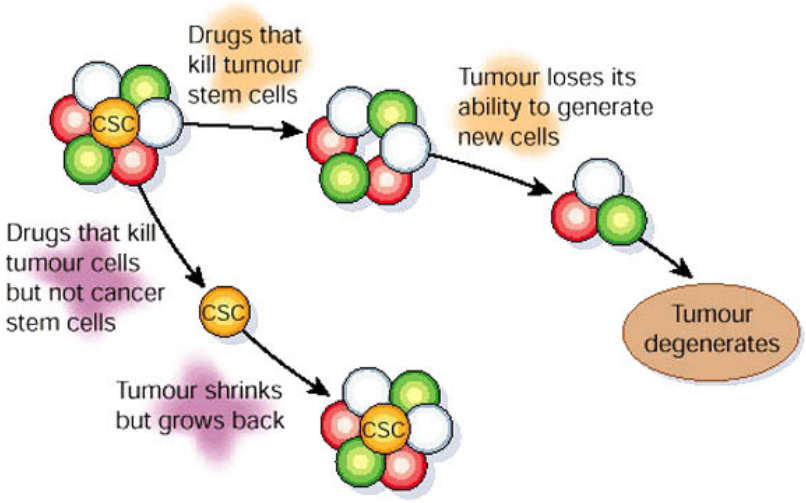

Figure 8: Targeting cancer stem cells. Conventional chemotherapeutics are able to remove bulk cancer tissue, but in most cases they are not able to kill CSCs leading to a disease recurrence. Therefore, a therapy might be more successful by targeting CSCs and causing permanent tumor degeneration. Image adapted from Reya *et al.* (91).

One valuable source for compounds that target CSCs are natural products. Many natural products have been described that affect cellular pathways relevant for CSCs, but have not been tested in these cell types specifically (92). Here, the effect of shikonin against CSCs was investigated by analyzing its effect against $CD44^{+}/CD24^{-/low}$ MCF-7 cancer stem cells cultured as mammospheres. In addition, the population distribution (non-CSCs versus CSCs) of MCF-7 cells was analyzed after shikonin treatment and the effect of shikonin against ABCB5 overexpressing cells was tested.

1.4 Drug uptake assays

Many pharmaceutical agents require intracellular presence to exert their therapeutic potential (93). Consequently, these substances must pass through the cell membrane by passive diffusion or via carrier-mediated transport. The complex procedure of intracellular accumulation differs among drug types, and important factors include uptake, retention, distribution in, and efflux from the cell (94). Thus, a precise detection of pharmaceutical drug uptake and knowledge of a drug's efficacy at the single cell level is crucial for understanding a compound's performance. A more thorough understanding of the associated steps and their respective kinetics would provide a clear advantage in drug identification, design, dosing and delivery, and could lead to improved efficiency in the lead compound identification process.

Over a time frame from around the 1940s to 2010, 49% of the small molecules used for cancer therapy were either natural products or directly derived therefrom (16). As such, they exhibit complex structures with many delocalized electrons and many of them, for example doxorubicin (95) and camptothecin (96), possess inherent fluorescence, a valuable trait most often neglected. Current methods in the analysis of drug uptake include assays using radioactively labeled compounds (97), limited fluorescence microscopy (94) or measuring residual amounts of drug remaining in the supernatant after cell treatment (98). These assays, besides being labor-intensive and time consuming, measure uptake indirectly using multiple samples in order to gain a limited endpoint-based kinetic analysis preventing any kind of multi-parametric co-analysis of effects caused by drug uptake.

In this study, FACS protocols for the measurement of real-time drug uptake kinetics have been established. The intrinsic fluorescence of the actual compounds was fundamental in order to perform flow cytometry allowing direct, single cell quantifications. Furthermore, it was shown that additional live functional assays can be easily coupled with drug uptake analysis and that flexible simple dye based analysis of multiple drug-dependent parameters at the same time is possible. Due to this, the presented method is advantageous as it combines multiple recommended cytotoxicity assays (99) into a single experimental setup and actually allows direct correlation of uptake efficiencies with drug efficacy. Furthermore, screening for drugs exhibiting inherent fluorescence can be easily performed by multi-parametric flow cytometry and hence the presented method has additionally the potential to be applied in a number of pharmaceutical areas including high-throughput screening in drug discovery and development. Especially, this approach can be a useful tool identifying potential inhibitors for MDR, representing a major challenge of the small molecule based treatment of various diseases.

2 Aim of the thesis

The naphthoquinone pigment shikonin is the most important pharmacologically active substance in the dried root of *Lithospermum erythrorhizon*. In TCM, its medical properties have been confirmed with a long history of usage. Shikonin was used for the treatment of inflammatory and infectious diseases, but in recent years it was recognized that shikonin has a strong anticancer activity. The substance developed to a promising lead compound for new anticancer agents, yet much uncertainty still exists about the molecular targets and the mode of action of shikonin in cancer cells. This knowledge is indispensible, in order to exploit the full therapeutic potential of shikonin and to minimize its unspecific toxicity. Furthermore, a detailed understanding of the cellular mechanisms of shikonin would provide a sound basis for the use of shikonin in a molecular targeted therapy. The ultimate goal of this study was:

- *Identification of the molecular targets and the mode of action of shikonin in cancer cells.*

In the first experimental approaches it was shown that shikonin disturbs the mitochondrial function and the mTOR signaling of cancer cells leading to two important aims of the research project:

- *Analysis of mitochondria as primary targets of shikonin.*
- *Analysis of the effect of shikonin on the IGF1R-Akt-mTOR signaling pathway.*

Cancer stem cells are a major cause for a relapse of the malignant disease after an initial response and therefore it is necessary that new chemotherapeutics are tested for their effect against this subpopulation of cancer cells. Hence, one purpose of this study was:

- *Analysis of the effect of shikonin against cancer stem cells.*

During the studies the intrinsic fluorescence of shikonin was used quite frequently for analysis by flow cytometry and confocal microscopy. This was leading to an additional aim of the study:

- *Establishment of an in vitro assay that is utilizing the inherent fluorescence of shikonin and other therapeutics to analyze real-time uptake and multi-parametric effector kinetics in cancer cells.*

3 Results

3.1 Shikonin directly targets mitochondria in cancer cells

The natural naphthoquinone shikonin exhibited outstanding anti-cancer activity in many recent *in vitro* and *in vivo* studies. However, the primary cellular mechanism of shikonin that accounts for its cytotoxic effect against cancer cells remains unknown. The primary aim of this thesis was to elucidate the exact cellular mode of action of shikonin in cancer cells. This could pave the way for its use in a molecular targeted therapy.[1]

3.1.1 Cytotoxic effect of shikonin against cancer cell lines

To analyze the cytotoxic effect of shikonin against various types of cancer, a panel of 15 sensitive and multidrug resistant cancer cell lines was treated with shikonin for 24 or 48 h and cell viability was evaluated using the resazurin reduction assay. The results are summarized in Table 1. Shikonin inhibited proliferation by 50% in nearly all cancer cell lines at concentrations below 10 μM after 24 h. Only the pancreatic carcinoma cell line SUIT 2 was more resistant to shikonin; it showed IC50 values of 12.9 and 18.5 μM after 24 and 48 h of treatment, respectively. Interestingly, all five tested leukemia cell lines had IC50 values below 1 μM, and the most sensitive cell line was the histocytic leukemia cell line U937, which was subsequently used for gene expression analysis under shikonin treatment.

[1] Parts of the results presented in this chapter were recently published in a peer-reviewed scientific journal and the publication is listed in the bibliography of the Johannes Gutenberg University (ID 9706):

Wiench B, Eichhorn T, Paulsen M, Efferth T. Shikonin directly targets mitochondria and causes mitochondrial dysfunction in cancer cells. Evid Based Complement Alternat Med. 2012; 2012:726025

All text passages, figures and tables of this publication that are used in a modified form in this dissertation were prepared or written by myself.

Table 1: IC50 values (mean ± SEM) of Shikonin for a panel of 15 different sensitive and resistant cancer cell lines after 24 and 48 h as assayed by resazurin reduction assay.

Cell line	Cancer type	Shikonin IC50 [µM]	
		24 h	48 h
U937	Histiocytic leukemia	0.30 ± 0.003	0.19 ± 0.003
CCRF-CEM	Acute lymphocytic leukemia	0.37 ± 0.01	0.24 ± 0.001
CEM/ADR5000*	Acute lymphocytic leukemia	0.36 ± 0.05	0.38 ± 0.01
HL-60	Acute myelocytic leukemia	0.39 ± 0.01	0.42 ± 0.001
HL-60/AR*	Acute myelocytic leukemia	0.95 ± 0.003	0.47 ± 0.001
MCF-7	Breast carcinoma	9.05 ± 0.08	10.51 ± 0.03
SK-BR-3	Breast adenocarcinoma	9.21 ± 0.08	8.70 ± 0.03
MDA-MB-231/pcDNA3	Breast carcinoma	1.23 ± 0.03	0.88 ± 0.03
MDA-MB-231/BCRP*	Breast carcinoma	2.61 ± 0.06	1.48 ± 0.04
786-O	Kidney carcinoma	9.44 ± 0.13	8.03 ± 0.06
SW-1116	Colorectal carcinoma (GIII)	6.63 ± 0.09	4.42 ± 0.06
HCT-116	Colorectal carcinoma	4.74 ± 0.07	8.54 ± 0.01
SW680	Colorectal carcinoma	7.21 ± 0.13	2.96 ± 0.06
Capan1	Pancreas adenocarcinoma	7.23 ± 0.28	6.21 ± 0.14
SUIT-2	Pancreatic carcinoma	12.92 ± 0.35	18.50 ± 0.09

*MDR cancer cell lines with various drug resistances

Drug resistance is a major problem in cancer chemotherapy. To assess the question of whether shikonin has the potential to circumvent drug resistance, the activity of shikonin against three multidrug-resistant cancer cell lines was tested: CEM/ADR5000, HL-60/AR, and MDA-MB-231-BCRP (Table 1). CEM/ADR5000 cells overexpress the multidrug-resistance protein 1 (MDR1, ABCB1) and exhibit high levels of resistance to DNA topoisomerase II inhibitors (e.g. doxorubicin, etoposide, and teniposide) and mitotic spindle inhibitors (e.g. vincristine, paclitaxel, and docetaxel) (18). HL-60/AR cells highly express the MDR-related protein 1 (MRP1, ABCC1) (100) that confers resistance to *Vinca* alkaloids, anthracyclines, doxorubicin, and mitoxantrone (101). MDA-MB-231-BCRP cells overexpress the breast cancer resistance protein (BCRP) (100) that mediates resistance to mitaxantrone, anthracyclines and camptothecine analogues (e.g. topotecan) (102). Similarly to their sensitive counterparts, all tested MDR cell lines showed no or negligible resistance against shikonin. The response rates obtained were compared with those of the established cytostatic drug doxorubicin (Table 2). In all MDR cell lines the degree of resistance to shikonin was much lower than to doxorubicin.

Table 2: Cross-resistance profile of three multidrug-resistant cancer cell lines to doxorubicin and shikonin. IC50 values (mean ± SEM) of doxorubicin were evaluated by resazurin reduction assay. The degree of resistance was calculated as the ratio of IC50 values of the resistant and the corresponding sensitive cell line.

Cell line	Doxorubicin			Shikonin
	IC50 [µM] (24 h)	IC50 [µM] (48 h)	Degree of resistance (24 / 48 h)	Degree of resistance (24 / 48 h)
CCRF-CEM	0.13 ± 0.002	0.03 ± 0.003	> 384.6 / > 1666.7	0.97 / 1.6
CEM/ADR500*	> 50	> 50		
HL-60	n.d.	0.73 ± 0.20†	n.d. / 225.5	2.4 / 1.1
HL-60/AR*	n.d.	164.6 ± 17.7†		
MDA-MB-231/pcDNA3	n.d.	1.10 ± 0.28†	n.d. / 7.12	2.1 / 1.7
MDA-MB-231/BCRP*	n.d.	7.83 ± 0.47†		

*MDR cancer cell lines with various drug resistances
†Values were evaluated by Dr. Victor Kuete using the same cells and methods used in this study

3.1.2 Gene expression profiling

mRNA Microarray

A gene expression analysis was performed to identify possible targets and mechanisms of shikonin's anti-cancer activities in histocytic leukemia U937 cells. Cells were treated with 0.3 µM (IC50) shikonin or DMSO solvent control for 24 h before total RNA was isolated for a whole human genome mRNA gene expression microarray. Bioinformatic analysis identified 683 molecules, out of which 465 were assigned to distinct genes, significantly deregulated ($p < 0.01$) after shikonin treatment. For a number of genes, the expression array was technically validated using RT-qPCR, which yielded comparable results (Table 3). The most deregulated genes identified in the microarray are summarized in Table 4.

Table 3: Results of microarray gene expression profiling and real-time reverse transcription-PCR for six selected genes.

Gene	Description	Fold change	
		Microarray	RT-qPCR
JUN	Transcription factor AP-1	+3.24	+4.03
YBX1	Nuclease-sensitive element-binding protein 1	-2.05	-3.30
HSP90AB1	Heat shock protein HSP 90-beta	-2.10	-1.92
TAF6	Transcription initiation factor TFIID subunit 6	-2.11	-2.35
CCNE1	G1/S-specific cyclin-E1	-2.14	-1.24
LYAR	Cell growth-regulating nucleolar protein	-2.15	-1.81

Table 4: Top up- and down-regulated genes in U937 cells after treatment with shikonin.

Gene	Description	Fold change
Up-regulated genes		
MLLT11	Myeloid/lymphoid or mixed-lineage leukemia	+6.15
S100A8	S100 calcium binding protein A8	+4.72
LY96	Lymphocyte antigen 96	+4.48
S100A9	S100 calcium binding protein A9	+4.24
CCL2	Chemokine (C-C motif) ligand 2	+4.16
VIM	Vimentin	+4.16
HMOX1	Heme oxygenase (decycling) 1	+4.14
ANXA1	Annexin A1	+4.14
MAFB	V-maf musculoaponeurotic fibrosarcoma oncogene homolog B	+3.49
JUN	Transcription factor AP-1	+3.24
Down-regulated genes		
ALDOA	Aldolase A, fructose-bisphosphate	-17,63
ACTG1	Actin, gamma 1	-11,88
CCT7	Chaperonin containing TCP1, subunit 7 (eta)	-7,84
ARPC1B	Actin related protein 2/3 complex, subunit 1B, 41kDa	-7,81
PSMC4	Proteasome (prosome, macropain) 26S subunit, ATPase, 4	-7,65
ACTB	Actin, beta	-6,80
HSPD1	Heat shock 60kDa protein 1 (chaperonin)	-6,59
SLC39A3	Solute carrier family 39 (zinc transporter), member 3	-6,19
ERP29	Endoplasmic reticulum protein 29	-5,98
NCF1	Neutrophil cytosolic factor 1	-5,92

Using the Ingenuity Pathway Analysis (IPA) tool, the deregulated genes were correlated with biological functions including cell death and proliferation, cell cycle, cellular movement, inflammatory response, protein folding and synthesis, energy production, DNA repair and free radical scavenging. Figure 9 displays the top cellular functions affected by shikonin treatment in U937 cells identified by IPA. In addition, subsequent analysis of the microarray data showed that a whole subset of genes responsible for mitochondrial function was deregulated.

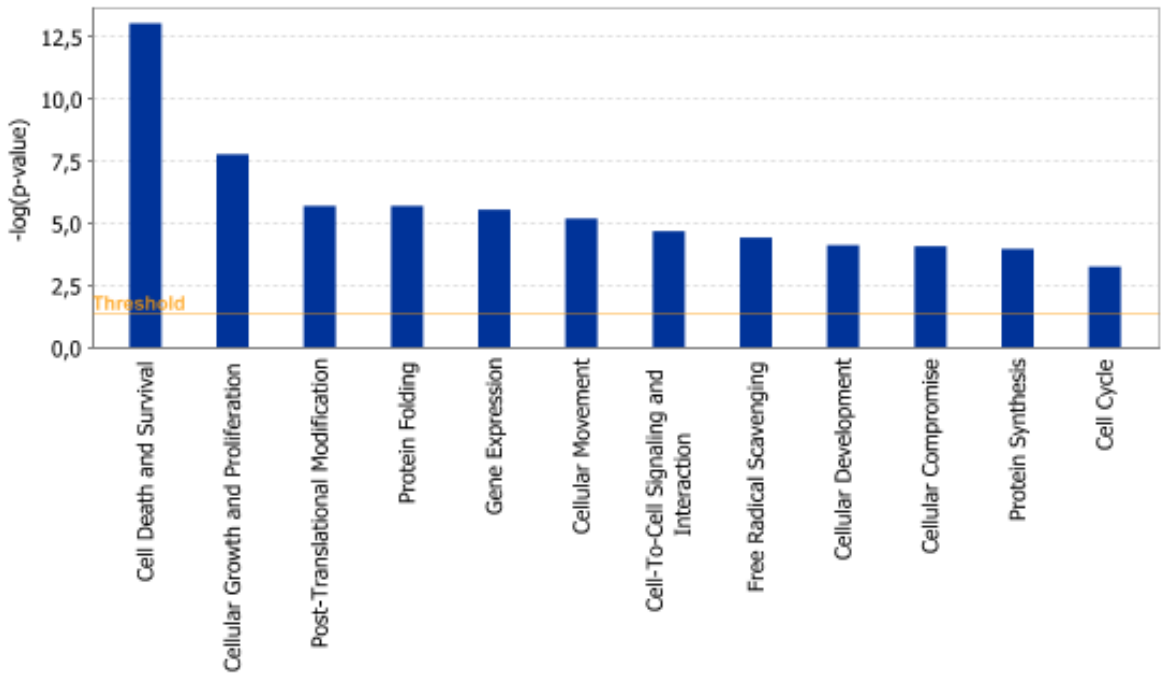

Figure 9: Top cellular functions affected by shikonin treatment in U937 cells examined by mRNA microarray. Right-tailed Fisher's exact test was used to calculate a p-value determining the probability that each biological function assigned to the datasets is due to chance alone.

Furthermore, several genetic networks were found to be significantly deregulated in U937 cells after shikonin treatment. The networks were correlated to discrete cellular functions like cell proliferation and cell death, cellular movement, DNA repair, energy production, cell-to-cell-signaling and inflammatory response. Figure 10 shows the two most affected genetic networks after shikonin treatment.

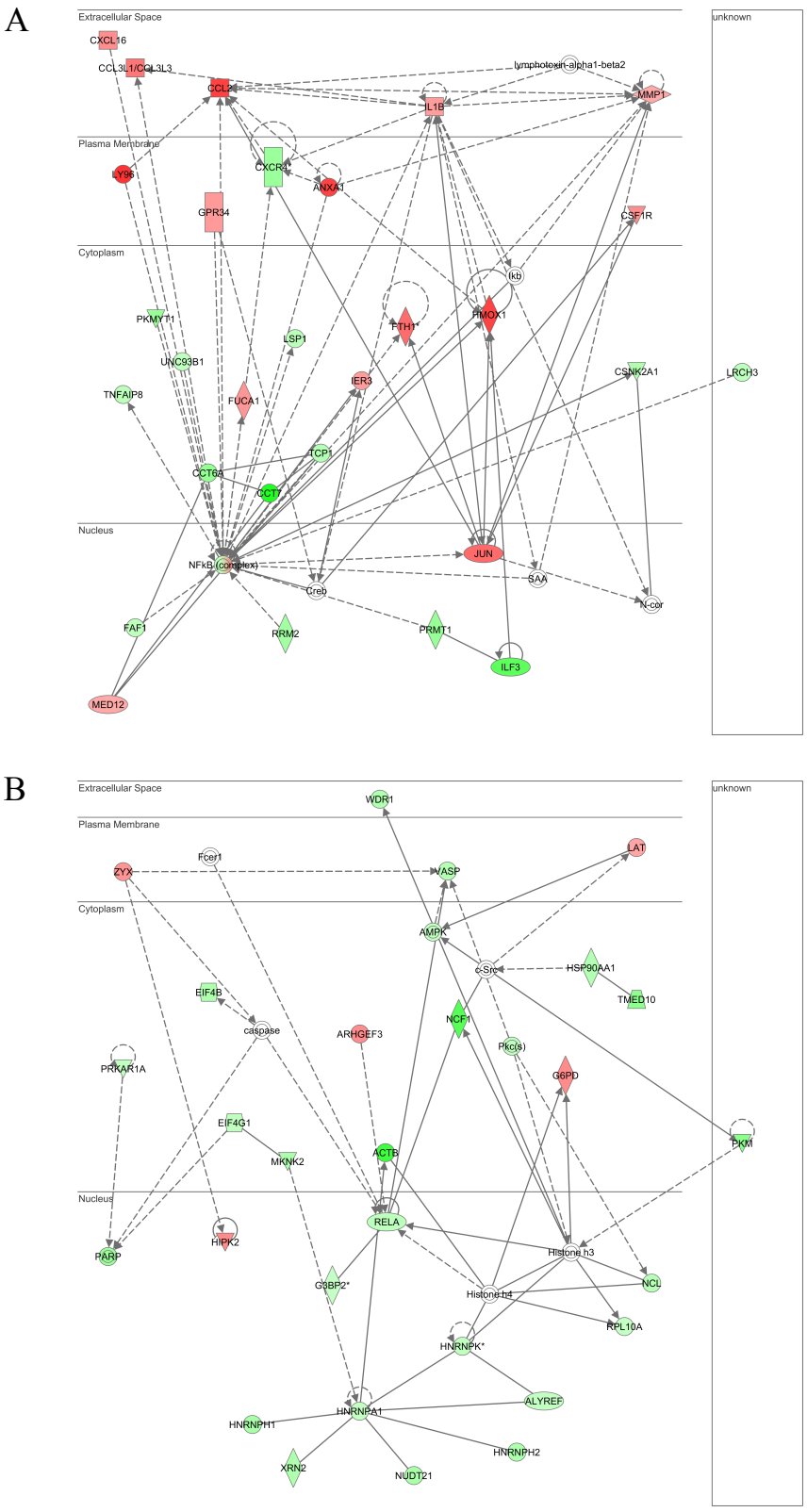

Figure 10: Two most deregulated genetic networks in U937 cells treated with shikonin. Molecules are represented as nodes, and the biological relationship between two nodes is represented as a line. The intensity of the node color indicates the degree of up- (red) or down- (green) regulation. Continuous lines show a direct interaction, dotted lines an indirect interaction. (A) The genetic network was correlated to distinct cellular functions like cell-to-cell signaling, cellular movement and inflammatory response. (B) The genetic network was correlated to distinct cellular functions like gene expression, RNA post-transcriptional modification and cellular movement.

Using IPA, an upstream regulator analysis was performed to identify transcription regulators that may be responsible for gene expression changes observed in U937 cells after shikonin treatment. Five upstream regulators were predicted to be activated (TP53, NFkB, TGM2, ERK, TREM) and three regulators were expected to be inhibited after shikonin treatment (CD24, KIAA1524, Mek). The most likely activated transcription factors were the cellular tumor antigen p53 (TP53, p53) and the nuclear factor kappa-light-chain-enhancer of activated B cells (NFkB) with 29 and 14 deregulated target molecules in the microarray experiment, respectively. Figure 11 displays a network of deregulated genes controlled by p53 and NFkB. Constitutive NFkB-activation was shown to protect different kinds of cancer cells against apoptosis (103). Therefore, activation of this pathway after shikonin treatment is presumably a resistance mechanism of U937 cells against cytotoxic drugs. Activation of the tumor suppressor protein p53 leads to cell cycle arrest, apoptosis, and growth inhibition in cancer cells (104). This emphasizes shikonin's potential as an anti-cancer drug.

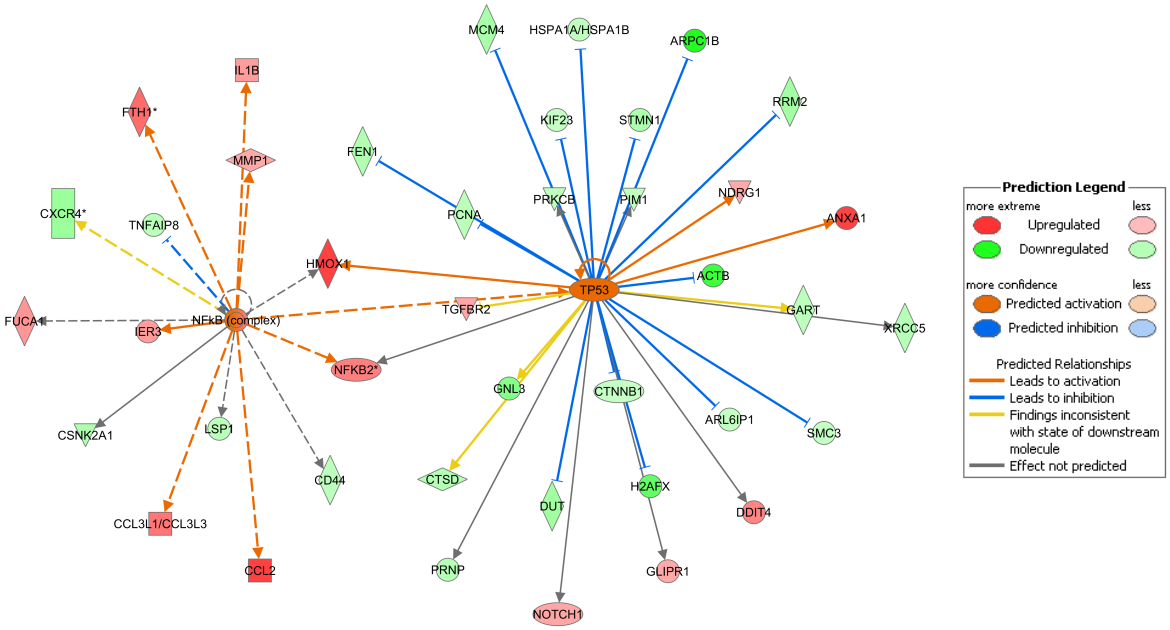

Figure 11: Network of deregulated genes under the control of TP53 and NFkB. An upstream regulator analysis predicted the transcription factors TP53 and NFkB to be activated after shikonin treatment.

Combining the information obtained from Ingenuity Pathway Analysis and an in-depth analysis of the deregulated genes, shikonin's most relevant cellular effects for cancer therapy

were divided into four categories: mitochondrial function, ROS induction and DNA damage, apoptosis and cell cycle arrest, and cytoskeleton and migration (Figure 12).

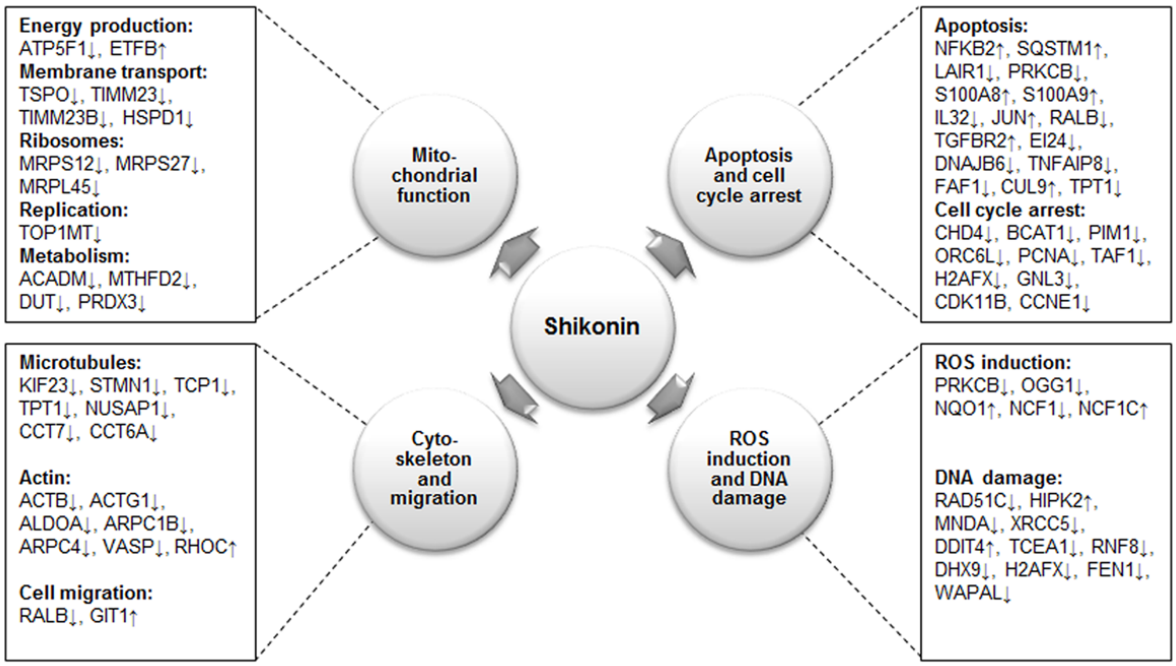

Figure 12: Summary of shikonin-affected mechanisms in U937 cells. Examples of deregulated genes important for each mechanism are shown laterally in the boxes. Arrows pointing downwards (↓) or upwards (↑) indicate down- or up-regulation of gene expression, respectively.

miRNA microarray

Micro RNAs (miRNAs) are small non-coding RNA molecules that play a key role in transcriptional and post-transcriptional regulation of gene expression (105). To complete the picture of shikonin's effect on transcription in U937 cells, a miRNA microarray was performed to identify deregulated miRNAs after shikonin treatment. U937 cells were treated with 0.3 µM (IC50) shikonin or DMSO solvent control for 24 h before miRNA was isolated for a miRNA microarray. Bioinformatic analysis identified 150 miRNAs significantly deregulated ($p < 0.05$) after shikonin treatment. The most deregulated miRNAs in response to shikonin treatment are summarized in Table 5. Using the Ingenuity target filter analysis 15082 mRNAs were predicted to be potentially targeted by the deregulated miRNAs.

Table 5: Top up- and down-regulated miRNAs in U937 cells after treatment with shikonin.

miRNA	Seed region	Fold change
Up-regulated miRNAs		
miR-19b-2-5p	GUUUUGC	+ 5,2
miR-20b-3p	CUGCAGU	+ 3.7
miR-155-3p	UCCUACA	+ 3.4
miR-181a-2-3p	CCACUGA	+ 3.1
miR-33b-5p	UGCAUUG	+ 3.1
miR-4286	CCCCACU	+ 2.9
miR-30a-3p	UUUCAGU	+ 2.8
miR-3907	GGUGCUC	+ 2.8
miR-223-5p	GUGUAUU	+ 2.7
miR-4284	GGCUCAC	+ 2.7
Down-regulated miRNAs		
miR-4299	CUGGUGA	- 30.6
miR-3656	GCGGGUG	- 17.3
miR-1915-3p	CCCAGGG	- 13.8
miR-2861	GGGCCUG	- 9.8
miR-1207-5p	GGCAGGG	- 6.3
miR-1290	GGAUUUU	- 6.2
miR-638	GGGAUCG	- 6.1
miR-1246	AUGGAUU	- 6.0
miR-1207-5p	GGCAGGG	- 5.9
miR-1225-5p	UGGGUAC	- 5.8

The deregulated miRNAs were correlated with cellular functions including cell cycle, cell death, cell-to-cell signaling and cellular movement (Figure 13). Furthermore, several genetic networks were found to be significantly deregulated in U937 cells after shikonin treatment and the most deregulated network is shown in Figure 14. The genetic network was correlated to discrete cellular functions like cellular growth and proliferation, cell death and cell cycle. Interestingly, the four most affected networks are correlated to inflammatory response.

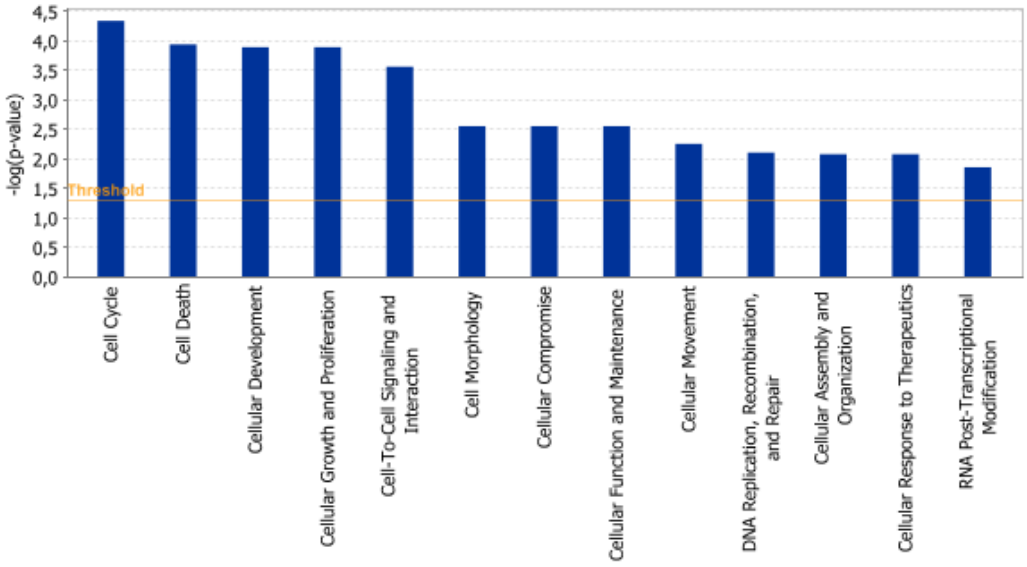

Figure 13: Top cellular functions affected by shikonin treatment in U937 cells examined by miRNA microarray. Right-tailed Fisher's exact test was used to calculate a p-value determining the probability that each biological function assigned to the datasets is due to chance alone.

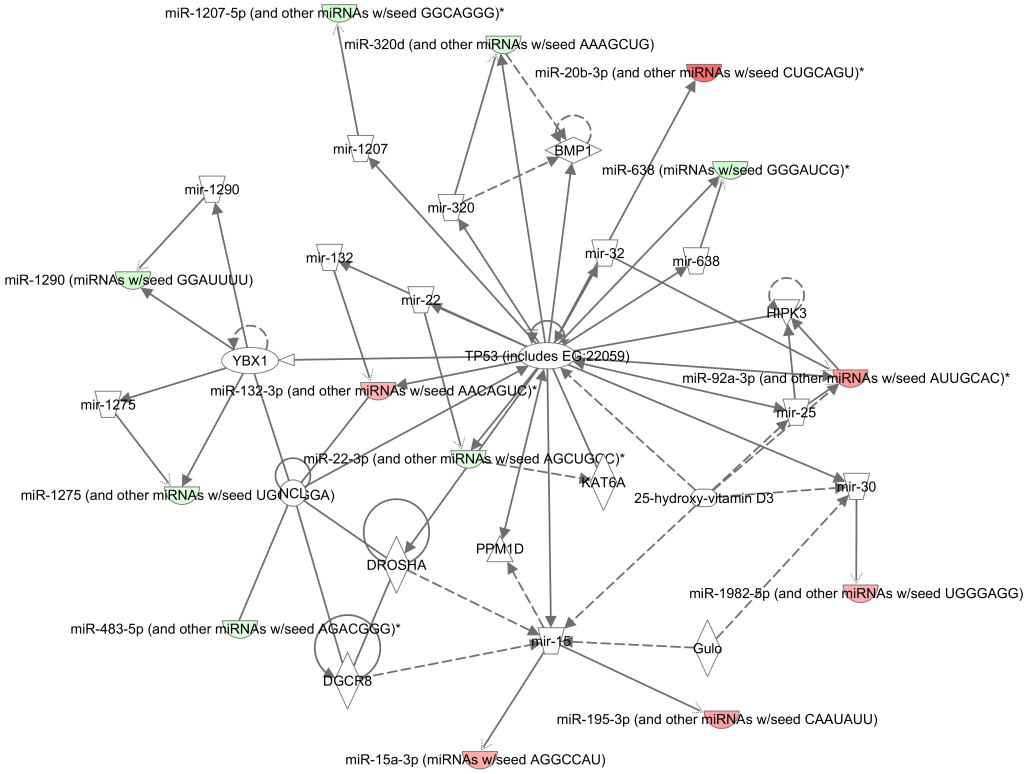

Figure 14: Most deregulated miRNA network in U937 cells treated with shikonin. Molecules are represented as nodes, and the biological relationship between two nodes is represented as an edge. The intensity of the node color indicates the degree of up- (red) or down- (green) regulation. Continuous lines show a direct interaction, dotted lines an indirect interaction. The network was correlated to discrete cellular functions like cellular growth and proliferation, cell death and cell cycle.

Comparison of mRNA and miRNA microarray data

Target filter analysis showed that the deregulated miRNAs target 15082 mRNAs from which 384 mRNAs were also deregulated in the mRNA microarray. This corresponds to 83% of all deregulated genes and indicates a functional correlation between mRNA and miRNA after shikonin treatment. The results of both microarrays were matched using the IPA comparative analysis tool. This revealed several cellular functions deregulated on mRNA as well as on miRNA level after shikonin treatment including cell death and proliferation, cellular movement and cell-to-cell signaling (Figure 15).

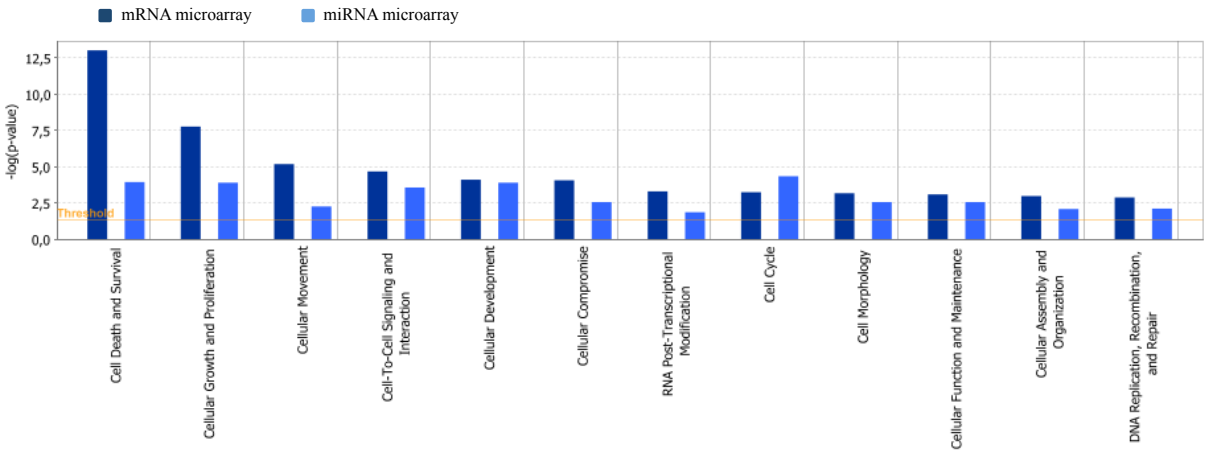

Figure 15: Comparison analysis of molecular and cellular functions affected by shikonin in mRNA and miRNA microarrays. The bar graph displays only functions disturbed in both assays. Right-tailed Fisher's exact test was used to calculate a p-value determining the probability that each biological function assigned to the datasets is due to chance alone.

3.1.3 Mitochondrial drug accumulation

Shikonin is a naphthoquinone derivative, and some substituted naphthoquinones have been shown to target mitochondria (106). Since shikonin had a strong effect on gene expression associated with mitochondrial function and metabolism, it seemed reasonable that the mitochondrion itself is a possible target of the compound. To be able to localize shikonin within cancer cells, the compound was tested for intrinsic fluorescence. A two-dimensional fluorescence spectrum of emission versus excitation wavelengths for shikonin was measured and a strong and specific fluorescence within the visible spectrum was observed (Figure 16). This specific inherent fluorescence was used in flow cytometry and confocal microscopy to detect and localize shikonin.

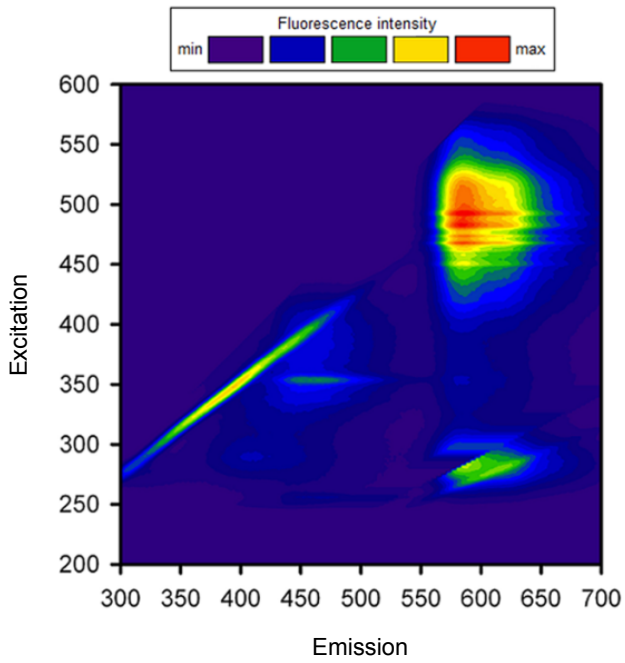

Figure 16: 2D excitation (200-600 nm) vs. emission (300-700 nm) fluorescence spectrum of 50 µM shikonin in aqueous buffer. Shikonin showed a strong and specific fluorescence in the far red range of the visible spectrum.

In a first experimental approach the intrinsic fluorescence of shikonin was used to perform flow cytometric cellular uptake assays. The cellular uptake of shikonin was best measured continuously at 730 nm after excitation with a 640 nm laser. The mean fluorescence of untreated cells was recorded for 2 min and subsequently shikonin was added to the cell suspension and the measurement was continued for a total recording time of 20 min. The results indicated that shikonin enters the cells within 10 min and that the cellular concentration increases with higher application doses (Figure 17). Washout experiments showed that shikonin remains stable inside the cells for at least 20 min, suggesting that no direct diffusion or transport out of the cell takes place (Figure 17, lower right panel).

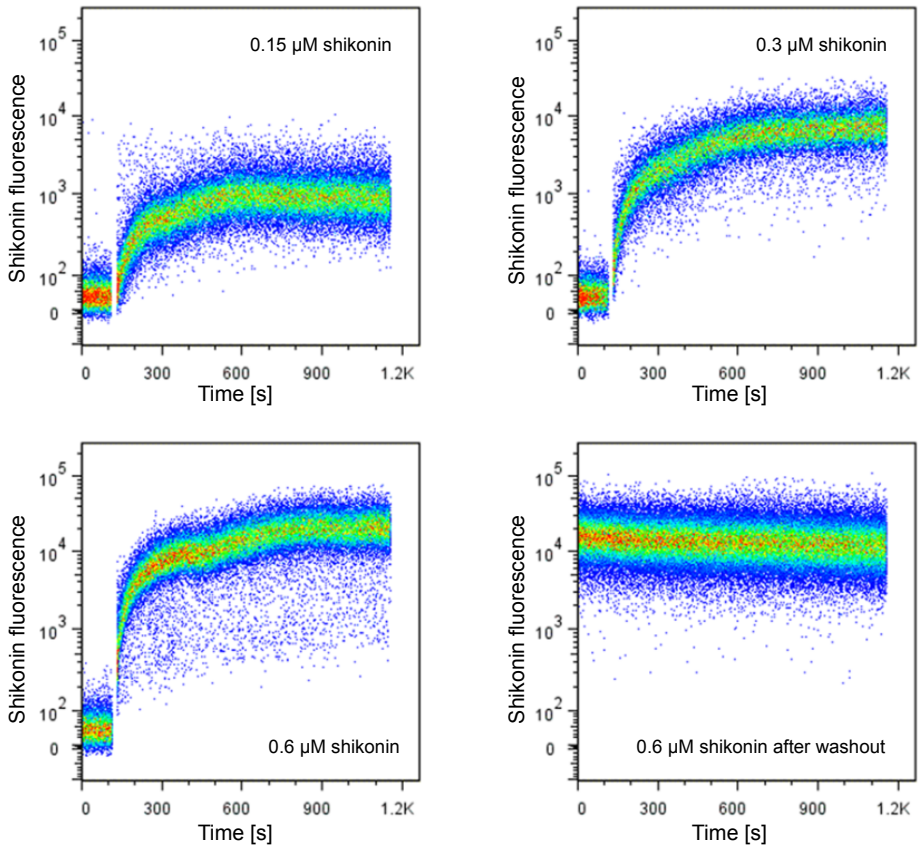

Figure 17: Real-time kinetics and quantification of cellular shikonin uptake by flow cytometry. The inherent fluorescence of intracellular shikonin was measured at 640 nm excitation with a 730/45 nm bandpass filter. A dose-dependent increase of the cellular shikonin fluorescence was observed after treatment with increasing concentrations (0.15, 0.3 and 0.6µM) of shikonin. After 20 min of incubation with 0.6 µM shikonin and subsequent washing of the cells, shikonin's fluorescence was still detectable in cells, indicating persistent intracellular accumulation of shikonin.

The inherent fluorescence of shikonin was further exploited to map its cellular localization in U937 and SK-BR-3 cells by confocal fluorescence microscopy. This examination revealed tubular structures with strong shikonin fluorescence, likely to be mitochondria, around the nucleus. In order to validate this assumption, U937 cells were stained with the mitochondrial dye MitoTracker Green and subsequently incubated with a higher dose of shikonin to enhance detection via confocal microscopy. As shown in Figure 18, shikonin (Figure 18, middle position) was clearly co-localized with the MitoTracker signal (Figure 18, left position) only minutes after shikonin application, corroborating the fact that shikonin accumulates directly in and around the mitochondria after its rapid cellular uptake. For improved visualization of the mitochondria, the experiment was repeated with the adherent SK-BR-3 breast cancer cell line, resulting in a similar accumulation of shikonin in and around the mitochondria (Figure 18).

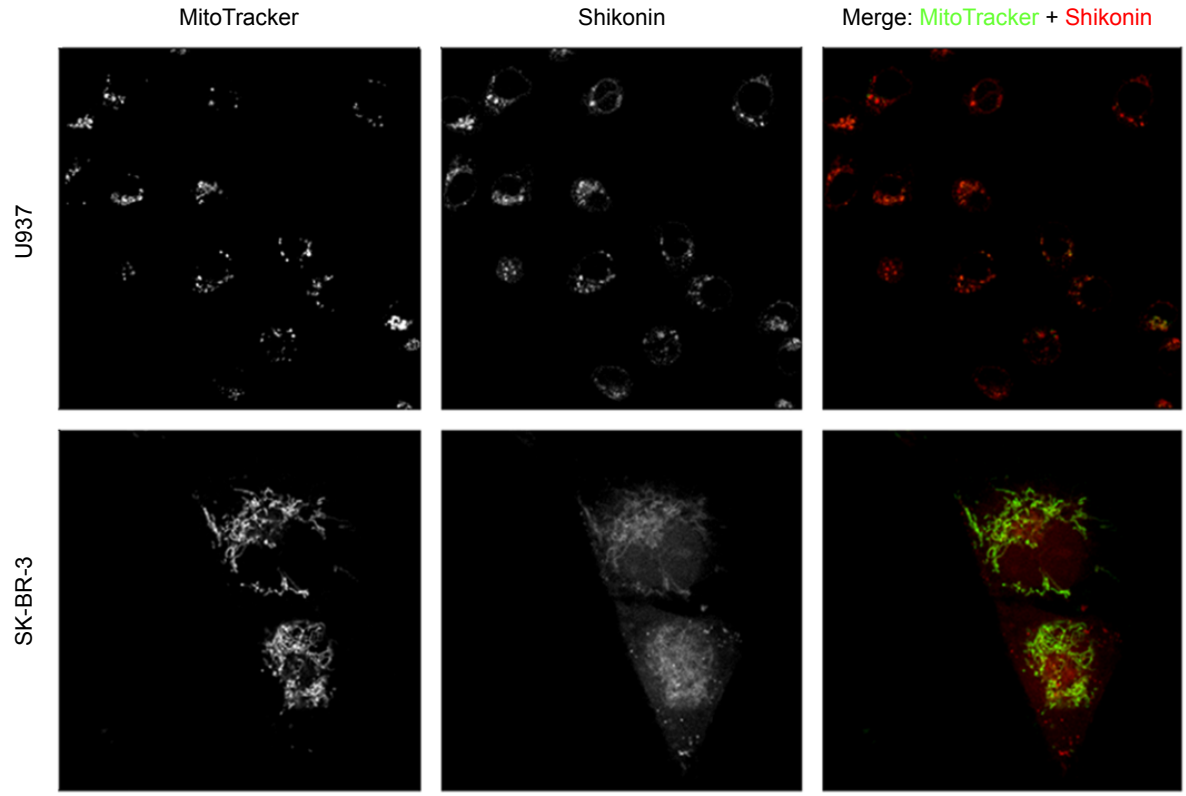

Figure 18: Shikonin localizes to mitochondria. U937 or SK-BR-3 cells were stained with MitoTracker Green and subsequently treated with 25 µM shikonin. Cells were then examined by confocal microscopy at an excitation wavelength of 488 nm and 561 nm and emission at 500-549 nm and 680-780 nm for MitoTracker Green and shikonin, respectively.

3.1.4 Breakdown of the mitochondrial membrane potential

The localization of shikonin to the mitochondria naturally led to the question of whether shikonin indeed negatively influences mitochondrial function as suggested by the gene expression profiling results. To investigate this, U937 cells were stained with JC-1, a marker for intact mitochondrial membrane potential, and treated with 0.3-1.2 µM shikonin for 6 h. Subsequently, the cellular shikonin signal and the JC-1 signal were analyzed by flow cytometry. The electron-potential across the mitochondrial membrane was significantly reduced in cells treated with shikonin, as indicated by reduced red fluorescence of JC-1 in these samples (Figure 19). This suggests that shikonin itself acts to reduce the membrane potential rather than interacting with or blocking a specific target protein.

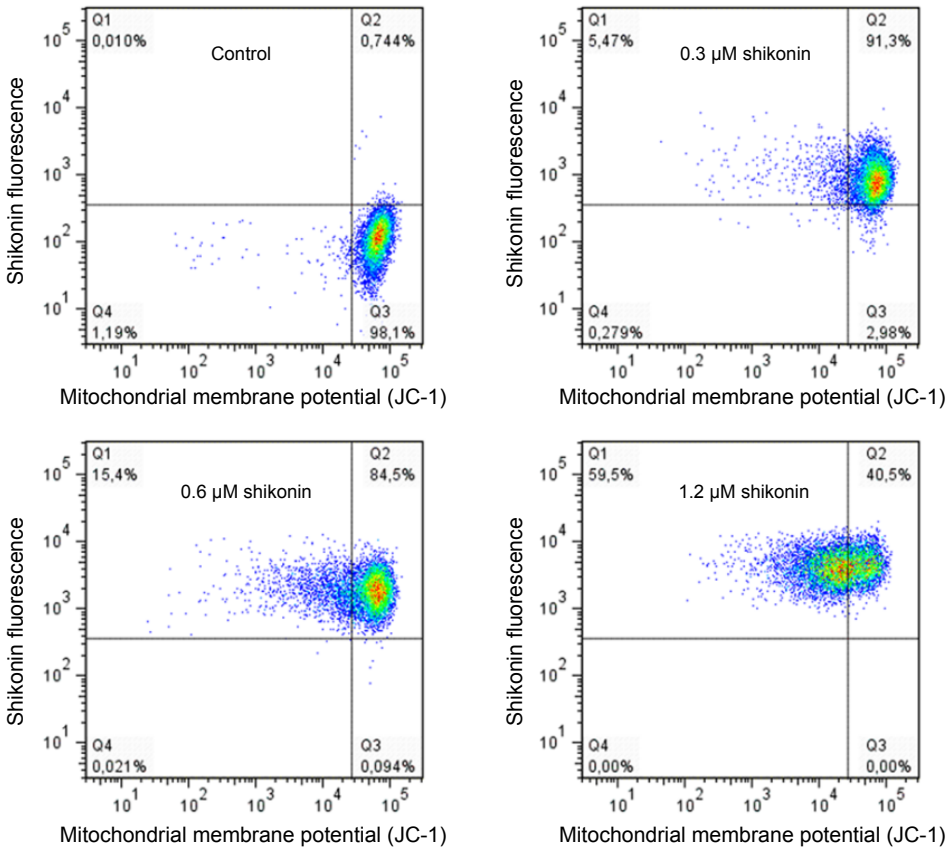

Figure 19: Breakdown of the mitochondrial membrane potential. U937 cells were stained with JC-1, which has a strong red fluorescence in healthy mitochondria. Shikonin induced a dose-dependent decrease of the red JC-1 fluorescence after 6 h of treatment with increasing concentrations of shikonin (0.3, 0.6 and 1.2 µM), indicating a breakdown of the mitochondrial membrane potential.

3.1.5 Induction of reactive oxygen species by redox cycling

ROS induction

Shikonin rapidly enters cells, accumulates in the mitochondria and negatively influences the mitochondrial membrane potential. However, the question remains whether the cytotoxicity of shikonin is mediated largely by mitochondrial deregulation. Mitochondria are the most significant source of cellular ROS (107). Given the previous results, particularly those on shikonin's effect on the mitochondrial membrane potential, cellular ROS levels after shikonin treatment were analyzed by 2′,7′-Dichlorodihydrofluorescein diacetate (H_2DCFH-DA) staining and flow cytometry. Indeed, a clear dose-dependent increase in cellular ROS levels after very short incubation periods (1 h) with shikonin was observed (Figure 20) confirming previous reports (24, 108). ROS levels after treatment with 0.6 µM shikonin are comparable

to those after incubation with the positive control of 50 µM H_2O_2. Thus, shikonin is indeed a potent ROS inducer (Figure 20).

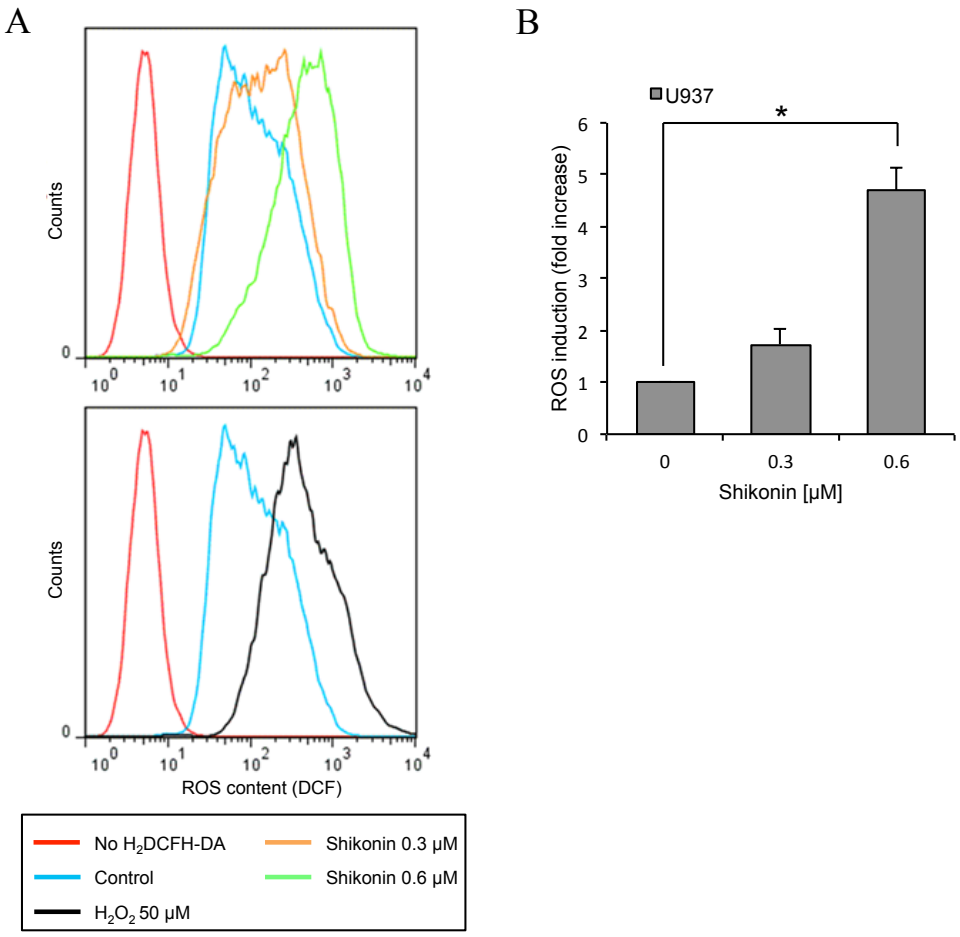

Figure 20: Induction of ROS by shikonin. (A) Flow cytometric analysis of ROS levels after treatment with different concentrations of shikonin for 1 h or 50 µM H_2O_2 for 15 min in living U937 cells. Cells were stained with H_2DCFH-DA and measured at 488 nm excitation and detected using a 530/30 nm bandpass filter. (B) Statistical quantification of ROS induction after shikonin treatment in U937 cells. Data points represent mean (fold change) ± SEM of at least three independent experiments. (*Significant different according to Student´s t-test, $P < 0.05$)

Life ROS induction kinetic

Real-time measurements of shikonin uptake and ROS induction were performed to correlate the kinetics of these two processes and to obtain stronger evidence that shikonin itself is the source of ROS induction. An increased ROS production was observed shortly after cellular shikonin uptake, and ROS levels continuously increased for at least 1 h after exposure to shikonin (Figure 21). The very quick kinetic of ROS induction suggests that it is a primary and direct effect of shikonin accumulation in the mitochondria rather than a downstream

effect mediated indirectly. Subsequent literature research supported this conclusion, revealing that naphthoquinones other than shikonin have been previously implicated in ROS induction via a futile redox cycle in isolated mitochondria (106).

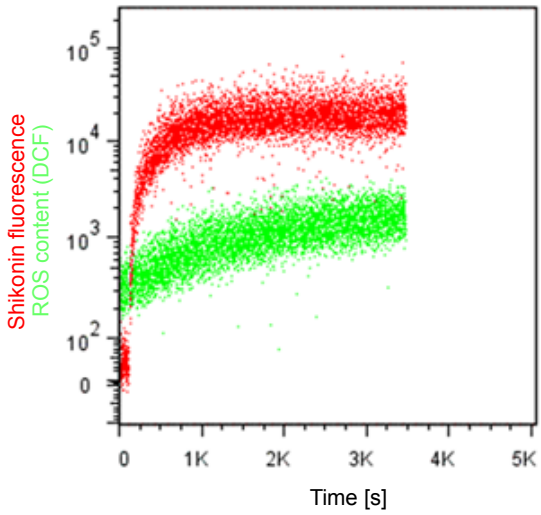

Figure 21: ROS induction kinetics in live cells. U937 cells were stained with H_2DCFH-DA and ROS induction was measured by flow cytometry. After 2 min, shikonin was added to the cells and measurement was continued for 1 h. Shikonin was excited at 640 nm and detected with a 730/45 nm bandpass filter. DCF was excited with a 488 nm laser and detected using a 530/30 nm bandpass filter.

Redox cycling

Due to the quinone structure of shikonin and its accumulation in the mitochondria, it was proposed that the ROS induction caused by shikonin is based on a futile mitochondrial redox cycle. To prove this hypothesis, an established colorimetric assay was performed to measure H_2O_2 generated by redox cycling of compounds incubated with the reducing agent dithiothreitol (DTT) (109). The assay is based on the ability of horseradish peroxidase (HRP) to catalyze the oxidation of phenol red by H_2O_2, producing a change in its absorbance at 610 nm. Figure 22 shows the reaction scheme for the interaction of shikonin and DTT to generate H_2O_2.

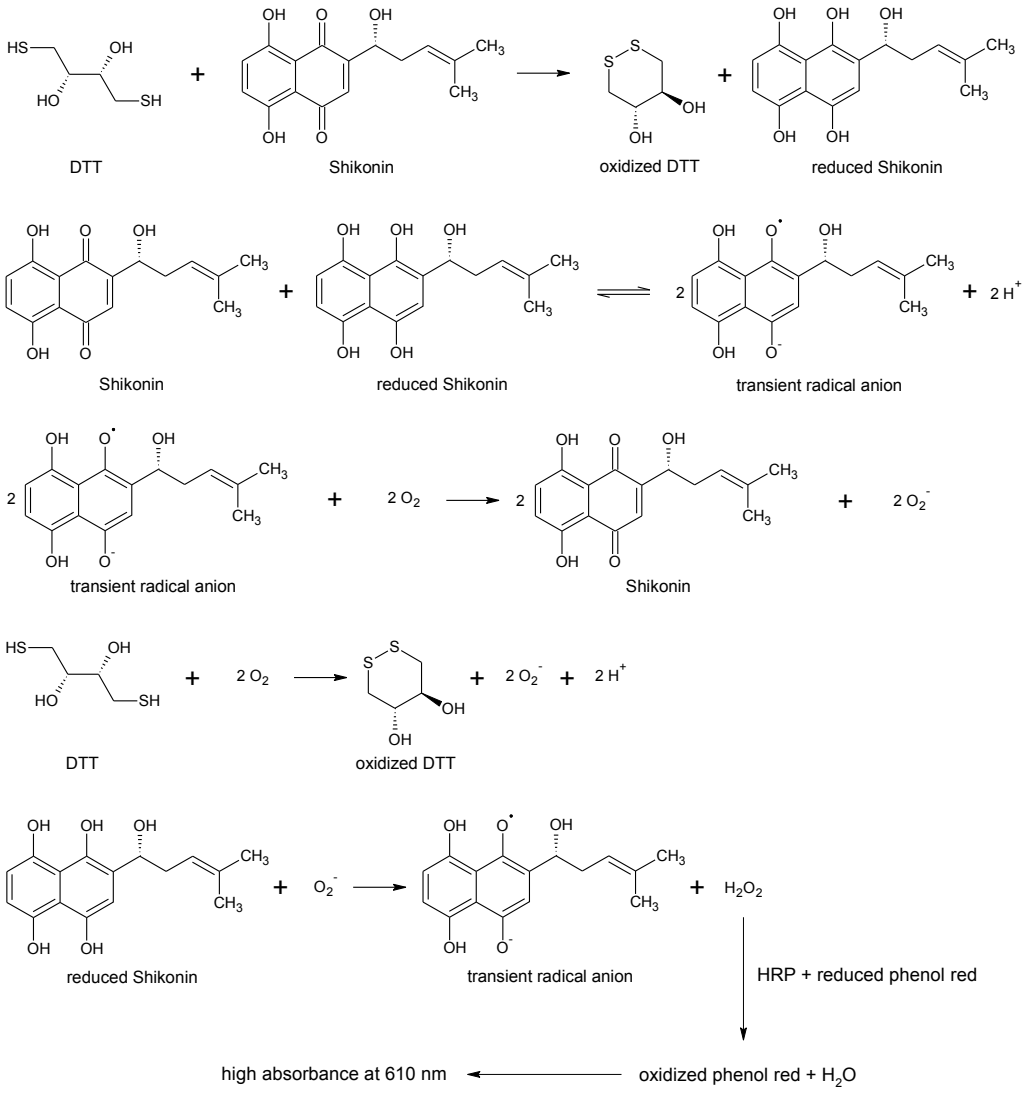

Figure 22: Reaction scheme for the interaction of shikonin and DTT to generate H_2O_2. Addition of DTT to shikonin results in the oxidation of DTT and the reduction of shikonin. When shikonin and reduced shikonin are present together they undergo a comproportionation reaction to form a transient anion. This anion reacts with oxygen to form superoxide (O_2^-). DTT also reacts with O_2 to generate O_2^-. O_2^- can then oxidize the reduced shikonin resulting in the production of H_2O_2. HRP catalyzes the reaction of phenol red and the generated H_2O_2 to oxidized phenol red with a high absorbance at 610 nm. Parts of the reaction scheme were adapted from Johnston *et al*. (109).

Figure 23 shows the results of the redox cycling assay. When tested individually, neither shikonin nor DTT produced an absorbance signal significantly different from the buffer control. In combination, shikonin (50 or 100 µM) plus DTT (0.5 mM) produced an absorbance signal in the same range like exogenously added H_2O_2 (100 µM). This data indicated that shikonin is capable to undergo redox cycling in the presence of reducing agents. In mitochondria NADH represents a source of electrons, which can drive the redox cycling of shikonin causing an overproduction of ROS.

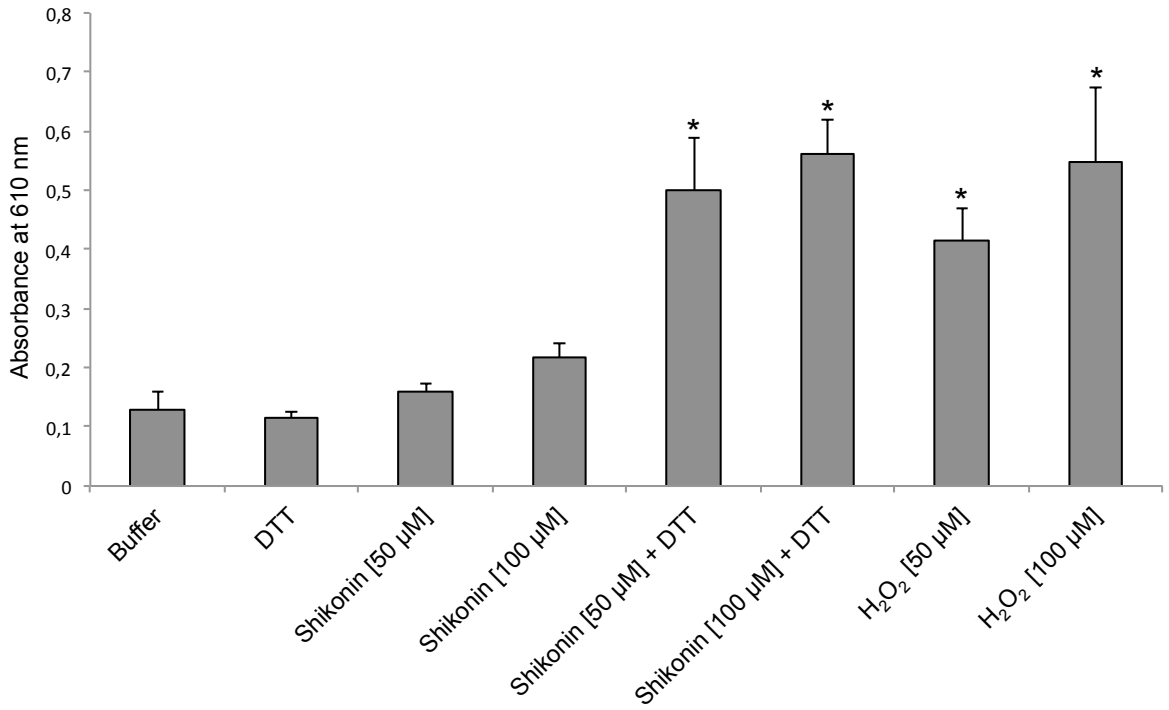

Figure 23: Shikonin- and DTT-dependent redox cycling generation of H_2O_2. Exogenously added H_2O_2 served as positive control. Data points represent mean ± SD of at least three independent experiments. (*Significant different according to Student´s t-test, $P < 0.05$)

3.1.6 Induction of DNA damage

Abnormal accumulation of ROS are likely to give rise to oxidative stress and cause DNA damage by modifications such as 7,8-dihydro-8-oxoguanine (8-oxoG) (110). Since the results of the gene expression profiling also indicated DNA damage after shikonin treatment, it was anticipated that shikonin-induced ROS was the cause of oxidative DNA damage. The alkaline elution technique was used to quantify DNA modifications sensitive to Fpg protein (formamidopyrimidine DNA glycosylase), a repair endonuclease that recognizes and nicks the DNA at sites of oxidative purine modifications such as 8-oxoG. Untreated U937 control cells showed few single-strand breaks, but had a mildly increased level of 0.3 oxidative DNA modifications/10^6bp (Figure 24). This elevated level of oxidative DNA damage corroborates previous findings showing an increased amount of oxidative stress and DNA damage in leukemia cells (111). Upon treatment of U937 cells with 0.3 µM shikonin, there was a 1.6 fold and 2.3 fold increase in the amount of oxidative DNA modifications after 3 and 6 h treatment, respectively (Figure 24). Interestingly, there was no significant generation of single-strand DNA breaks observed in cells treated with 0.3 µM shikonin during the short

incubation periods (3 and 6 h). This observation agrees with a model in which shikonin causes oxidative DNA damage mediated primarily by inducing ROS.

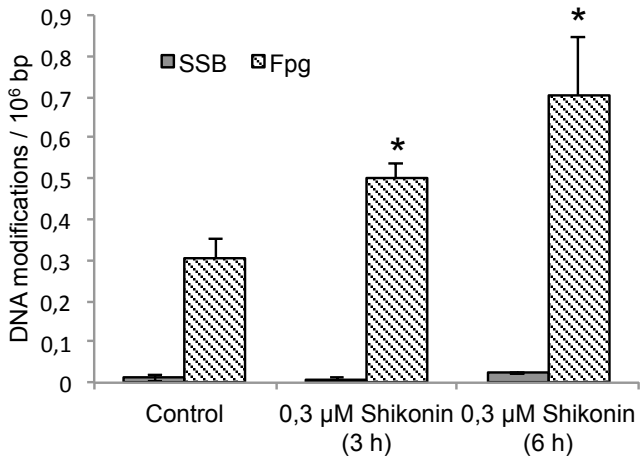

Figure 24: Induction of DNA damage by shikonin measured using alkaline elution technique. Columns indicate the number of DNA single-strand breaks (SSB) and of Fpg-sensitive modifications (oxidative DNA damage) after shikonin treatment. Data points represent mean ± SEM of at least three independent experiments. (*Significant different according to Student´s t-test, $P < 0.05$)

3.1.7 Induction of intracellular calcium signaling

Increased intracellular ROS levels are known to disturb cellular calcium signaling (44). Since several genes involved in calcium homeostasis were found to be strongly deregulated after shikonin treatment (e.g. genes coding for the calcium binding proteins S100A8 and S100A9), the effect of shikonin on the intracellular calcium concentration $[Ca^{2+}]_I$ was analyzed by ratiometric indo-1 staining using flow cytometry. In contrast to ionomycin, an ionophore molecule used to increase $[Ca^{2+}]_I$, treatment with shikonin caused a very short and weak decrease in free $[Ca^{2+}]_I$ that quickly reversed into a slow but continuous increase in $[Ca^{2+}]_I$ in U937 cells (Figure 25). After 30 min of treatment with shikonin, the concentration of intracellular calcium was more than 1.2 fold higher than that in the DMSO treated control cells. Furthermore, the effect was stable for at least 1 h. Interestingly, different concentrations of shikonin (0.6 and 1.2 µM) appeared to have the same effect, and no obvious dose dependency was detected. The slow release of $[Ca^{2+}]_I$ after treatment with shikonin suggests that shikonin doesn't interact directly with calcium storage regulators or serves itself as a calcium ionophore/shuttle as does ionomycin. Instead, it is likely that shikonin induces release

of $[Ca^{2+}]_I$ by the well-known ROS-calcium signaling pathway (44), which would also explain the rather slow kinetics of calcium signaling observed (Figure 21 and Figure 25).

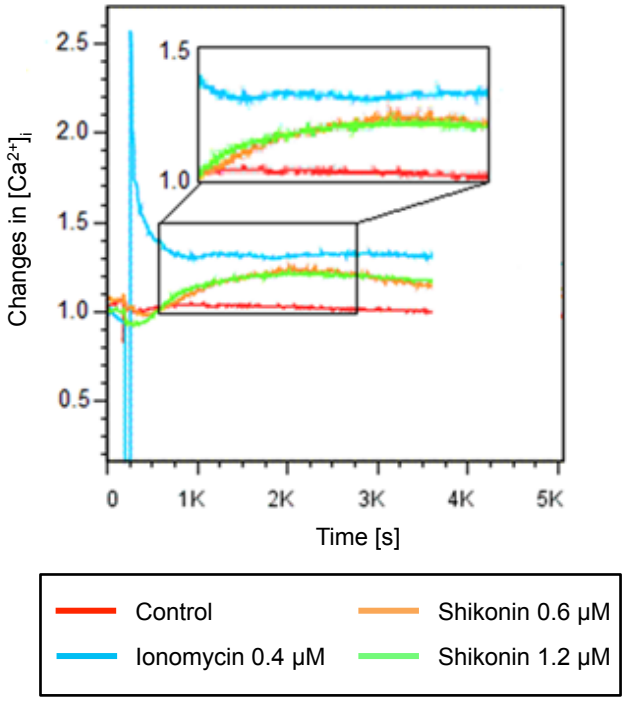

Figure 25: Real-time kinetics of intracellular Ca^{2+} levels after treatment with different concentrations of shikonin or ionomycin in U937 cells. Cells were stained with indo-1 and $[Ca^{2+}]_I$ was measured by flow cytometry. After 2 min, shikonin was added to the cells and measurement was continued for 1 h. Indo-1 was excited with a 355 nm laser and the ratio of the signals detected using a 405/20 nm filter and a 530/30 filter (405/20 nm / 530/30 nm) was used as an index for intracellular calcium concentration.

3.1.8 Induction of cell-cycle arrest and the mitochondrial pathway of apoptosis

Given the effects of shikonin on ROS generation, oxidative genotoxic stress induction, and calcium signaling, the long-term effects of shikonin on the cell cycle were further explored. Flow cytometric cell cycle analysis was performed on U937 cells after 24 h of treatment with different concentrations of shikonin (Figure 26). Shikonin significantly increased the percentage of cells in the sub-G1 phase in a dose-dependent manner (Figure 26A, B), representing an increase in cell death, possibly by apoptosis (112). However, the amount of cells in the G1 and S phase was less affected than the G2 cell population at 0.3 µM (IC50) shikonin (Figure 26B). At this concentration, the population of cells in the G2 phase was decreased by nearly half, indicating that, although the cells were still able to enter S phase to some extent, they were significantly stalled therein. In summary, effective doses of shikonin

seem to cause an arrest of cells in the G1 and S phase, preventing them from entering G2 phase. Ultimately, this arrest leads to a strong increase in the number of apoptotic cells (sub-G1 phase).

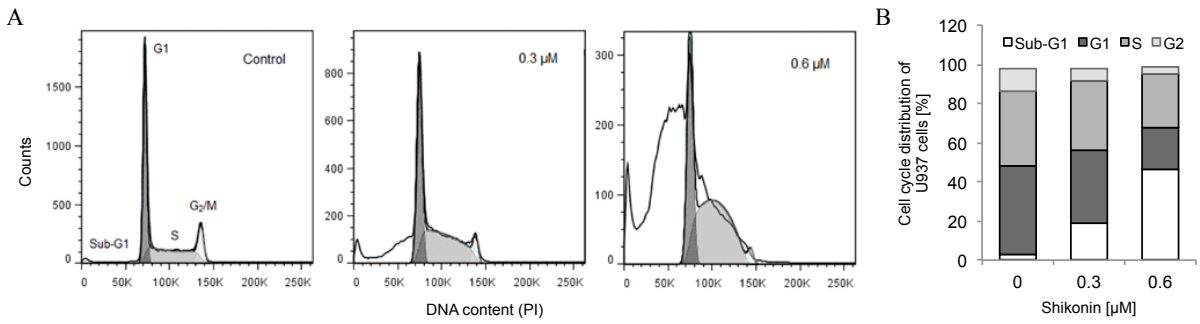

Figure 26: Shikonin induces cell cycle arrest in U937 cells. (A) Typical DNA content histograms of U937 cells treated with increasing concentrations of shikonin for 24 h. (B) Statistical analysis of cell cycle distribution of U937 cells after treatment with different concentrations of shikonin for 24 h. Data points are means of at least three independent experiments.

Since shikonin accumulates in the mitochondria and disrupts the mitochondrial membrane potential, it was hypothesized that induction of cell death in shikonin-treated cells may be due to the activation of the mitochondrial or intrinsic apoptotic pathway leading to caspase 9 activation. Caspase 9 is activated after the release of cytochrome c from the mitochondria, and once activated it cleaves and activates the effector caspases 3 and 7, which mediate apoptotic cell death (42, 113). The activation of caspases 3, 7 and 9 was analyzed in U937 cells after 6 h of treatment with different concentrations of shikonin. A significant dose-dependent increase in the activity of all three caspases in shikonin treated samples was observed consistent with the hypothesis that shikonin activates the intrinsic pathway of apoptosis (Figure 27).

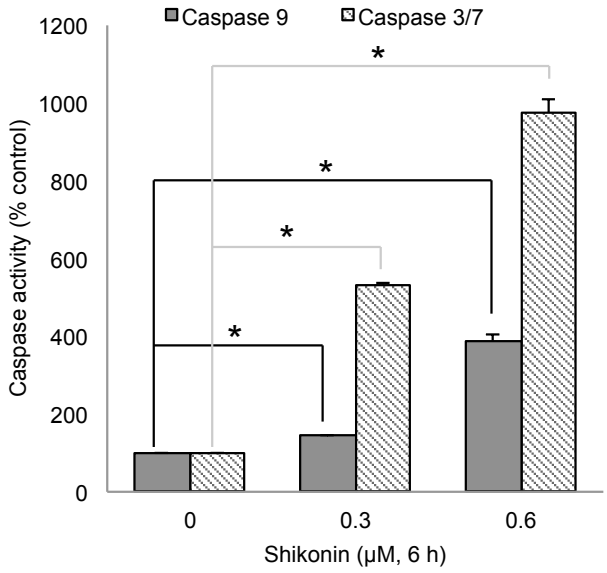

Figure 27: Shikonin induces apoptosis in U937 cells. Enzymatic activity of caspase 3/7 and caspase 9 after 6 h of shikonin treatment in U937 cells. The caspase activity (mean ± SD of at least three experiments) is expressed as percentage relative to the untreated control. (*Significantly different according to Student´s t-test, $P < 0.05$)

3.1.9 Inhibition of cancer cell migration and microtubule dynamics

The initial microarray experiment identified a set of genes sensitive to shikonin and correlated with cytoskeleton formation, cellular movement and morphology. Thus, it was hypothesized that shikonin negatively influences cell motility. Scratch migration assays using the highly metastatic breast cancer cell line SK-BR-3 were performed to investigate the effect of shikonin on cancer cell migration (Figure 28). Experiments with SK-BR-3 cells treated with DMSO solvent control demonstrated complete scratch closure in most cases after 12 h. However, cells treated with 1.2 µM shikonin (IC50/8) showed a considerably delayed closure of the scratch; after 12 h only 55% of the initial scratch width was closed. At a concentration of 2.3 µM shikonin (IC50/4), only 22% of the initial scratch width was recolonized after 12 h (Figure 28 A and B). The results strongly indicate that shikonin inhibits migration of SK-BR-3 breast cancer cells at sub-toxic concentrations.

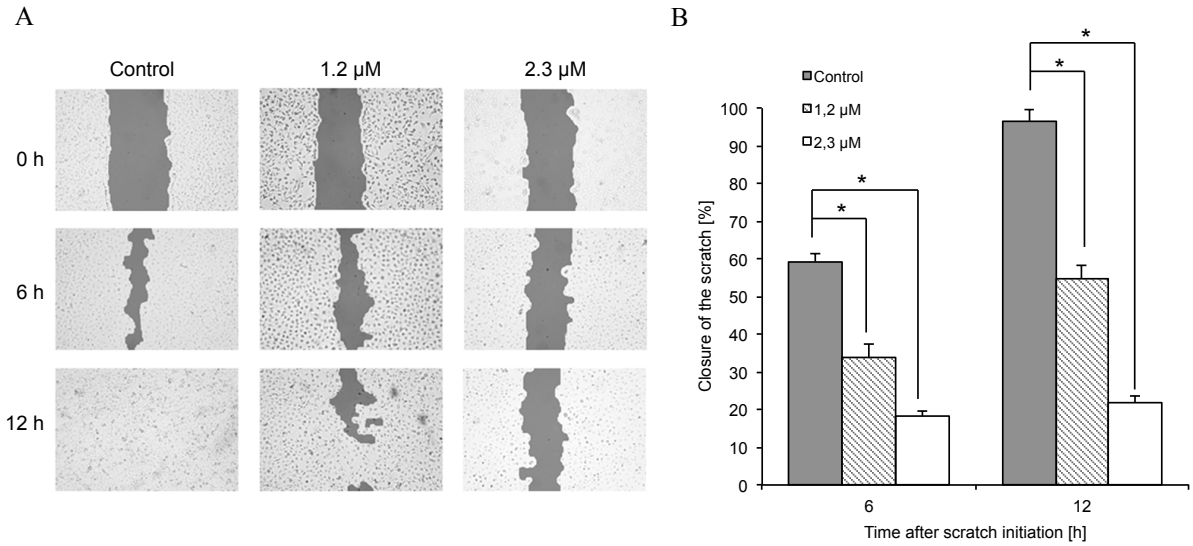

Figure 28: Shikonin inhibits cancer cell migration. (A) Typical pictures at 0, 6 and 12 h of scratch migration assays using SK-BR-3 cells treated with different effective, but in this time-frame sub-toxic, concentrations of shikonin. (B) Statistical quantification of the scratch migration assay. Data points represent the mean ± SEM of at least three independent experiments. (*Significantly different according to Student´s t-test, $P < 0.05$)

Microtubules are essential for the directional migration of cells (114). Since the gene expression profiling showed a high number of deregulated genes associated with the microtubule cytoskeleton, it was presumed that shikonin's effect on microtubules was responsible for its ability to inhibit breast cancer cell migration. Therefore, U2OS-GFP-αTubulin cells were treated with 25 µM shikonin and drug uptake, as well as the direct effect of shikonin on the microtubule cytoskeleton were analyzed using real-time high-resolution confocal microscopy (see Video 1 provided on the attached CD). A rapid accumulation of shikonin within the cells' mitochondria was observed, but no colocalization of shikonin with tubulin filaments was detected. However, with increasing cellular concentrations of shikonin, the number of distinct tubulin filaments decreased and the tubulin staining became progressively more diffuse (Figure 29). Due to highly specific accumulation of shikonin in and around the mitochondria, it was concluded that the disassembly of the tubulin network is an indirect downstream effect of shikonin. The tubulin filament disassembly could be a consequence of the reduced amount of ATP generated in the mitochondria by oxidative respiration and/or deregulated calcium signaling.

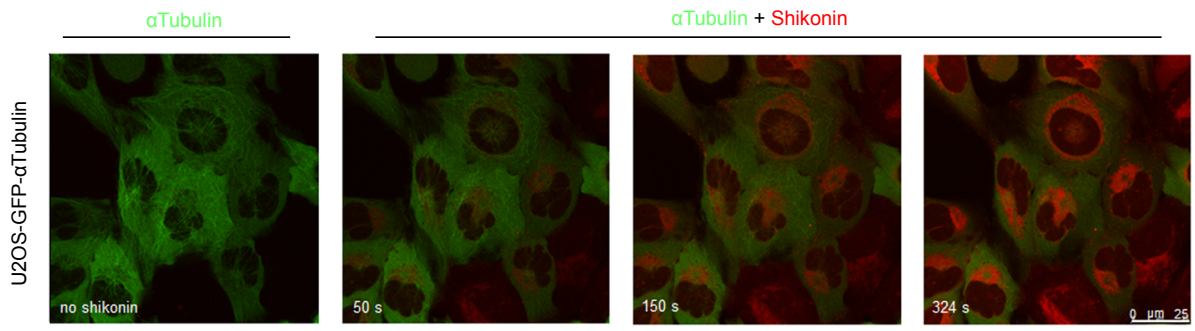

Figure 29: Live imaging of U2OS-GFP-αTubulin cells stably transfected with a GFP fusion construct of α-tubulin and treated with 25 µM shikonin. With increasing cellular concentrations of shikonin, the number of distinct tubulin filaments decreased and the tubulin staining became progressively diffuse. See also Video 1 provided on the attached CD.

The microtubule-associated End binding protein-3 (EB3) binds to growing microtubule plus ends. The GFP-EB3 fusion proteins generate a punctuate pattern of EB3-GFP comets throughout the cell and serve as an elegant marker for visualizing microtubule growth events and dynamics (115, 116). In order to examine variations in microtubule dynamics after shikonin treatment, RPE-1-GFP-EB3 cells were treated with 25 µM shikonin and drug uptake as well as effects on EB3-GFP particle dynamics were analyzed in real-time experiments using high-resolution confocal microscopy (see Video 2 provided on the attached CD). As expected, there was no colocalization of shikonin with EB3 comets. However, shikonin treatment did cause a strong slowdown and finally a complete disappearance of EB3 particles within 3 min of application (Figure 30). EB3-GFP particles are known to disappear when microtubule growth is paused or switches from a state of growth into a state of shrinkage (115). Furthermore, microtubule formation is dependent on sufficient amounts of ATP (117) and is sensitive to changes in calcium levels (118), both of which are significantly affected by shikonin.

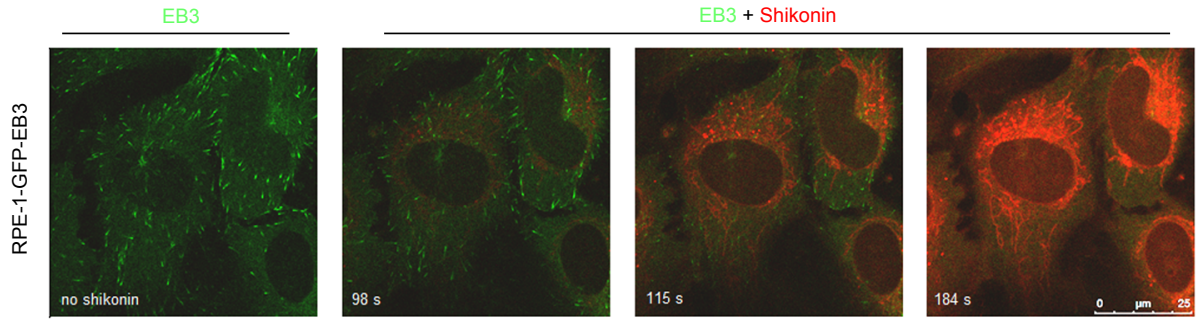

Figure 30: Live imaging of RPE-1-GFP-EB3 cells stably expressing GFP-EB3 and treated with 25 µM shikonin. Shikonin caused a slowdown and finally a complete disappearance of EB3 particles within 3 min after application, indicating disrupted microtubule formation. See also Video 2 provided on the attached CD.

3.1.10 Summary: Shikonin directly targets mitochondria of cancer cells

The results presented in the previous parts indicated that shikonin has a strong cytotoxic effect on a wide variety of cancer cell lines, especially different types of leukemia and several known MDR cell lines. Microarray based gene expression analysis of U937 leukemia cells suggested that the cytotoxicity of shikonin is based on the disruption of normal mitochondrial function, overproduction of ROS, inhibition of cytoskeleton formation, and finally induction of cell cycle arrest and apoptosis. All these effects were confirmed by *in vitro* cell culture experiments exploiting the specific natural fluorescence of shikonin. Most importantly, the deregulated mitochondrial function was caused by a direct accumulation of shikonin in the mitochondria of cancer cells. In the reductive environment of the mitochondria shikonin is capable to undergo redox cycling causing an overproduction of ROS. Thereby, direct targeting of mitochondria was identified as possible primary cellular mechanism of shikonin's cytotoxicity. The deregulation of calcium signaling and microtubule disintegration were downstream effects mediated not by a direct interaction of shikonin with the suggested targets but rather by the direct generation of ROS, the subsequent dysregulation of mitochondria and induction of oxidative damage.

3.2 Shikonin inhibits mTOR signaling in leukemia cells

In the previous chapter it was shown that shikonin has a strong cytotoxic effect against different cancer cell lines, especially sensitive and resistant leukemia cells, and that the basal cellular mechanism of shikonin is the direct targeting of mitochondria and the induction of the mitochondrial pathway of apoptosis. However, the question why shikonin is particularly effective against leukemia and lymphoma cells remains unresolved. Thus, the effect of shikonin on the myeloid leukemia cell line U937 was further analyzed using dimethyl labeling for quantitative proteomics. This technique allowed a detection of quantitative changes in the proteome after shikonin treatment. The obtained data was evaluated with IPA and subsequently integrated with the results from the transcriptomic studies (mRNA and miRNA microarray). The proteomic versus transcriptomic approach indicated that one of the most affected signaling pathways in U937 leukemia cells was the PI3K-Akt-mTOR cascade. The effect of shikonin on the PI3K-Akt-mTOR pathway was validated by demonstrating a decreased phosphorylation and activation of Akt after shikonin treatment using phospho-specific antibodies and flow cytometric analysis. In addition, kinase activity tests revealed

that shikonin inhibits the kinase activity of the insulin-like growth factor 1 receptor (IGF1R), which is an important trigger of the PI3K-Akt-mTOR signaling cascade.[2]

3.2.1 Proteomics analysis using dimethyl labeling

Using stable-isotope labeling, coupled with mass spectrometry-based methods is a simple and practical way to quantify changes in protein abundance. Here, quantitative changes in the proteome of U937 cells after shikonin treatment were studied by stable-isotope dimethyl labeling. The technique uses formaldehyde to globally label the N-terminus and ε-amino group of lysine through reductive amination. Samples are digested with trypsin and the derived peptides of the different samples are labeled with isotopomeric dimethyl labels. The labeled samples are mixed and simultaneously analyzed by LC-MS whereby the mass difference of the dimethyl labels is used to compare the peptide abundance in the different samples (119, 120). U937 cells were treated with 0.3 µM (IC50) shikonin or DMSO solvent control for 24 h before proteins were isolated for stable-isotope dimethyl labeling and LC-MS/MS analysis. Bioinformatic evaluation identified 918 proteins significantly deregulated ($p < 0.05$) after shikonin treatment. The most deregulated proteins in consequence to shikonin treatment are summarized in Table 6.

Using the Ingenuity Pathway Analysis tool, the deregulated proteins were correlated with cellular functions including RNA post-transcriptional modification, nucleic acid metabolism and energy production (Figure 31).

[2] Parts of the results presented in this chapter were recently published in a peer-reviewed scientific journal:

Wiench B, Chen YR, Paulsen M, Hamm R, Schroeder S, Yang NS, Efferth T. Integration of different "-omics" technologies identifies inhibition of the IGF1R-Akt-mTOR signaling cascade involved in the cytotoxic effect of shikonin against leukemia cells. Evid Based Complement Alternat Med. 2013; Accepted 7 May 2013

All text passages, figures and tables of this publication that are used in a modified form in this dissertation were prepared or written by myself.

Table 6: Top up- and down-regulated proteins in U937 cells after treatment with shikonin.

Gene name	Protein name	Fold change
Up-regulated proteins		
HMOX1	Heme oxygenase 1	+14.3
WDR3	WD repeat-containing protein 3	+12.1
HIST1H4	Histone H4	+11.1
RQCD1	Cell differentiation protein RCD1 homolog	+10.0
SNX17	Sorting nexin-17	+9.1
MPI	Mannose-6-phosphate isomerase	+7.7
HIST2H2BE	Histone H2B type 2-E	+7.1
SLFN11	Schlafen family member 11	+6.7
LIMA1	LIM domain and actin-binding protein 1	+6.7
SEPT3	Neuronal-specific septin-3	+6.7
Down-regulated proteins		
HK1	Hexokinase-1	-20.5
VPS11	Vacuolar protein sorting-associated protein 11 homolog	-20.0
RPL24	60S ribosomal protein L24	-7.5
NT5DC2	5'-nucleotidase domain-containing protein 2	-5.4
HNRNPH2	Heterogeneous nuclear ribonucleoprotein H2	-4.5
DDX3Y	ATP-dependent RNA helicase DDX3Y	-4.3
WDR77	Methylosome protein 50	-4.0
GOLPH3	Golgi phosphoprotein 3	-3.5
LRRC58	Leucine-rich repeat-containing protein 58	-3.5
ARHGAP4	Rho GTPase-activating protein 4	-3.1

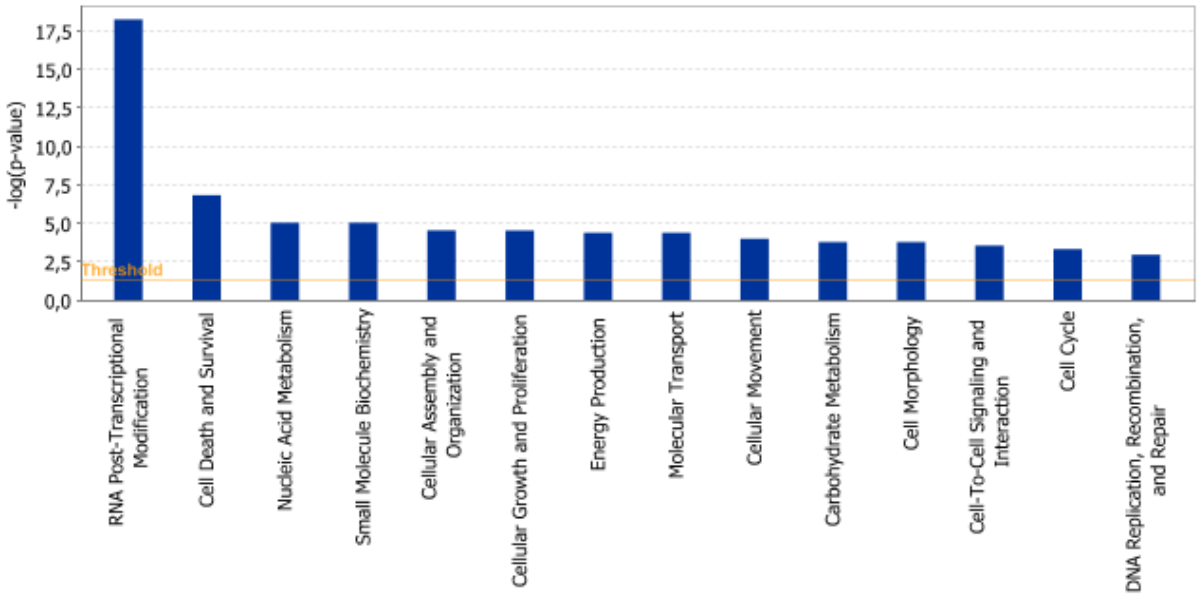

Figure 31: Top cellular functions affected by shikonin treatment in U937 cells examined by proteomics analysis using dimethyl labeling. Right-tailed Fisher's exact test was used to calculate a p-value determining the probability that each biological function assigned to the datasets is due to chance alone.

Furthermore, several protein networks were found to be significantly deregulated in U937 cells after shikonin treatment and the most deregulated network is shown in Figure 32. The figure indicates that a whole set of 40S ribosomal proteins as well as the ribosome maturation protein SBDS were deregulated after shikonin treatment. A central node of the network is the heme oxygenase 1 (HMOX1), which is the most up-regulated protein after shikonin treatment. The network was correlated to discrete cellular functions like RNA post-transcriptional modification, cell death and protein synthesis.

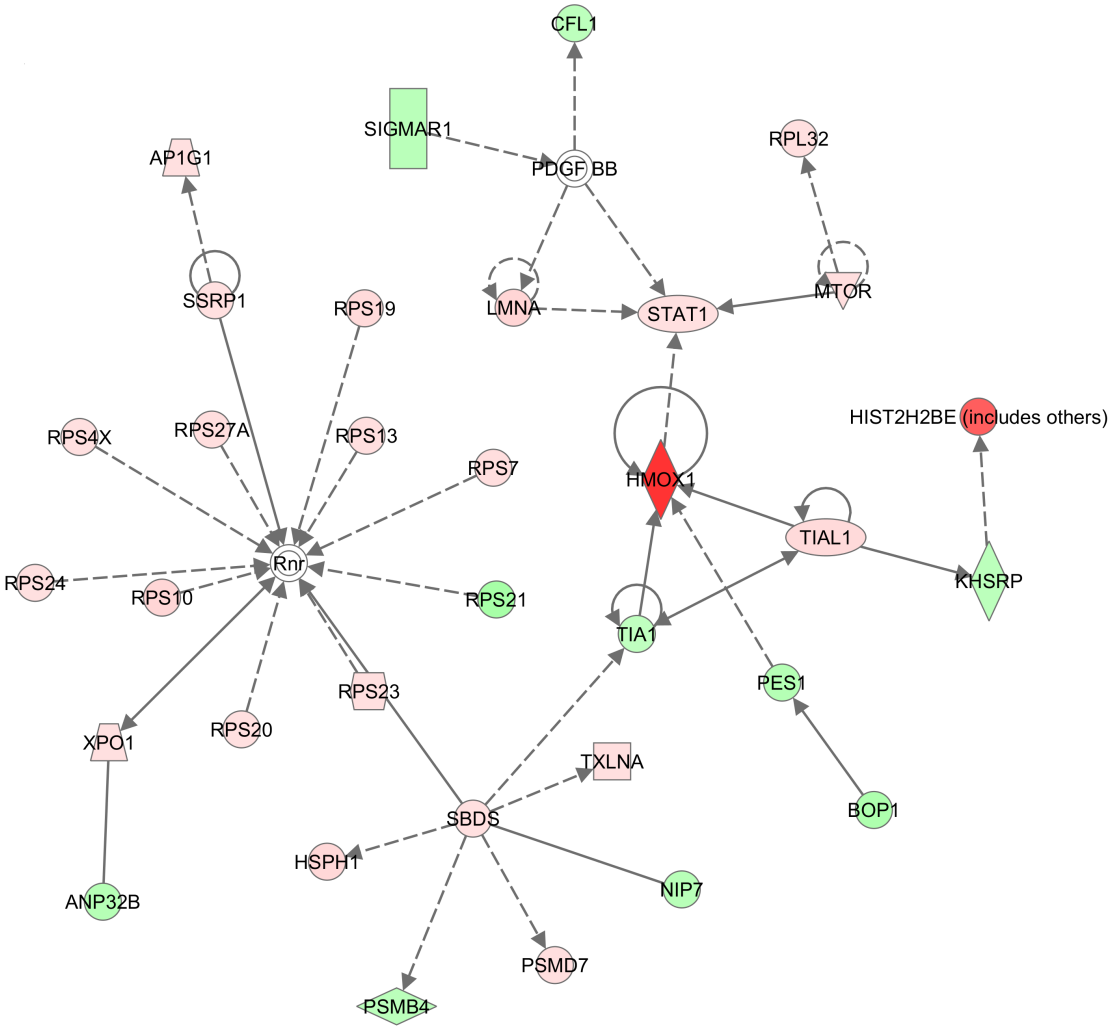

Figure 32: Most deregulated protein network in U937 cells treated with shikonin. Proteins are represented as nodes, and the biological relationship between two nodes is represented as an edge. The intensity of the node color indicates the degree of up- (red) or down- (green) regulation. Continuous lines show a direct interaction, dotted lines an indirect interaction. The network was correlated to discrete cellular functions like RNA post-transcriptional modification, cell death and protein synthesis.

3.2.2 Comparison of transcriptomics and proteomics

Recently, it was shown that the integration of different quantitative *omics* technologies is a promising tool for elucidating molecular mechanisms of new drugs in a fast and precise manner (121). Since each of the three *omics* assays performed in this study (mRNA and miRNA microarray, and proteomics analysis using dimethyl labeling) resulted in a plethora of information about shikonin's cellular mechanisms, it was decided to evaluate the datasets in a comparative transcriptomics versus proteomics approach to extract the most significant results (Figure 33).

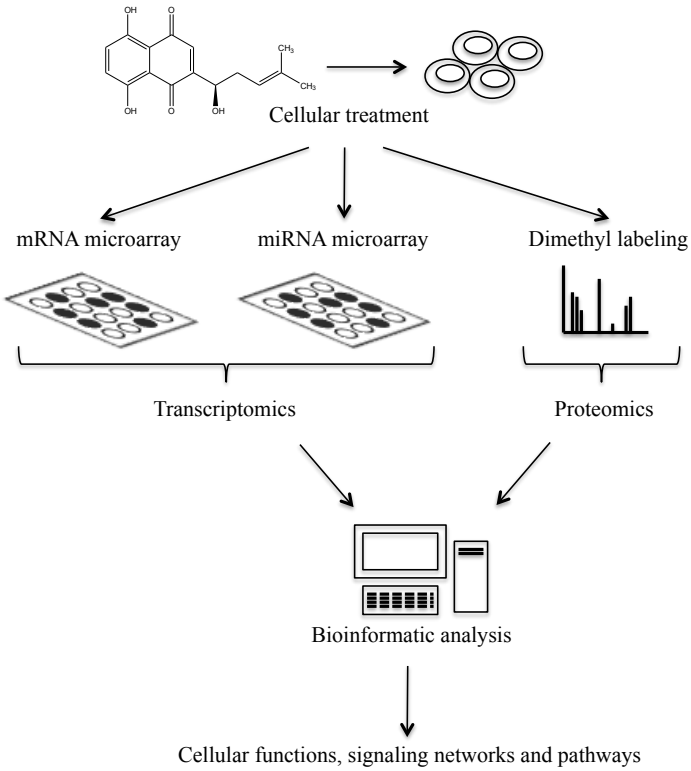

Figure 33: Complementarity of various *omics* technologies provides a system-level understanding of shikonin's effects in U937 cells and provides new insights into cellular functions, signaling networks and pathways affected by shikonin. Figure adapted from Rix and Superti-Furga (122).

Figure 34 shows the number of deregulated molecules in each assay, and the number of predicted mRNA targets of deregulated miRNAs. The intersections of the *Venn* diagram indicate the number of corresponding molecules deregulated in different assays independently from the direction of their deregulated expression. The overlap of deregulated genes and proteins comprises 88 molecules (19%). Filtered to cases where the corresponding molecules

are expressed in the same direction - resulting in the same biological consequence - it is limited to 52 molecules (11%).

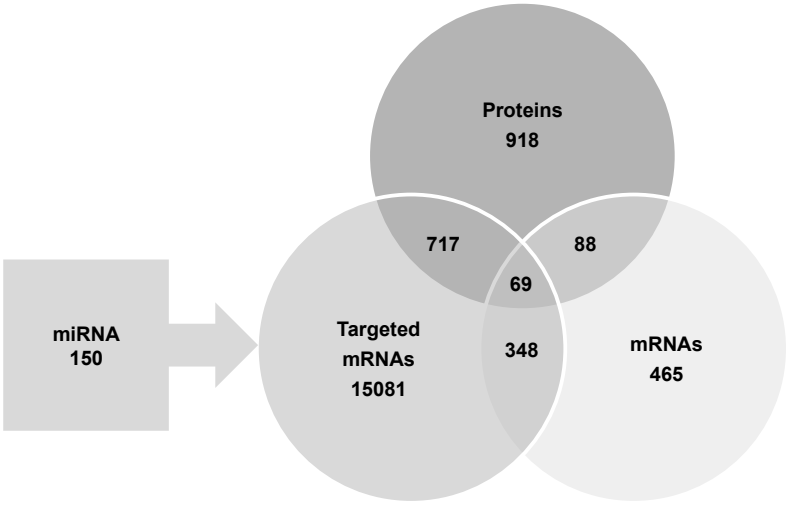

Figure 34: Results and relations of mRNA microarray, miRNA microarray and proteomics analysis using dimethyl labeling. Only molecules from the *omics* datasets that met the expression fold change cutoff of ≥ ±1.2 are shown in this diagram. The intersections of the Venn diagram indicate the number of corresponding molecules deregulated in different assays independently from the direction of their deregulated expression.

The data of the single assays were matched using the Ingenuity Pathway Analysis (IPA) comparative analysis tool, revealing cellular functions deregulated by shikonin treatment on the transcriptome as well as on the proteome (Figure 35). The data confirms previous findings indicating that shikonin has strong effects on cell proliferation, cell cycle progression, cellular movement and DNA integrity of cancer cells. Interestingly, shikonin also affects the post-transcriptional modification of RNA and disturbs cell-to-cell signaling and interaction.

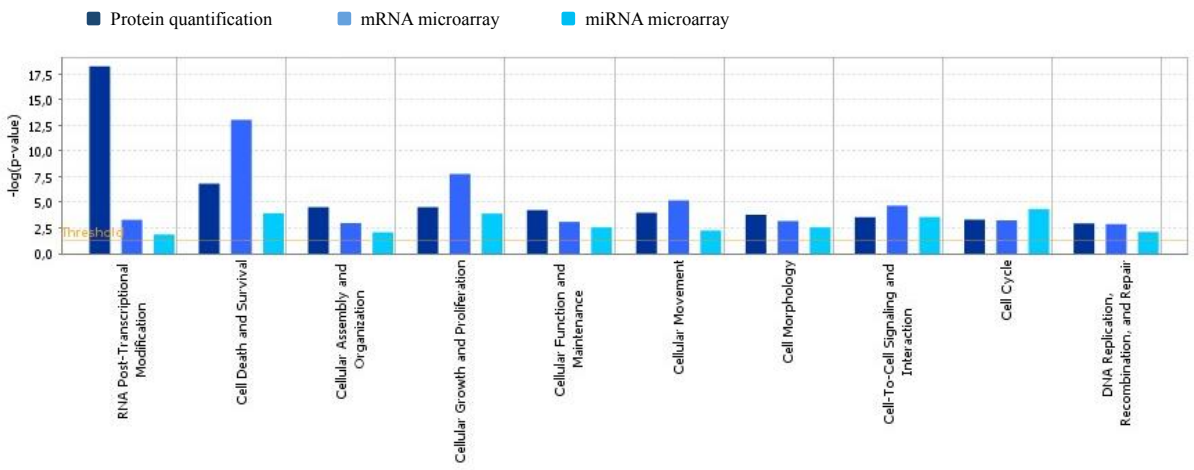

Figure 35: Comparison analysis of molecular and cellular functions affected by shikonin in three *omics* assays. The bar graph displays only functions disturbed in all three assays. Right-tailed Fisher's exact test was used to calculate a p-value determining the probability that each biological function assigned to the datasets is due to chance alone.

The data of the three *omics* assays were compiled to one data set and a pathway analysis was performed using IPA. This reanalysis identified a signaling network around the PI3K-Akt-mTOR axis, which was strongly affected by shikonin treatment (Figure 36).

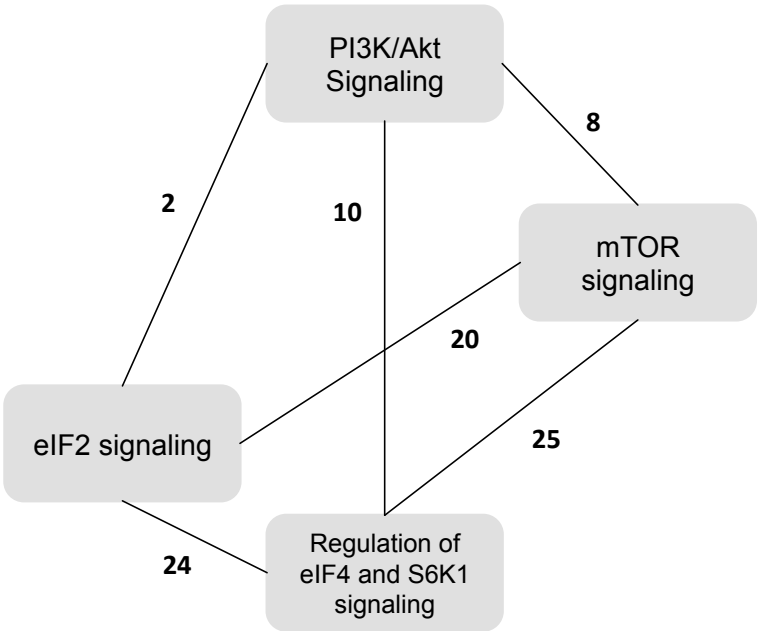

Figure 36: Overlapping signaling pathways deregulated after shikonin treatment. Numbers of identical molecules deregulated in overlapping pathways are shown.

3.2.3 Effect of shikonin on the PI3K-mTOR signaling cascade

The effect of shikonin on PI3K-Akt-mTOR signaling pathway was analyzed by a close examination of the upstream marker p-Akt and the downstream marker p-ribosomal protein S6 (pRiboS6) by flow cytometry. Samples with and without shikonin treatment were stained with directly conjugated antibodies against p-Akt and pRiboS6. Shikonin significantly inhibits the phosphorylation of Akt, while the phosphorylation of RiboS6 remained almost unchanged (Figure 37). This result indicates an effect of shikonin upstream of the PI3K-mTOR signaling cascade.

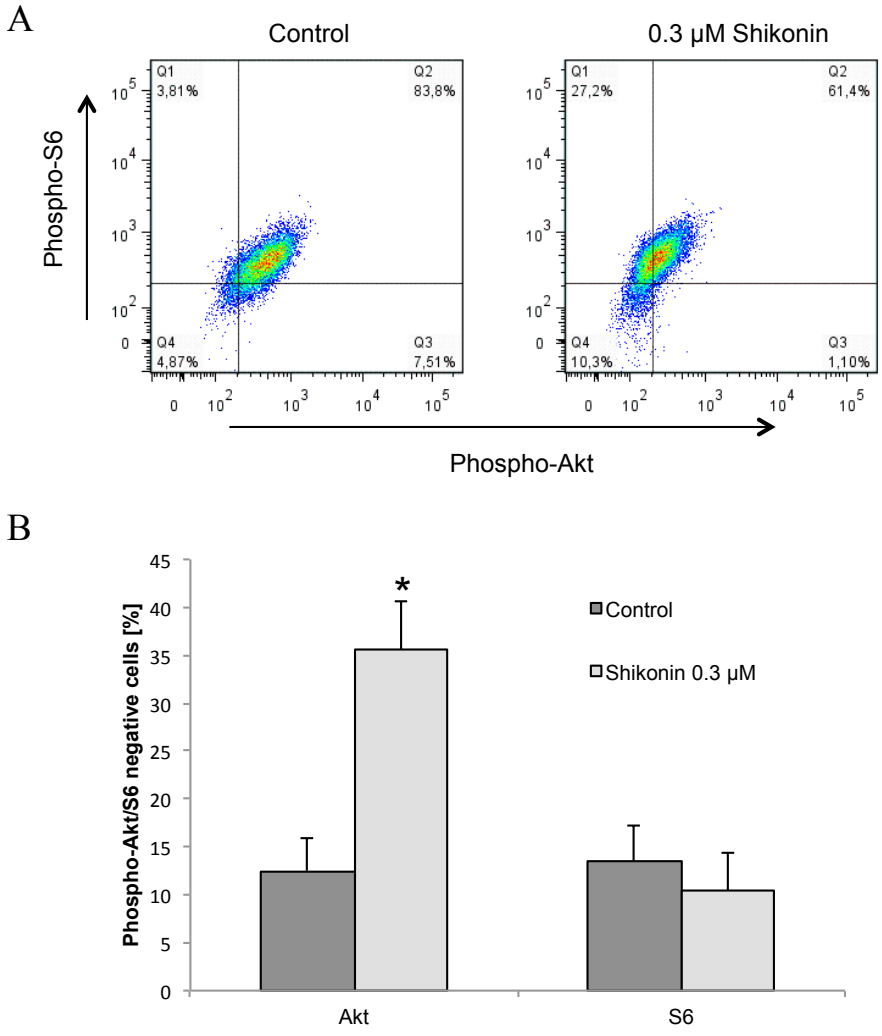

Figure 37: Effect of shikonin on the PI3K-mTOR signaling cascade. (A) U937 cells were treated with 0.3 µM shikonin for 24 h and subsequently stained with phospho-specific antibodies against p-Akt and p-ribosomal protein S6. Shikonin treatment significantly decreased the amount of phosphorylated Akt (left shift), but no effect on the phosphorylation status of ribosomal protein S6 was detected. (B) Statistical quantification of p-Akt or p-ribosomal protein S6 negative cells after shikonin treatment. (*Significantly different according to Student´s t-test, $P < 0.05$)

3.2.4 Virtual screening of shikonin on proteins of the mTOR signaling pathway

To identify possible targets of shikonin in the PI3K-mTOR pathway, a virtual screening approach was conducted. Binding energies of shikonin and key proteins of the signaling cascade – with available crystal structures – were calculated using the AutoDock Vina tool (123). Proteins involved in the PI3K-mTOR pathway were selected according to a recent publication by Laplante and Sabatini (64). Table 7 summarizes the ranking of the predicted target proteins of shikonin.

Table 7: Calculate binding energies of shikonin and key proteins of the IGF1R-Akt-mTOR signaling pathway. Virtual screening was performed using the AutoDock Vina software.

Symbol	Description	Binding energy [kcal/mol]
EGFR	Epidermal growth factor receptor	-8.8
SGK1	Serine/threonine-protein kinase Sgk1	-8.8
IGF1R	Insulin-like growth factor 1 receptor	-8.6
GSK3B	Glycogen synthase kinase-3 beta	-8.5
4E-BP1	Eukaryotic translation initiation factor 4E-binding protein 1	-8.5
S6K1	Ribosomal protein S6 kinase beta-1	-8.4
PKCA	Protein kinase C alpha type	-8.4
PIK3C3	Phosphatidylinositol 3-kinase catalytic subunit type 3	-8.3
PDK1	3-phosphoinositide-dependent protein kinase 1	-8.3
eIF4E	Eukaryotic translation initiation factor 4E	-8.3
RND3	Rho-related GTP-binding protein RhoE	-8.2
AKT2	RAC-beta serine/threonine-protein kinase	-8.1
RSK1	Ribosomal protein S6 kinase alpha-1	-8.1
Rheb	GTP-binding protein Rheb	-7.9
AMPK2	5'-AMP-activated protein kinase catalytic subunit alpha-2	-7.9
RHOA	Transforming protein RhoA	-7.9
AKT1	RAC-alpha serine/threonine-protein kinase	-7.8
RRAGD	Ras-related GTP-binding protein D	-7.8
mTOR	Serine/threonine-protein kinase mTOR	-7.5
RHOC	Rho-related GTP-binding protein RhoC	-7.3
RHOB	Rho-related GTP-binding protein RhoB	-7.2
ERK1	Extracellular signal-regulated kinase 1	-7.1
RHOD	Rho-related GTP-binding protein RhoD	-6.9
IRS1	Insulin receptor substrate 1	-6.4
IKKB	Inhibitor of nuclear factor kappa-B kinase subunit beta	-5.1

Within the top potential binding partners, the receptor tyrosine kinases EGFR and IGF1R, as well as the serine/threonine-protein kinase Sgk1 (SGK1) were found. Since the results of the Akt/RiboS6 phosphorylation by FACS showed no effect of shikonin on the phosphorylation status of ribosomal S6 protein, a target of SGK1, the kinase was not further investigated as binding partner of shikonin. EGFR and IGF1R are both important transmembrane receptors that trigger the PI3K-mTOR signaling cascade after binding to their respective growth factors like EGF, TGFα and IGF. Previous studies showed that shikonin inhibits EGFR phosphorylation and modulates the EGFR signaling cascade (124). Since little is known about an interaction of shikonin and IGF1R and due to the evolvement of IGF1R in drug evasion (67), further studies on shikonin´s mode of action focused on IGF1R.

3.2.5 Inhibitory effect of shikonin on IGF1R

Since IGF1R showed a very high binding activity towards shikonin in the virtual screening experiment, the inhibitory effect of shikonin on this kinase was tested using a radiometric protein kinase activity assay. The dose response curve of shikonin on the IGF1R activity clearly indicates a dose-dependent inhibition of the kinase after shikonin application (Figure 38). An IC50 concentration of 2.6 µM was calculated for shikonin on the purified IGF1R kinase activity by nonlinear regression using Prism 5.04 (Graphpad, CA, USA). This IC50 of shikonin on the IGF1R kinase is very similar to the IC50 of about 3µM observed for U937 cells suggesting that shikonin – besides inducing mitochondrial dysfunction – also exerts additional anti-cancer activities specifically by inhibiting the IGF1R.

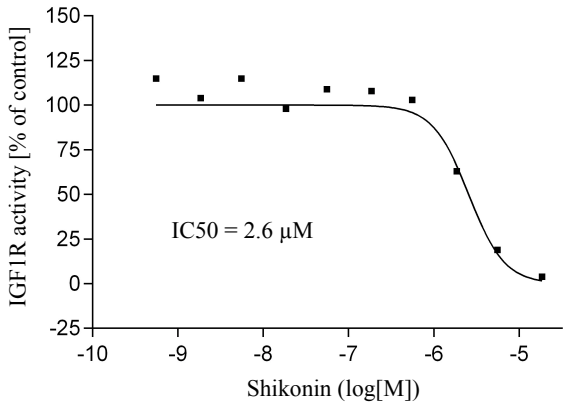

Figure 38: Dose response curve of shikonin in an IGF1-R kinase assay. A radiometric protein kinase assay (33PanQinase® Activity Assay) was used for measuring the kinase activity of IGF1R. IC50 values were calculated by nonlinear regression using Prism 5.04 (Graphpad, CA, USA).

An *in silico* blind docking approach was undertaken to evaluate possible binding sites of shikonin on the entire surface of the IGF1-R molecule. Two possible binding sites were identified by this approach (Figure 39). One of the detected binding sites (Figure 39, B) correlates with the already described binding region of known IGF1-R inhibitors.

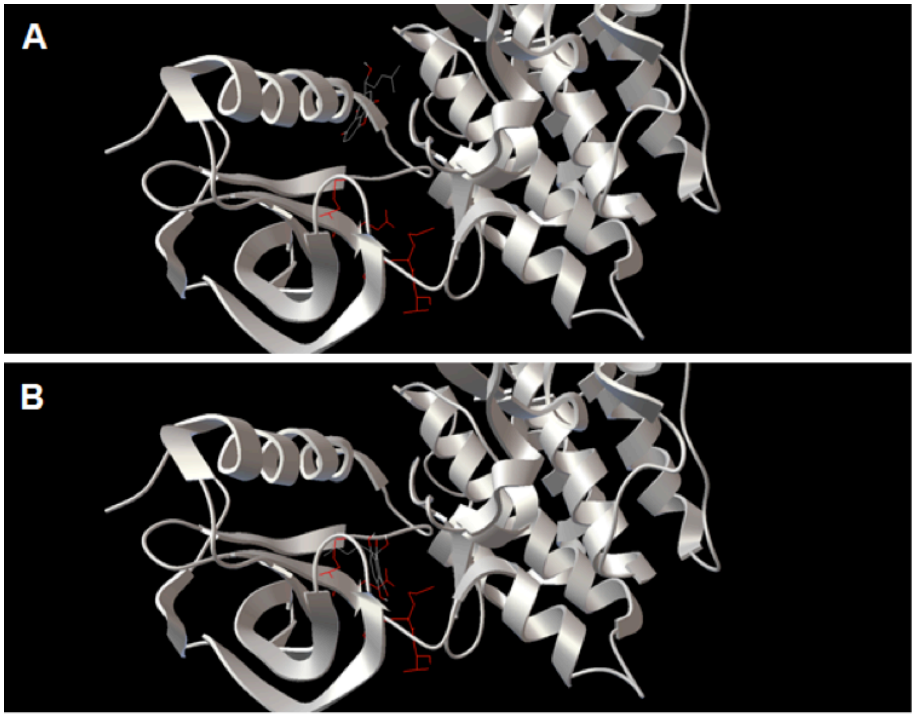

Figure 39: Potential shikonin binding sites of IGF1-R identified by *in silico* blind docking analysis. Best docked shikonin molecules were found at two different binding sites (A, B). Shikonin is drawn as sticks (carbon atoms are colored grey, oxygen atoms are colored red). IGF1-R is colored grey, secondary structures of the protein are displayed. Residues involved in the binding of known IGF1-R inhibitors are highlighted red.

3.2.6 Summary: Shikonin inhibits mTOR signaling

The basal cellular mechanism of shikonin is the direct targeting of mitochondria and the induction of the mitochondrial pathway of apoptosis. Cytotoxicity screenings showed that the compound is particularly effective against sensitive and resistant leukemia and lymphoma cell lines, suggesting an additional cellular mechanism of shikonin action. mRNA and miRNA microarrays were used to analyze changes in gene expression in myeloid leukemia cells after shikonin treatment and those results were combined with proteomics analysis using dimethyl labeling. The integration of bioinformatics and the three *omics* assays revealed that the strongly cross-linked PI3K-Akt-mTOR axis was intensely affected by shikonin. This signaling pathway plays a critical role in cellular growth control and survival. Deregulations

of the PI3K-Akt-mTOR pathway are frequently associated with cancerogenesis, especially in a wide range of hematological malignancies where the pathway is constitutively active, creating a promising target for cancer therapy (61). The effect of shikonin on the PI3K-Akt-mTOR signaling cascade was functionally validated by demonstrating a decreased phosphorylation and activation of Akt after shikonin treatment. Kinase activity tests revealed that shikonin inhibits the kinase activity of IGF1R, which is an important trigger of the PI3K-Akt-mTOR signaling cascade. Up-regulation of IGF1R is a major evasion mechanism of cancer cells against currently used drugs targeting the pathway (67-69). Ultimately, the results indicate that inhibiting the IGF1R-Akt-mTOR signaling cascade is a new cellular mechanism of shikonin strengthening its potential for the treatment of hematological malignancies.

3.3 Effect of shikonin against cancer stem cells

CSCs are a small subpopulation of cancer cells that possess the abilities of unlimited growth, self-renewal and differentiation into other, more specialized cancer cell types (77). Furthermore, CSCs are more resistant to anticancer agents representing a major cause for a relapse of the disease after an initial response (85, 86). For a successful therapy it is insufficient to kill only the differentiated bulk cells without targeting the CSCs. Here, the effect of shikonin against CSCs was analyzed by performing a mammosphere formation assay, population distribution and uptake studies, and cytotoxicity tests against ABCB5 overexpressing cells.

3.3.1 Mammosphere culture of MCF-7 cells

One breakthrough in CSC research was the detection of $CD44^{+}/CD24^{-/low}$ breast cancer stem cells (BCSCs) (70). In the last decade, these cells were investigated extensively and it was shown that an *in vitro* propagation of BCSCs is possible by culturing the cells in a reconstituted 3D culture system as so-called mammospheres (125, 126). This comprises culturing of breast cancer cell lines or isolated breast cancer progenitor cells under serum-free, non-adherent conditions leading to the formation of spherical cell clusters that are highly enriched for BCSCs. The experimental procedure represents a common test system for analyzing the effect of compounds against *in vitro* formed CSCs (127). Here, a modified protocol from Guttilla *et al.* (128) was used to maintain a prolonged mammosphere culture of

MCF-7 breast cancer stem cells. According to the protocol, MCF-7 cells were cultured for 5 weeks as mammospheres and then returned to standard adherent culture conditions. The morphological development and the CD44/CD24 phenotype of the complete culture were analyzed at several time points during the prolonged culture (Figure 40). Each generation of mammospheres was named after the week of culture since the mammosphere generation was initiated (MS P1, MS P2, and so forth). Mammosphere formation was already obtained after one week of culture under non-adherent conditions (MS P1). The cells in the first passage of mammosphere culture showed a 2-fold increase in the number of cells with a $CD44^{+}/CD24^{-/low}$ phenotype in comparison to normal MCF-7 cells (3.9 vs. 1.9 %). During the mammosphere culture the tightly adherent spheroids (MS P1) switched to small and loosely aggregated spheroids after five passages (MS P5) (Figure 40). Mammospheres in the fifth passage showed a strong increase in the number of $CD44^{+}/CD24^{-/low}$ CSCs (12.5%). Upon transfer back to adherent flasks, cells attached to the bottom again and started growing as a monolayer (MS P6 and MS P7). During mammosphere culture, MCF-7 cells continuously developed a $CD44^{+}/CD24^{-/low}$ phenotype, which reached a maximum one week after reseeding to adherent flaks (MS P6). At this stage more than half of the cells showed a CSC phenotype (51.6%). Two weeks after reseeding, the amount of $CD44^{+}/CD24^{-/low}$ cells started to decrease again (MS P7). An experimental layout was designed that performs cytotoxicity testing of mammospheres one week after reseeding into adherent culture flasks (Figure 41).

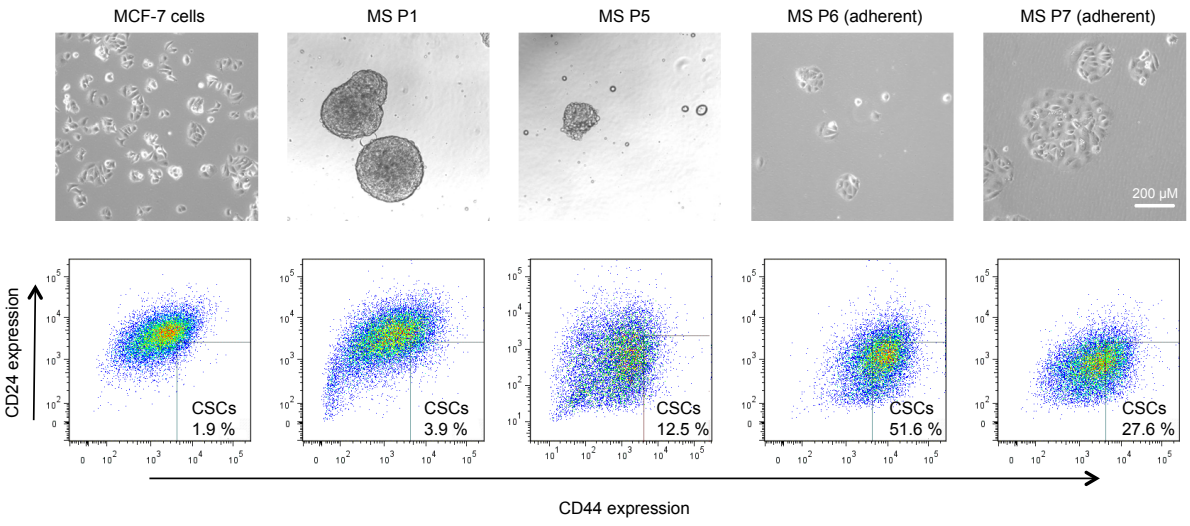

Figure 40: Morphological development and changes in the CD44/CD24 phenotype during prolonged mammosphere culture. Each generation of mammospheres was designated by the week of culture since mammosphere generation was initiated (MS P1, MS P2, and so forth).

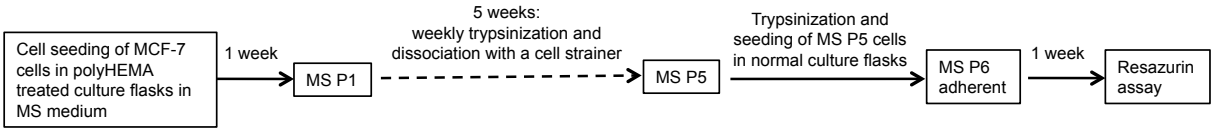

Figure 41: Experimental layout of MS culture and subsequent cytotoxicity testing.

3.3.2 Effect of shikonin against BCSCs-enriched MCF-7 cells

Resistance to cytotoxic chemotherapy is one characteristic of CSCs (85). The established mammosphere culture was used to test the cytotoxic effect of shikonin and the conventional anti-cancer drug docetaxel against MCF-7 cells highly enriched with CSCs as described in Figure 41. The results were compared to the effect of both drugs against normal MCF-7 cells. The CSC-enriched cell line revealed a higher resistance than normal MCF-7 cells to both compounds at all tested concentrations (Figure 42).

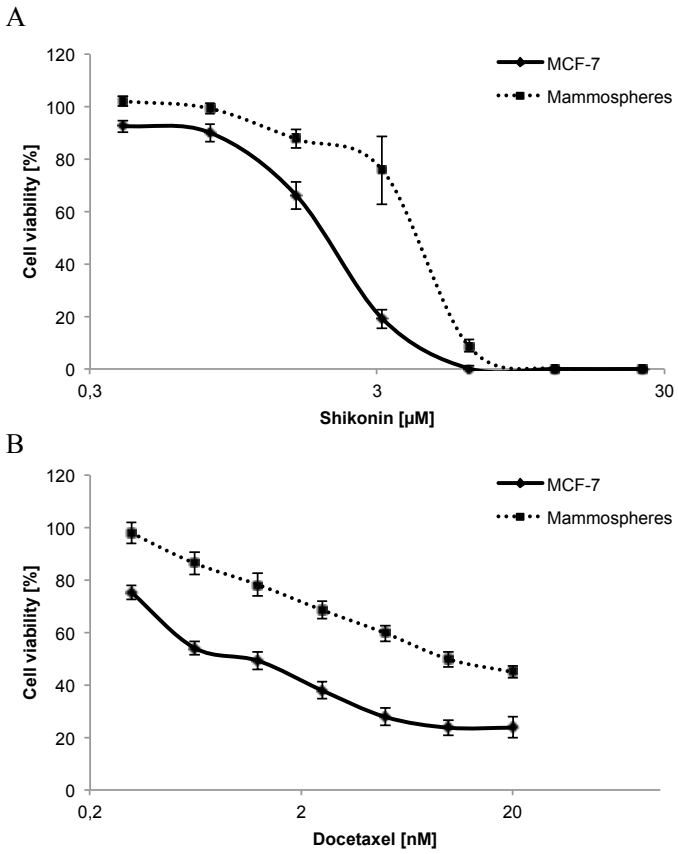

Figure 42: Cytotoxic effect of shikonin (A) and docetaxel (B) against MCF-7 cells and MCF-7 cells cultured as mammospheres. Both cell lines were treated with different compound concentrations or vehicle control for 24 h and subsequently a resazurin reduction assay was performed. Viability of cells is represented by mean ± SEM of three independent experiments and it is expressed as percentage survival of control.

Shikonin showed IC50 values of 2.1 µM and 4.3 µM in normal MCF-7 cells and CSC-enriched MCF-7 cells, respectively. This resulted in a degree of resistance of 2.0 (Table 8). Docetaxel inhibited proliferation by 50% in MCF-7 cells at a concentration of 1.1 nM and in CSC-enriched cells at 9.9 nM resulting in a degree of resistance of 9.9. This indicated that CSCs possess a certain cross-resistance against shikonin, but the resistance is less pronounced than that against the established cytostatic drug docetaxel.

Table 8: Cross-resistance profile of CSC-enriched MCF-7 cells to shikonin and docetaxel. IC50 values (mean ± SEM) were evaluated by resazurin reduction assay. The degree of resistance was calculated as the ratio of IC50 values of the resistant and the corresponding sensitive cell line.

Compounds	IC50 values		Degree of resistance
	MCF-7 cells	CSC enriched MCF-7 cells	
Shikonin	2.1 µM	4.3 µM	2.0
Docetaxel	1.1 nM	9.9 nM	9.9

3.3.3 Effect of shikonin on the population distribution of MCF-7 cells

It was shown that a prolonged treatment with chemotherapeutics leads to an enrichment of BCSCs (129). To examine if shikonin treatment causes a selection pressure on MCF-7 cells leading to an enrichment of CSCs, the CD44/CD24 phenotype of a heterogeneous MCF-7 population was analyzed after shikonin treatment. MCF-7 cells were incubated with shikonin and subsequently stained with antibodies against CD44 and CD24 to investigate the effect of shikonin on different subpopulations of MCF-7 cells (Figure 43). After 24 h shikonin incubation, there was no significant change in the percentage of CSCs, but treatment with 10 µM shikonin for 48 h increased the fraction of $CD44^{+}/CD24^{-/low}$ MCF-7 cells by more than 3-fold (Figure 43 upper panel, Figure 44 A). Like the cytotoxicity data obtained on MCF-7 cells cultured as mammospheres, this is again an evidence for a limited resistance of BCSCs against shikonin. Simultaneously to the phenotype analysis, the cellular content of shikonin in different MCF-7 subpopulations (anti-CSC with a $CD44^{-}/CD24^{+}$ phenotype vs. CSC) was examined (Figure 43, lower panel). At both time points (24 and 48 h) the shikonin content in anti-CSCs was significantly higher than in CSCs (Figure 43 lower panel, Figure 44 B). This indicates that there is an increased export of shikonin out of CSCs probably causing the higher resistance of the cells.

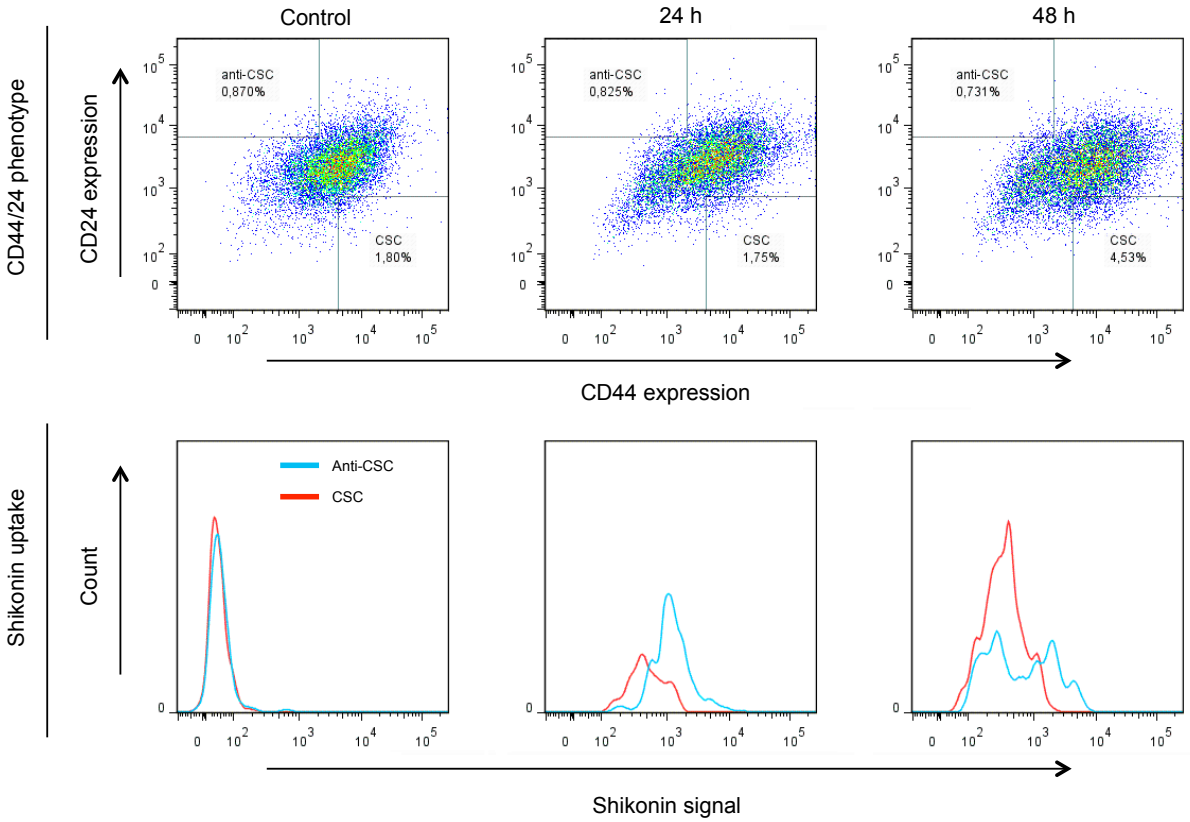

Figure 43: Population distribution and drug uptake of MCF-7 cells after shikonin treatment. Cells were treated with shikonin (10 µM) for 24 or 48 h and subsequently stained with antibodies against CD44 and CD24. Shikonin content and the respective CD44/CD24 phenotype were analyzed by flow cytometry.

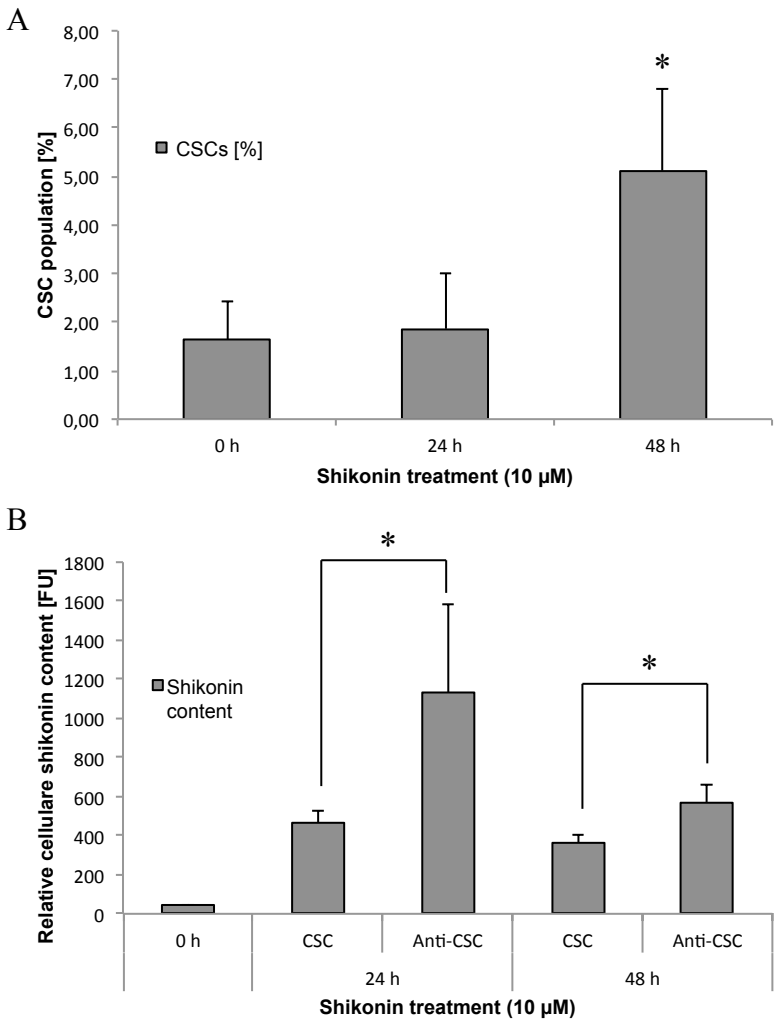

Figure 44: Statistical quantification of CSC population size (A) and drug uptake (B) in MCF-7 cells after shikonin treatment. Data points represent the mean ± SD of at least three independent experiments. (*Significant different according to Student´s t-test, $P < 0.05$)

3.3.4 Effect of shikonin treatment on ABCB5-overexpressing cells

CSCs overexpress several ABC transporters that serve as drug efflux pumps and reinforce their resistance against chemotherapeutics [reviewed in (90)]. A cytotoxicity screening at the beginning of the studies on shikonin indicated that MDR1, MRP1 and BCRP-overexpressing cancer cells showed no or only negligible resistance against shikonin in comparison to their sensitive counterparts. The ATP-binding cassette sub-family B member 5 (ABCB5) transporter represents a new member of the ABC family that plays a crucial role in the resistance of CSCs against cytotoxic drugs (76). ABCB5 acts as an energy-dependent drug efflux transporter and marks tumor cells of a putative CSC compartment (130). Especially among melanoma, ABCB5-expressing cells were proposed to display an enhanced

tumorigenicity with stem cell-like properties (131) and its expression confers resistance to taxanes and anthracyclines (132). Here, the effect of shikonin against ABCB5 overexpressing HEK293 cells and the corresponding sensitive cell line was tested (Figure 45).

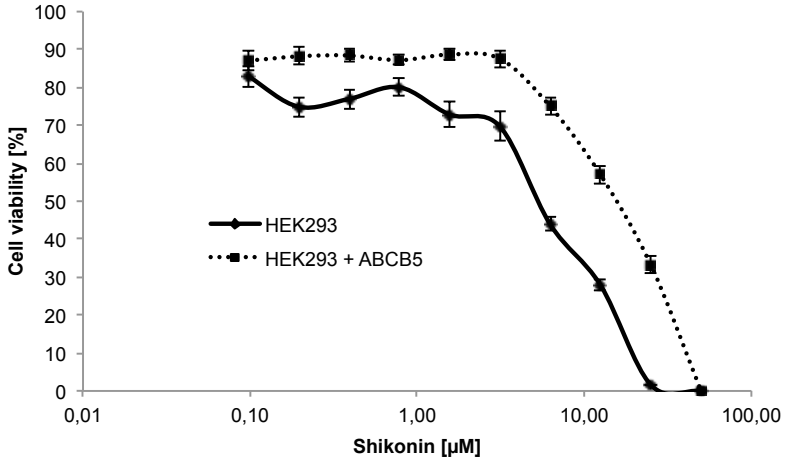

Figure 45: Cytotoxic effect of shikonin against ABCB5 overexpressing HEK293 cells and normal HEK293 cells. Both cell lines were treated with different shikonin concentrations or vehicle control for 48 h and subsequently a resazurin reduction assay was performed. Viability of cells is represented by mean ± SEM of at least two independent experiments and it is expressed as percentage survival of control.

The ABCB5-overexpressing cells revealed a higher resistance than their sensitive counterparts at all tested concentrations (Figure 45). After 24 h treatment, shikonin inhibited proliferation of HEK293 cells by 50% at a concentration of 2.7 µM and in ABCB5-overexpressing HEK293 cells at 13.8 µM resulting in a degree of resistance of 5.1 (Table 9). After 48 h incubation, shikonin showed IC50 values of 5.3 µM and 15.3 µM on sensitive and ABCB5-overexpressing HEK293 cells, respectively. This results in a degree of resistance of 2.9 indicating that shikonin is a substrate of the ABCB5 transporter and is therefore less toxic against CSCs in comparison to sensitive cancer cell populations.

Table 9: Cross-resistance profile of ABCB5-overexpressing HEK293 cells to shikonin after 24 or 48 h treatment. IC50 values (mean ± SEM) were evaluated by resazurin reduction assay. The degree of resistance was calculated as the ratio of IC50 values of the resistant and the corresponding sensitive cell line.

Shikonin treatment	IC50 values [µM]		Degree of resistance
	HEK293 cells	ABCB5 expressing HEK293 cells	
24 h	2.7 ± 0.1	13.8 ± 0.2	5.1
48 h	5.3 ± 0.1	15.3 ± 0.4	2.9

3.3.5 Summary: Effect of shikonin agains CSCs

A prolonged mammosphere culture was established to enrich MCF-7 cells with $CD44^{+}/CD24^{-/low}$ CSCs. Cytotoxicity screenings using this CSC-enriched cell line indicated a moderate resistance of CSCs to shikonin. The well-established anti-cancer drug docetaxel was much less active against CSCs than shikonin. Analysis of the CD44/CD24-phenotype after shikonin treatment showed a selection and an enrichment for CSCs in the surviving MCF-7 population and thereby confirmed the results of the cytotoxicity tests. Drug uptake assays revealed that a decreased intracellular concentration of shikonin is the reason for the enhanced resistance of CSCs. Since shikonin is a substrate of the ABCB5 transporter that is overexpressed in various CSC-populations, this could be a possible reason for the lower shikonin concentrations in CSCs.

3.4 Utilizing inherent fluorescence of therapeutics to analyze drug uptake

During the studies on shikonin, it was examined that the compound exhibits a strong intrinsic fluorescence that can be exploited for analysis by flow cytometry and confocal microscopy. The natural fluorescence of shikonin was used to investigate its cellular uptake and localization in cancer cells. Furthermore the uptake assays of shikonin were coupled to additional endpoint measurements using multi-parametric flow cytometry. This provided the opportunity to analyze for example the effect of shikonin on ROS production or MMP and cellular shikonin uptake simultaneously. Since a high number of pharmaceutical drugs exhibit an intrinsic fluorescence that can be readily exploited for research purpose, the experimental procedure of the shikonin uptake assays was assigned to a small compound library. A method was proposed that analyzes simultaneously in real-time the efficiency, effects and the associated kinetics of compound-uptake and efflux in mammalian cells by flow cytometry.[3]

[3] Parts of the results presented in this chapter were recently published in a peer-reviewed scientific journal and the publication is available via the electronic journals library of the Johannes Gutenberg University:

Wiench B, Eichhorn T, Korn B, Paulsen M, Efferth T. Utilizing inherent fluorescence of therapeutics to analyze real-time uptake and multi-parametric effector kinetics. Methods. 2012 Feb 3

All text passages, figures and tables of this publication that are used in a modified form in this dissertation were prepared or written by myself.

3.4.1 Real-time high-resolution analysis of compound uptake kinetics

Doxorubicin is an established cytostatic compound commonly used in the chemical treatment of a wide range of cancers (133). The drug has an inherent fluorescence frequently used in a variety of different assays (94, 98). Here, doxorubicin was used as the principle model substance to examine the general applicability of the experimental procedure used for shikonin to other compounds. At first the real-time kinetics of doxorubicin uptake in U937 leukemia cells were recorded and analyzed. The cellular uptake of doxorubicin was best measured continuously at 610 nm (BP 610/20) after excitation with a 150 mW 561 nm laser in a flow cytometer (Table 10). The mean fluorescence of untreated cells was recorded and limited to 10x the SD. Doxorubicin was added to the cells and the suspension was briefly mixed before being measured for a total recording time of 20 min. Figure 46 shows the experimental layout of the drug uptake assays.

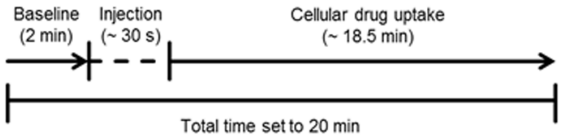

Figure 46: Experimental layout of drug uptake assays. All measurements were performed according to the same workflow**.**

A rapid uptake of doxorubicin into the cells that plateaued after approximately 5 min of incubation was observed (Figure 47). The absolute doxorubicin fluorescence thereafter did not change significantly with increasing time, suggesting that the drug was not transported actively into the cells, but entering via membrane association coupled with a slow cellular permeabilization leading to an equilibrium concentration of doxorubicin in the cells. The rapid-uptake kinetic profile agrees with recently published data in which doxorubicin influx into MDA-MB-435 cells was analyzed by confocal microscopy (94). To analyze the dose dependency of doxorubicin uptake, high-resolution kinetics for five concentrations of doxorubicin in U937 cells were recorded (Figure 47). A simple dose-dependent increase of total cellular fluorescence correlated to increasing doxorubicin concentrations after subtracting the increasing background fluorescence of doxorubicin in the sample stream (Gate 3 – Gate 2) was observed. It is evident that the increase in fluorescence was due to doxorubicin uptake into the cells, because washing the cells did not reduce the fluorescence

signal to a similar extent as was initially characterized as the background signal in the sample stream (Figure 47, lower right panel) (Gate 2). The remaining fluorescence was stable, probably due to the high affinity of doxorubicin for DNA (134), which prevents its efflux from the cell.

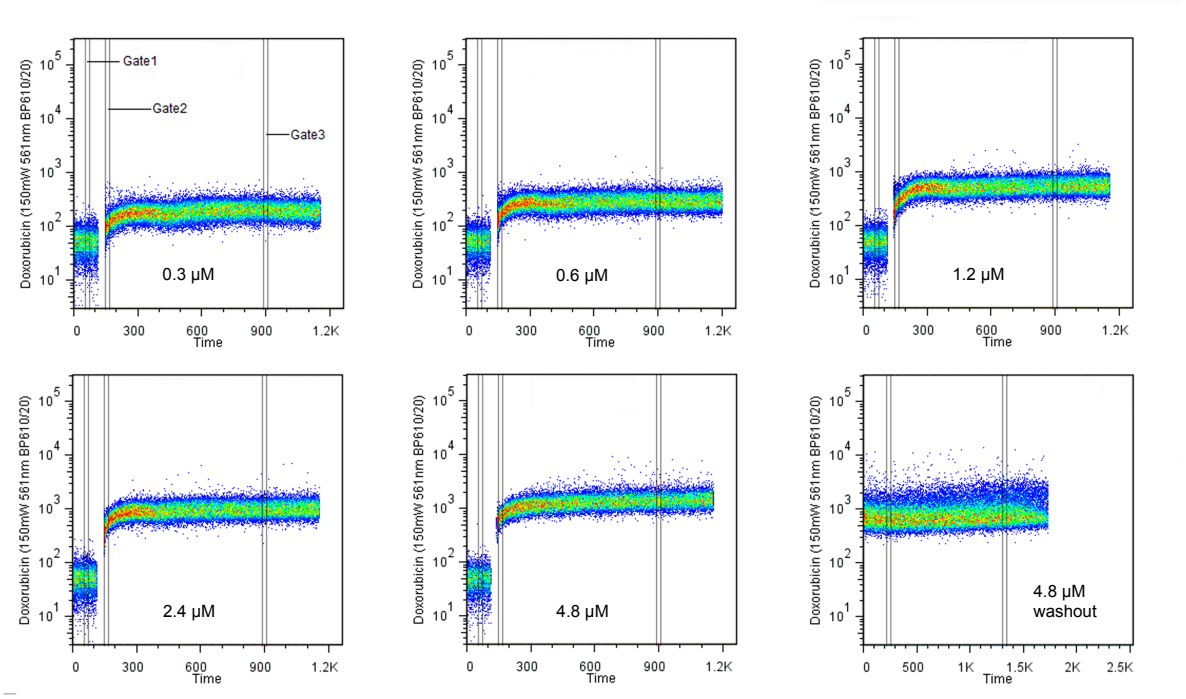

Figure 47: Real-time kinetics of cellular doxorubicin uptake and efflux by flow cytometry. Time (t) is in seconds. The inherent fluorescent emission of doxorubicin was best measured at 610nm with a band width filter at 610/20nm after excitation with a 150mW 561nm laser. The mean fluorescence of non-treated U937 cells was recorded for 2min (Gate 1) and doxorubicin was subsequently added at a concentration of 0.3 µM, 0.6 µM, 1.2 µM, 2.4 µM or 4.8 µM. Measurement continued until a total recording time of 20 min was reached. A washout experiment measured fluorescence after 20 min incubation with 4.8 µM doxorubicin and washing, indicating persistent intracellular accumulation of doxorubicin (lower right panel).

Commonly, the cellular uptake of drugs is quantified by indirect methods such as analyzing the remaining amount of drug in the supernatant of treated cultures (98). To compare this indirect method with the direct measurement of cellular fluorescence via flow cytometry, the doxorubicin fluorescence remaining in the supernatant after 20 min was quantified according to a protocol from Effenberger-Neidnicht *et al*. (98). The calculated uptake correlated directly with the increase in fluorescence for each respective doxorubicin concentrations applied (Figure 48). The obtained results prove that the direct measurements of cellular fluorescence described are consistent with the indirect measurements obtained from data for the reduction of fluorescence measured in the supernatants, at least for 0.3 to 2.4 µM doxorubicin doses.

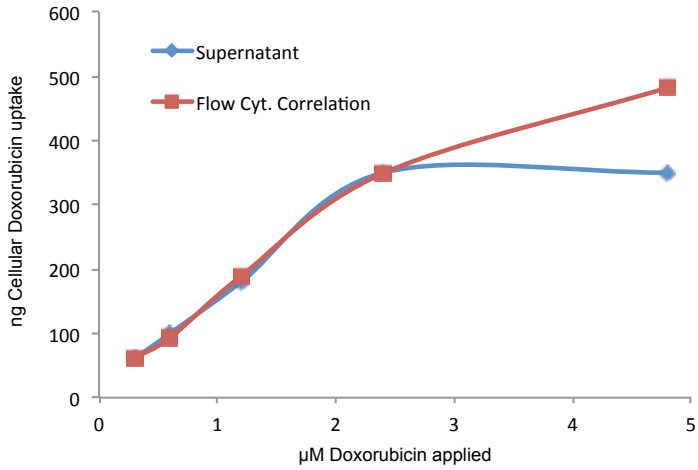

Figure 48: Quantification of cellular doxorubicin uptake and efflux by flow cytometry. To quantify the amount of cell-bound doxorubicin, the fluorescence in the supernatant after 20 min incubation with doxorubicin was measured for each of the applied concentrations and the calculated uptake was correlated with the respective increase of fluorescence measured by flow cytometry. To correct for the increase of total fluorescence due to the increasing background fluorescence of doxorubicin in the sample stream, the geometric mean of Gate 3 was deducted from the geometric mean of Gate 2 (Figure 47).

3.4.2 Small scale screen for inherent fluorescence and drug uptake kinetics

To expand the application area of the developed drug uptake assay, a small library of medically used cytostatic compounds (etoposide, irinotecan, methotrexate, mitoxantrone and topotecan) was screened for possible inherent fluorescence. Three of these compounds possessed an inherent fluorescence measurable in the FACS setup and their respective optimal excitation differed from UV to red light (Table 10).

Table 10: Compound-specific fluorescence characteristics measured by flow cytometry. The table reflects the most common bandpass filter (BP) setups used in FACS with respect to the excitation board available. The specific fluorescence strength of each compound is indicated by – (none), + (measurable), ++ (strong), +++ (very bright) based on the intermediate dose of 1.2 µM.

Excitation (nm)	Emission (nm)	Substances					
		Doxo-rubicin	Etoposide	Irinotecan	Metho-trexate	Mito-xantrone	Topotecan
355 or 405	450/50	-	-	+++	-	-	-
	525/50	-	-	+	-	-	+
	560/40	-	-	-	-	-	+++
	610/20	+	-	-	-	-	+++
488	530/30	-	-	-	-	-	+
	610/20	-	-	-	-	-	-
	670/30	+	-	-	-	+	-
561	586/14	+	-	-	-	-	-
	610/20	+++	-	-	-	-	-
	660/20	++	-	-	-	+	-
	710/50	+	-	-	-	+	-
640	670/30	-	-	-	-	++	-
	710/50	-	-	-	-	++	-
	780/60	-	-	-	-	++	-

Irinotecan is optimally excited with UV and showed a similar quick cellular uptake kinetic as observed for doxorubicin (Figure 49, upper panel). In contrast, mitoxantrone was best excitable with red light and its absorbance into the cell was much slower than seen for doxorubicin or irinotecan (Figure 49, lower panel). Mitoxantrone uptake was still seen even after 15 min of drug application highlighting the feasibility of flow cytometry based kinetic studies to identify small but significant differences in drug uptake.

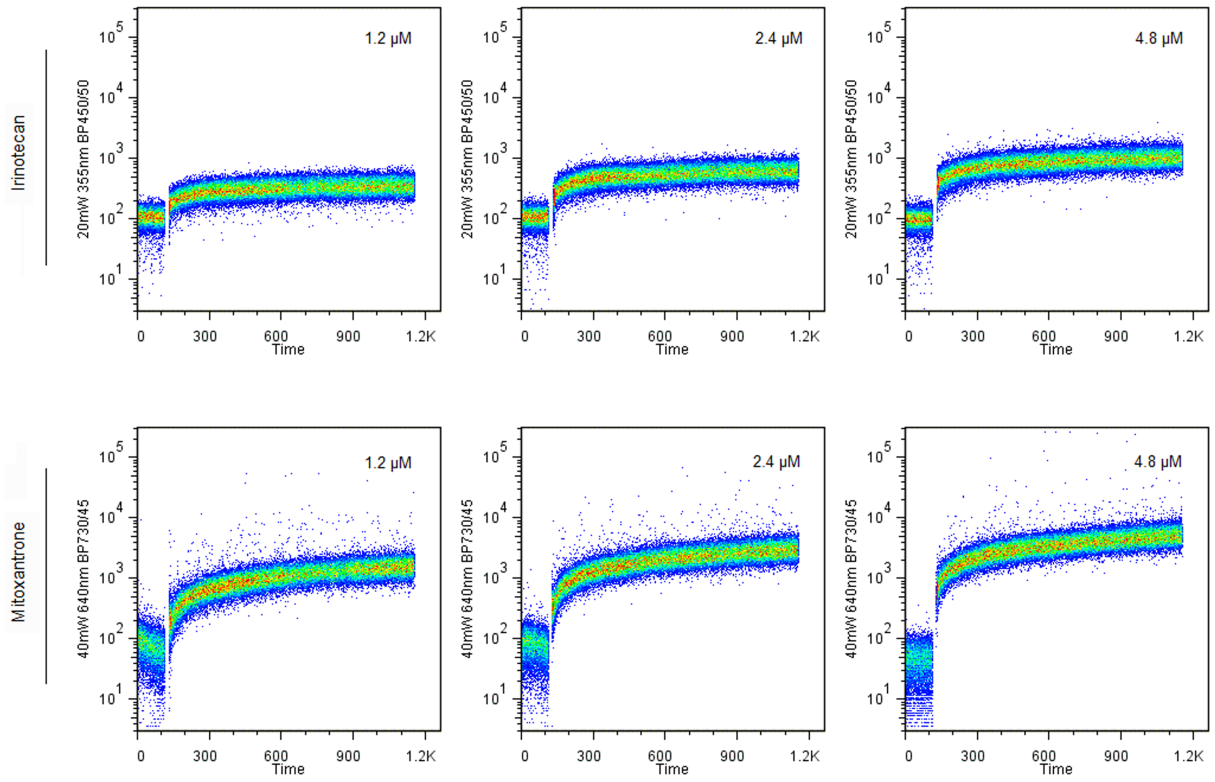

Figure 49: Real-time kinetics and quantification of cellular irinotecan and mitoxantrone uptake by flow cytometry. The inherent fluorescence of irinotecan as excited at 355 nm was best measured in the 450/50 channel. A dose-dependent increase of the cellular irinotecan fluorescence can be observed after treatment with increasing concentrations (1.2, 2.4 and 4.8 µM) of the drug. The inherent fluorescence of mitoxantrone as excited at 640nm was best measured in the 730/45 channel. The cellular fluorescence signal increases with increasing drug concentrations (1.2, 2.4, 4.8 µM) and mitoxantrone showed a much slower saturation kinetic than did irinotecan. All measurements followed the workflow in Figure 46; time is measured in seconds.

3.4.3 Multiplexing live drug uptake and cellular endpoint measurements

Taking advantage of the flexible and high-throughput nature of flow cytometry, the uptake of doxorubicin was coupled with live functional assays based on viable dyes suitable for screening approaches to demonstrate the method's capability to monitor i) drug uptake and ii) detecting its effect on multiple parameters in live samples. To demonstrate this capability, the published knowledge that doxorubicin induces ROS after short term incubation (135) and causes cell cycle arrest at G1 and G2 (136) was used. ROS can be detected in cells by staining them with H_2DCF-DA, which reacts to the fluorescent DCF in the presence of ROS. Cells treated for 3 h with doxorubicin at a final concentration of 4.8 µM robustly report its uptake as well as induction of ROS in the 561nm excited 610/20 channel (Geo-Mean:122) as anticipated, while control cells reported a lower level of ROS (Geo-Mean: 77.2) (Figure 50). The observed induction of ROS is consistent with previously reported results using H_2DCFH-DA in flow cytometry (135).

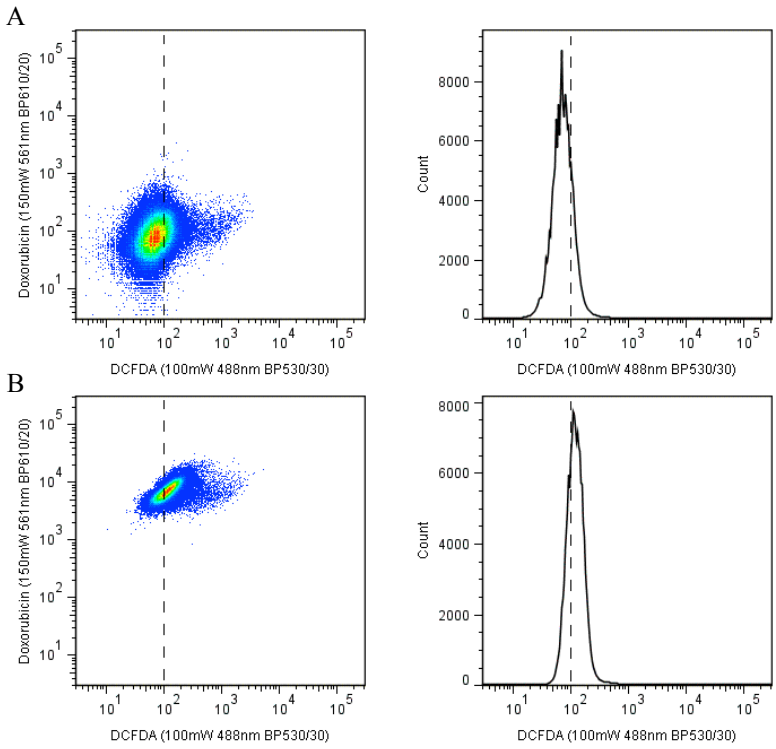

Figure 50: Live Co-measurement of doxorubicin uptake and ROS induction. (A) H_2DCF-DA loaded cells treated with normal media served as an untreated control, and showed no doxorubicin signal in the 561 nm excited 610/20 channel and very little DCF signal in the 488 nm excited 530/30 channel (A, left). The DCF fluorescence signal was plotted as histogram (A, right). (B) After 3h incubation with 4.8 µM doxorubicin, H_2DCF-DA loaded cells showed a strong increase in the doxorubicin signal in the 561nm excited 610/20 channel as well as the DCF signal in the 488nm excited 530/30 channel.

In a next step, the assay was improved by multiplexing the uptake of doxorubicin with three endpoint measurements: cell cycle analysis, live/dead cell ratio determination and the above-described ROS analysis (Figure 51). This provided a suitable live and multi-parametric staining panel useful for initial drug-screenings. The cells were incubated with 0, 0.07, 1.2, or 2.4 µM doxorubicin for 16 h and then stained with commercially available viable dyes. Cells treated with 0.07 µM doxorubicin showed no increased ROS reporter signals (Figure 51 B, left panel), but they did undergo doxorubicin-mediated G2 cell cycle arrest as compared to control cells, which had a very low incidence of cell death (16.1%) (Figure 51 A, right panel). Increasing the dose of doxorubicin to 1.2 µM shifts the cell cycle arrest to the G1 phase and induces a small increase of ROS levels (Figure 51 C). 2.4 µM doxorubicin dosage leads to a strong induction of cell death (40.2%) in the G1 arrested population that is associated with a threefold increase in ROS (combining ROS positive cells in Q2 and Q3, Figure 51 A vs. D). The shift in cell cycle arrest by different doses of doxorubicin is well known (136), but here it was demonstrated that using live-cell flow cytometry with dyes that fluoresce at different wavelengths, it is possible to extract multiple parameters with biological significance from a

single experiment. In addition to acquiring measurements of multiple factors concurrently, this technique also provides direct proof and quantification of the uptake of therapeutic compounds at the single cell level. Thus, the method represents a truly elegant, economic and fast screening tool in working with inherently fluorescent therapeutic compounds.

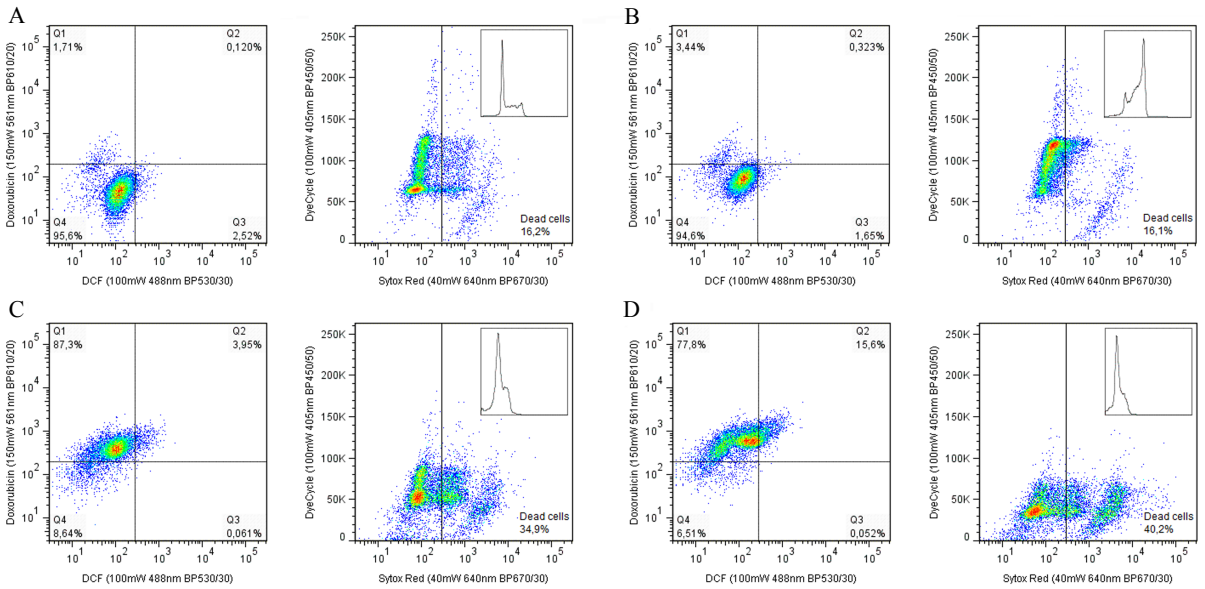

Figure 51: Four-parametric analysis of doxorubicin uptake and treatment using commercially available viable dyes: DyeCycle mapping cell cycle, SytoxRed indicating live/dead ratio, DCF measuring generated ROS. Doxorubicin was applied in the following doses for 16 h as indicated in the respective figure panels: (A) 0, (B) 0.07, (C) 1.2, (D) 2.4 µM. The inlay in each right panel shows the distribution of cells in each stage of the cell cycle in the corresponding plot as a histogram to clearly illustrate the switch in cell-cycle-arrest stage that resulted from increasing doxorubicin doses.

3.4.4 Summary: Drug uptake assay

Here, a drug uptake assay utilizing the intrinsic fluorescence of therapeutics to analyze real-time uptake and multi-parametric effector kinetics was established. Using the natural fluorescence characteristics of the model substance doxorubicin it was shown that the experimental procedure used for shikonin is applicable to other compounds with inherent fluorescence. Real-time kinetics of cellular doxorubicin uptake and efflux were measured by flow cytometry according to the acquired experimental layout. A comparison of the direct measurement of doxorubicin uptake by flow cytometry with the commonly used indirect method showed that the results of both approaches are mostly consistent. To expand the application area of the developed drug uptake assay, a small library of medically used cytostatic compounds were screened for possible inherent fluorescence. Three of the six

tested compounds possessed an inherent fluorescence measurable in the FACS setup and their real-time kinetics of cellular uptake and efflux were measured. In a final step the live drug uptake assay was multiplexed with various additional endpoint measurements including ROS analysis, cell cyle analysis, and determination of live/dead cell ratio. In summary, a flow cytometric assay was established and optimized, that enables a fast and simple screening of pharmaceutical drug uptake and analysis of several additional endpoints, simultaneously.

4 Discussion

4.1 Shikonin directly targets mitochondria and causes mitochondrial dysfunction in cancer cells

Shikonin exhibited a strong cytotoxic effect on a wide variety of cancer cell lines, especially different types of leukemia and several known MDR cell lines. Microarray-based gene expression analysis of U937 leukemia cells suggested that the cytotoxicity of shikonin is based on the disruption of normal mitochondrial function, overproduction of ROS, inhibition of cytoskeleton formation, and finally induction of cell cycle arrest and apoptosis. All of these effects were validated using *in vitro* cell culture experiments exploiting the specific natural fluorescence of shikonin. During this in depth analysis, the primary cellular mechanism of shikonin's cytotoxicity was identified: shikonin immediately accumulates in the mitochondria of cancer cells and disrupts mitochondrial function, as evidenced by the loss of the mitochondrial membrane potential. It was recently shown that shikonin induces ROS and apoptosis in cancer cells (24) and the results of this study fully concur with this assertion. However, other previously described mechanisms of action for shikonin, such as the induction of necroptosis (25), inhibition of topoisomerase II activity (26), down-regulation of NFκB signaling (27), cell cycle arrest through up-regulation of p53 and down-regulation of cyclin-dependent protein kinase 4 (28), inhibition of proteasome function (29), inhibition of tumor necrosis factor alpha (30), deregulation of calcium signaling and microtubule disintegration are actually downstream effects mediated (in most cases) not by a direct interaction of shikonin with the suggested targets, but rather by the direct generation of ROS, the subsequent dysregulation of mitochondria, and induction of oxidative damage.

The activation of the cellular tumor antigen p53 shown by Wu *et al.* (28) is in accordance with the results of the gene expression profiling and the subsequent up-stream regulator analysis, that also predicted an activation of p53. Presumably, the shikonin-induced oxidative DNA damage caused the activation of p53. P53 is a tumor suppressor protein regulating DNA repair, cell cycle, and apoptosis. It becomes activated in response to several stress types including DNA damage, oxidative stress or deregulated oncogene expression (137). *In vivo* studies showed that the activation of the p53 pathway leads to cell cycle arrest, apoptosis, and growth inhibition in cancer cells (104). Therefore, activation of p53 strengthens the potential use of shikonin for cancer treatment. In contrast, the results of the up-stream regulator analysis contradict findings of Cheng *et al*. that indicate a down-regulation of NFκB signaling

after shikonin treatment (27). The protein complex NFκB controls the transcription of DNA and thereby regulates cellular stress and immune responses. An enhanced activation of NFκB was observed in different types of cancer (138). This constitutive NFkB-activation was shown to protect cancer cells against apoptosis (103). Therefore, activation of this pathway after shikonin treatment is presumably a resistance mechanism of U937 cells against cytotoxic drugs.

A recent study showed that shikonin interferes with the energy generation of cancer cells by targeting tumor pyruvate kinase-M2 and inhibiting glycolysis (31). The results of this study confirmed that shikonin treatment causes reduced energy production in cancer cells by affecting the mitochondrial membrane potential, but the observed effects of shikonin on ROS and mitochondrial function are not likely to be purely based on blocking glycolysis. If glycolysis is unable to serve as a source of acetyl-CoA for energy generation, cells can compensate by shift to other metabolic pathways such as fatty acid oxidation (139) or glutamine utilization (140). The obtained data doesn't exclude the possibility that shikonin has an effect on pyruvate kinase-M2, but the direct targeting of mitochondria and the complete loss of the mitochondrial membrane potential as well as the rapid induction of ROS make the electron chain the more likely target of shikonin.

Shikonin can be categorized as a mitocan (141), a class of compounds that act by interfering with energy-generating mitochondrial processes, which in turn leads to ROS accumulation, mitochondrial destabilization and induction of apoptosis (50). Shikonin itself is a naphthoquinone derivative, and various substituted naphthoquinones have been shown to be capable of redox cycling in isolated mitochondria (106). During this process, reductive enzymes, e.g. mitochondrial NADH-ubiquinone oxidoreductase (complex 1), metabolize quinones to unstable semiquinones through one-electron reduction reactions (142). When molecular oxygen is present, such semiquinones enter into a redox cycle leading to reformation of the original quinone, with the associated generation of reactive oxygen species. Ultimately, this cycle results in excessive ROS accumulation, depolarization of the mitochondrial membrane and induction of apoptosis (143). Figure 52 displays the redox cycling reaction of shikonin in mitochondria.

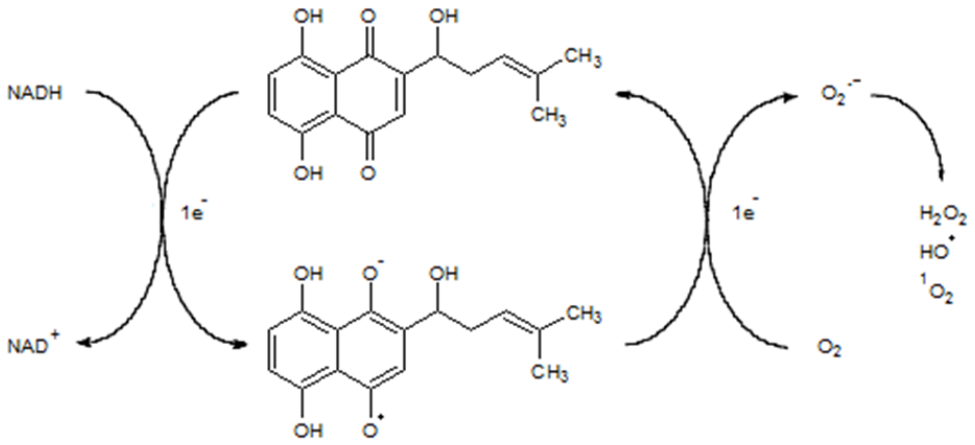

Figure 52: Redox cycling of shikonin initiated by a one electron reduction. During this reaction NADH serves as electron donor and shikonin is reduced to a semiquinone. In a subsequent reaction with oxygen the semiquinone is oxidized to shikonin resulting in the concomitant production of a superoxide radical anion that further reacts to H_2O_2. Image modified from Gutierrez (144).

Using a well established *in vitro* assay for testing the capacity of redox cycling, it was shown that a futile mitochondrial redox cycling is indeed the cellular mechanism by which shikonin induces ROS. The elevated levels of ROS strain the mitochondria, leading to a breakdown of the mitochondrial membrane potential and finally to the release of pro-apoptotic compounds and thus the activation of caspases involved in the intrinsic pathway of apoptosis. The oxidative DNA damage detected is also a consequence of the elevated ROS production, and could likely be the trigger of the observed cell cycle arrest (145).

Besides inducing ROS, some quinones have been shown to cause release of calcium from isolated mitochondria (106). This is consistent with the elevated levels of $[Ca^{2+}]_I$ observed after shikonin treatment. In contrast to ionomycin, shikonin caused a slow and continuous increase in intracellular calcium concentrations. This suggests that shikonin doesn't shuttle extracellular or intracellular stored calcium actively or triggers fast calcium-channels, but rather causes a calcium release from calcium stores or other organelles, e.g. mitochondria, by an indirect mode such as via ROS signaling pathway (44). Nevertheless, elevated levels of $[Ca^{2+}]_I$ and ROS together appreciably disturb normal calcium signaling (44). Increased calcium levels promote the disassembly of microtubules by direct destabilization of growing microtubule ends (118), which is in accordance with the findings that shikonin inhibits cancer cell migration by the disruption of microtubule cytoskeleton dynamics (see 3.1.9). Indeed, shikonin treatment results in a complete inhibition of EB3 protein dynamics and a loss of distinct microtubule filaments, suggesting that the ATP shortage and deregulation of calcium

levels are dually destructive. These findings motivate further investigations on the effect of shikonin in the treatment of highly invasive cancer types.

Many established anticancer agents affect upstream signaling pathways that ultimately converge on mitochondria as regulators of cell death and survival (146). These signaling pathways are often deregulated in human cancers, and for this reason many MDR phenotypes are resistant to classical anticancer agents (3). Compounds that directly target mitochondria can bypass deregulated upstream signaling events and thereby circumvent the resistance mechanisms of cancer cells (43). However, due to its basic mode of action, it is likely that shikonin also has an effect on non-cancer cells and the mode of delivery needs to confer specificity. Yet, shikonin bypasses resistances of known MDR cell types and this makes further research on better and more direct application methods an interesting project. Numerous animal studies showed that the therapeutic effects of shikonin apparently outweigh the side effects (21, 108) and a clinical trial with shikonin showed that it can be utilized in therapy (23). Future studies should concentrate on the reduction of side effects by chemical derivatization or tissue targeted application.

In summary, our results indicate that shikonin accumulates in the mitochondria of cancer cells, disrupts mitochondrial function and finally causes apoptosis. As mitochondria generate the majority of the cellular ATP supply and also regulate the cell death machinery, they are promising targets for cancer therapy. Hence, shikonin may have potential for cancer treatment as part of a poly-drug approach within classic chemotherapy.

4.2 Integration of *omics* technologies identifies inhibition of IGF1R-Akt-mTOR signaling involved in the cytotoxicity of shikonin against leukemia cells

As discussed in the previous chapter, targeting of mitochondria is the basal cellular mechanism of shikonin, which is primarily responsible for the induction of apoptosis in cancer cells. However, the particular activity of shikonin against leukemia cells indicated a secondary mechanism of shikonin in these cells, which reinforces its cytotoxic effect. Therefore, a comparative approach of different quantitative *omics* technologies was undertaken to identify additional effects of shikonin in leukemia cells. The combination of *omics* data is a powerful tool to investigate the cellular effects and mechanisms of small molecules (122). In the present study, the experimental approach was used to show that the natural naphthoquinone shikonin strongly affects the IGF1R-Akt-mTOR signaling cascade in

U937 myeloide leukemia cells. Three different *omics* assays indicated that the signaling pathway is disturbed at transcriptomic and proteomic level. Functional validation studies showed that shikonin indeed inhibits two central signaling nodes of the pathway: the kinase activity of IGF1R (a central receptor of the signaling cascade) was inhibited and in addition the phosphorylation of Akt was significantly decreased upon shikonin application.

The signaling network around the mTOR kinase has been shown to be frequently deregulated in a wide range of hematological malignancies, especially in different types of leukemia (61). For example, in acute myelogenous leukemia (AML) the mTORC1-signaling pathway is constitutively activated in almost 100% of all patients (147, 148). Blocking this pathway might be an effective new treatment strategy for leukemia and other hematological malignancies. At the moment, rapamycin and its derivatives (rapalogs), e.g. RAD001 (everolimus), CCI-779 (temsirolimus) and AP23573 (deforolimus), are used to partially inhibit the signaling pathway by direct binding to the mTORC1 complex (65, 66). However, results of respective clinical trials were mostly disappointing and showed only modest anti-cancer effects of the drugs (61). A combination of rapalogs with other targeted molecules was more successful and clinical trials have shown that rapalogs synergize with different conventional chemotherapeutics to overcome resistance (61, 149, 150). Recent findings indicated that a positive feedback loop is responsible for the rapamycin-resistance phenotype: mTOR inhibition by rapalogs leads to an up-regulation of IGF1R signaling, which in turn activates the PI3K-Akt-mTOR cascade again (67-69). Thus, combining an mTOR inhibitor and an IGF-1R inhibitor may be an appropriate strategy to enhance mTOR-targeted anticancer therapy (69). Since shikonin strongly deregulates the mTOR signaling pathway and in addition also directly inhibits the kinase activity of IGF1R, it is a promising candidate for a co-treatment with rapalogs.

Our results are consistent with recent findings indicating that shikonin also modulates cell proliferation by inhibiting EGFR signaling (124). EGFR is a further RTK that triggers the PI3K-Akt-mTOR cascade. Results showed that simultaneous targeting of EGFR and mTOR inhibits the growth of cancer cells (151). An additional inhibition of EGFR signaling makes shikonin even more valuable for targeting the PI3K-Akt-mTOR cascade since a second important starting point of the pathway is eliminated.

Nevertheless, deregulation of the PI3K-Akt-mTOR signaling cascade is only a secondary mechanism of shikonin that strengthens its cytotoxic effect against leukemia cells. The basal mode of action of shikonin is direct targeting of mitochondria and subsequent induction of

apoptosis. Mitochondria-targeting drugs were suggested to synergize with the common and clinically established antileukemic drug arsenite trioxide (152). This makes shikonin even more interesting for the treatment of leukemia. On the one hand it is directly targeting mitochondria of cancer cells, and in addition it inhibits the PI3K-Akt-mTOR signaling cascade, which is frequently deregulated in leukemia, what makes shikonin to a promising candidate for a combined treatment with established anti-leukemic drugs.

Ultimately, the direct targeting of mitochondria and the simultaneous deregulation of the IGF1R-Akt-mTOR signaling cascade make shikonin a promising compound for the treatment of hematological malignancies.

4.3 Effect of shikonin against cancer stem cells

Chemotherapy-resistant cancer stem cells are a major cause for a relapse of a malignant disease after an initial therapy success (77). New experimental therapeutics should be tested for their activity against this certain kind of cancer cell population. Routinely, many therapeutic compounds are screened for targeting bulk cancer cells and the primary end point assessed in most clinical studies is reduction of tumor volume. In order to detect the effect of compounds on cancer stem cells, it is necessary to perform several assays including high throughput FACS analysis to measure changes in the $CD44^{+}/CD24^{-/low}$ cell population, as well as *in vitro* mammosphere formation assays depending on the self-renewal and anchorage-independent growth properties of these cells (153). Here, both approaches were used to analyze the effect of the natural compound shikonin against CSCs.

In a first step, a prolonged mammosphere culture of MCF-7 cells was established according to a recently published protocol (128). Culturing breast cancer cells as mammospheres under non-adherent and serum-free conditions increased the number of $CD44^{+}/CD24^{-/low}$ CSCs drastically. After five weeks of mammosphere culture and one subsequent week under normal culture conditions, the highest enrichment of CSCs in the MCF-7 cell population was reached. More than half of all cells showed a $CD44^{+}/CD24^{-/low}$ phenotype. Cells at this stage were used for cytotoxicity testing of shikonin and docetaxel. In comparison to normal MCF-7 cells the CSC-enriched population showed a 2-fold degree of resistance to shikonin. Nevertheless, at a shikonin concentration of 12.5 µM all cells of the CSC-enrich MCF-7 cell population were killed, indicating that slightly increased shikonin concentrations are effective against CSCs. In contrast, the CSC-enrich cell line showed a 10-fold increased resistance to the anti-mitotic

drug docetaxel. The clinical profile of docetaxel as an effective cytotoxic agent in the treatment of metastatic breast cancer is well established (154). However, even at docetaxel concentrations 18-fold higher than the IC50 of normal MCF-7 cells, more than 40% of the CSC-enriched cells remained vital. Other studies confirm this distinct resistance of CSCs against common cytostatic drugs. For example, MCF-7 cells cultured as mammospheres showed a strong resistance to tamoxifen (128) and doxorubicin (129). This indicates that shikonin – despite a certain degree of resistance – is much more effective against CSCs within a MCF-7 cell population than clinically well-established drugs.

Recently, it was shown that standard chemotherapy treatment increased the percentage of $CD44^+/CD24^{-/low}$ cells in tumors of breast cancer patients significantly (155). To further investigate the resistance of CSCs to shikonin, MCF-7 cells were treated with shikonin and the percentage of $CD44^+/CD24^{-/low}$ cells was analyzed. After 24 h, shikonin treatment caused no significant change in the population distribution of MCF-7 cells, but after 48 h the cytotoxic selection pressure of shikonin led to an enrichment of CSCs in the surviving MCF-7 cell population. This is in accordance with the results of the mammosphere assays indicating that CSCs are able to resist the cytotoxic effect of shikonin to a certain degree. Simultaneously to the analysis of the CD44/CD24 phenotype, a measurement of the shikonin content in different MCF-7 cell populations was performed. Results showed that in $CD44^+/CD24^{-/low}$ cells the shikonin content is significantly lower than in $CD44^-/CD24^+$ cells (anti-CSCs) after 24 and 48 h, whereas directly after substance injection both populations showed the same level of intracellular shikonin. Therefore it was proposed that an increased efflux of shikonin out of the cell or an increased metabolism of shikonin reduced the intracellular concentration of the drug in CSCs. A well-known resistance mechanism of CSCs is the overexpression of ABC-transporters that shield them from chemotherapeutic insult (89). Since MDR1 (ABCB1), MRP1 (ABCC1) and BCRP overexpressing cell lines showed no or negligible resistance against shikonin in comparison to their sensitive counterparts, it was excluded that these transporters play a key role in shikonin resistance. A further important ABC-transporter that protects CSCs from cytotoxic drugs is the ABCB5 transporter. Expression of human ABCB5 confers resistance to taxanes and anthracyclines (132). In melanoma, ABCB5 serves as marker for CSCs and its expression correlates with clinical progression (156, 157). In the context of breast cancer, it was shown that ABCB5 is up-regulated in MCF-7 cell populations resistant to doxorubicin (158). Therefore, it was suggested that ABCB5 expression plays in a role in the resistance of CSCs against shikonin. To test this, HEK293 cells transfected with an ABCB5-plasmid and their sensitive

counterparts were treated with shikonin. The ABCB5 overexpressing cells showed a 3- to 5-fold increased resistance to shikonin depending on the incubation time. This strongly suggested that shikonin is a substrate of the ABCB5 transporter and that overexpression of ABCB5 is a possible resistance mechanism of CSCs against shikonin.

Nevertheless, shikonin showed better results against CSC-enriched breast cancer cells than docetaxel. One possible reason could be its inhibitory effect on the mTOR signaling pathway. Recent studies showed that the activation of the mTOR signaling cascade is critical for the survival and proliferation of breast cancer stem cells (159). In pancreatic cancer, a combination treatment of mTOR inhibitors, hedgehog inhibitors and standard chemotherapy reduced the number of CSCs to virtually undetectable levels *in vitro* and *in vivo* (160). Due to the critical role of mTOR signaling in the survival and proliferation of CSCs, it is conceivable that a combination of shikonin and other targeted therapeutics could be effective against this cell population. Since ABCB5 overexpression can attenuate the effects of shikonin, a combination with inhibitors of this transporter should also be considered in future studies.

4.4 Establishment of an flow cytometric assay to analyze real-time uptake and multi-parametric effector kinetics of therapeutics

Analyzing drug uptake based on the frequently observed inherent fluorescence of pharmaceutical compounds by flow cytometry exhibits several analytical advantages. Cytometry couples directly measured, quantifiable data acquisition with a high temporal resolution based on continuous randomized sampling of an adjustable percentage of the respective specimen. The resulting real-time kinetic data of drug uptake can be used to compare the specificity of drug delivery, membrane permeability, accumulation and efflux of different compounds. Therefore, a simple and fast screening of important characteristics of new drugs is possible and furthermore, the assay can be performed on nearly all cell types and thus allows for example the comparison of drug effects on cancer versus normal or resistant versus sensitive cell lines in a high-throughput system. In addition, the resulting kinetic data of drug uptake can be used to compare the effects of modifying compounds to improve or negatively influence their cell permeability to generate a higher specificity of drug application and delivery independent of antibody carriers or nanoparticle vehicles (161).

Using the natural fluorescence characteristics of doxorubicin along with functional viable dyes it was demonstrated that live-monitoring of multiple downstream drug effects by multi-

parametric flow cytometry is easily performed. The approach can be readily used to perform high-throughput screens, directly correlating drug uptake efficiency with drug efficacy (99) and thereby rationalizing the usually tedious workflow of cytotoxicity screening. Additionally, this flow-based analysis can be either focused or expanded in analytical depth due to the plethora of different reporter systems available, for example signaling processes (162), DNA damage (163, 164), and cell death and apoptosis (165). Using – if available – natural fluorescence in analytical assays circumvents the necessity of indirect reporter assays with artificial 'drug-like' fluorescent probes or specially-tailored cell models (166) indirectly reporting drug properties that could be substantially different from the natural product.

Multi-parametric screening of drug effects using flow cytometry is broadly employed in research; yet, combining these screening approaches with the inherent fluorescence of pharmaceutical compounds has discrete analytical advantages. In case inherent drug fluorescence is observed, the combination of flow-cytometrically measured kinetic data and drug efficacy for inherently fluorescent drugs provides researchers with even more significant and quantitative biological data. Taken together, the high-parametric and flexible screening approach by flow cytometry is superior to the standard laborious cell culture-based 'cytotox' screening approaches using XTT or MTT to monitor viability or other single-parametric and population based screening platforms (99).

A further application of the flow-based performance analysis of inherently fluorescent drugs is the screening and identification of compounds inhibiting resistance mechanisms for MDR. Indeed, such resistance mechanisms represent a major challenge to the targeted treatment of diseases; for example antibiotic resistant bacteria (e.g. EHEC), malaria or even more pressing cancer (167-169). Along these lines and since flow cytometry is already one of the key diagnostic methods in clinical workflows (170), the use of inherent compound fluorescence could be well extended to antibiotics in general. Many antibiotics are fluorescent (171) and it would be fairly easy to screen bacterial, protozal or fungal patient samples for an abnormal reduction of intracellular fluorescence indicating a resistance mechanism aiding the process of precise and functional medication of a patient. Again, this approach could also be exploited in large scale pharmaceutical research identifying new antibiotics to fight the upcoming shortage of reliable antibiotics (167).

5 Summary and Conclusion

In this study, the primary mode of action that underlies the anti-cancer effects of shikonin was identified. Shikonin directly targeted mitochondria of cancer cells and the mitochondrial drug accumulation was associated with a shikonin-dependent deregulation of cellular Ca^{2+} and ROS levels. This deregulation led to a breakdown of the mitochondrial membrane potential, dysfunction of microtubules, cell cycle arrest and ultimately induction of the mitochondrial pathway of apoptosis. Seeing as both the metabolism and the structure of mitochondria show marked differences between cancer cells and normal cells, shikonin is a promising candidate for the next generation of chemotherapy.

In addition, cytotoxicity screenings showed that shikonin is particularly effective against sensitive and resistant leukemia and lymphoma cell lines suggesting an additional cellular mechanism of action of shikonin. The integration of bioinformatics and three *omics* assays showed that the strongly cross-linked PI3K-Akt-mTOR axis was intensely affected by shikonin. This signaling pathway plays a critical role in cellular growth control and survival. The effect of shikonin on the PI3K-Akt-mTOR signaling cascade was functionally validated by demonstrating a decreased phosphorylation and activation of Akt after shikonin treatment. Kinase activity tests revealed that shikonin inhibits the kinase activity of IGF1R, which is an important trigger of the PI3K-Akt-mTOR signaling cascade. Since mTOR signaling is constitutively activated especially in hematological malignancies, this could explain the outstanding effect of shikonin against leukemia and lymphoma cells. The results indicate that inhibiting the IGF1R-Akt-mTOR signaling cascade is a new cellular mechanism of shikonin strengthening its potential for the treatment of hematological malignancies.

To further complete the picture of the anti-cancer activities of shikonin, its effect against CSCs was tested. A prolonged mammosphere culture of MCF-7 breast cancer cells was established and cytotoxicity tests showed that a CSC enriched cell population exhibits slightly increased resistance to shikonin. Nevertheless, the clinically established drug docetaxel was much less active against CSCs than shikonin. Analysis of changes in the $CD44^{+}/CD24^{-/low}$ cell population confirmed the resistance of CSCs to shikonin and uptake measurements showed that the intracellular shikonin concentration in this cell type is decreased in comparison to other subpopulations. It was shown that at least to some extent the ABCB5 transporter is responsible for the increased transport of shikonin out of the cells and for the resistance of CSCs to shikonin. Nevertheless, shikonin showed better results against CSCs than clinically used chemotherapeutics.

In an additional project, the gained experience with the experimental use of shikonin's inherent fluorescence was used to develop an assay utilizing the intrinsic fluorescence of therapeutics to analyze real-time uptake and multi-parametric effector kinetics. Many pharmaceutical drugs have a distinct natural fluorescence that can be readily exploited for research purpose. Utilizing this respective fluorescence, a method was established analyzing simultaneously in real-time the efficiency, effects and the associated kinetics of compound uptake and efflux in mammalian cells by flow cytometry. Furthermore, the uptake measurements were coupled with various live dye-based multi-parametric screenings of pharmaceutical compound activity. The precise detection of pharmaceutical drug uptake and knowledge of a drug's efficacy at single-cell level are crucial for understanding a compound's performance. Therefore, the established experimental approach enables a simple and fast screening of important characteristics of new drugs and it is applicable in multiple research areas, e.g. cytotoxicity screenings or examination of MDR mechanisms.

6 Material and Methods

6.1 Chemicals and equipment

Shikonin

Shikonin was purchased from Enzo Life Sciences (Lausen, Switzerland) and a 50 mM stock solution was prepared by dissolving it in DMSO. The shikonin solution was stored in aliquots of 10 µl at -20°C for up to 3 months. Freeze/thaw-cycles of dissolved shikonin were avoided.

Chemotherapeutics

Doxorubicin and daunorubicin were provided by the University Medical Center of the Johannes Gutenberg University (Mainz, Germany) and dissolved in DPBS at a concentration of 10 mM. Both chemotherapeutics were stored in the dark at 4 °C for a maximum of 4 weeks.

Etoposide, irinotecan, methotrexate, mitoxantrone and topotecan were also provided by the University Medical Center of the Johannes Gutenberg University. The drugs were dissolved in DPBS at concentration of 100 µM and stored in the dark at 4 °C for a maximum of 3 days.

Cell culture media, reagents and disposable material

Table 11: Cell culture media, reagents and disposables

Compound	Producer
12-well cell culture microplate, clear, Nunclon®	Thermo Scientific, Germany
24-well cell culture microplate, clear, Nunclon®	Thermo Scientific, Germany
6-well cell culture microplate, clear, Nunclon®	Thermo Scientific, Germany
96-well cell culture microplate, clear, Nunclon®	Thermo Scientific, Germany
96-well cell culture microplate, white, Nunclon®	Thermo Scientific, Germany
B27 supplement	Invitrogen, Germany
Cell culture flasks (25 cm^2), Nunclon®	Thermo Scientific, Germany
Cell culture flasks (75 cm^2), Nunclon®	Thermo Scientific, Germany
Centrifuge tube (15 ml)	Sarstedt, Germany
Centrifuge tube (50 ml)	Sarstedt, Germany
Daunorubicin	JGU Medical Center, Germany
DMEM, High Glucose, GlutaMAX™, Pyruvate	Invitrogen, Germany

DMEM/F-12, GlutaMAX™	Invitrogen, Germany
Doxorubicin	JGU Medical Center, Germany
DPBS, no calcium, no magnesium	Invitrogen, Germany
Epidermal growth factor (recombinant human protein)	Invitrogen, Germany
FACS test tube	Becton-Dickinson, USA
FACS test tube with cell strainer cap	Becton-Dickinson, USA
Fetal Bovine Serum (FBS), Qualified, E.U. Approved, South America Origin	Invitrogen, Germany
Fibroblast growth factor	Invitrogen, Germany
Geneticin	Sigma-Aldrich, Germany
IbiTreat µ-slides	Ibidi, Germany
Penicillin (10000 U/ml)-streptomycin (10000 µg/ml)	Invitrogen, Germany
Poly(2-hydroxyethyl methacrylate)	Sigma-Aldrich, Germany
RPMI 1640 Medium	Invitrogen, Germany
RPMI 1640 Medium, no Phenol Red	Invitrogen, Germany
Trypsin-EDTA 0.25% (1X), Phenol Red	Invitrogen, Germany
Zeocin	Invivogen, USA, CA

Chemicals, dyes, antibodies, enzymes and commercial kits for molecular biology

Table 12: Chemicals, dyes, antibodies, enzymes and commercial kits for molecular biology

Compound	Producer
^{33}PanQinase® Activity Assay	ProQinase GmbH, Germany
4-(2-hydroxyethyl)-1-piperazineethanesulfonic acid (HEPES)	Sigma-Aldrich, USA, MO
40% acrylamide/bis-acrylamide (37.5:1) solution	Sigma-Aldrich, USA, MO
acetonitrile (ACN)	J. T. Baker, USA, NJ
Ammonium hydroxide	Sigma-Aldrich, USA, MO
Ammonium persulfate (APS)	Sigma-Aldrich, USA, MO
Biotin-16-UTP	Roche, Germany
Bovine beta casein	Sigma-Aldrich, USA, MO
Bovine serum albumin (BSA)	Sigma-Aldrich, USA, MO
Caspase-Glo® 3/7 Assay Kit	Promega, Germany
Caspase-Glo® 3/7 Assay Kit	Promega, Germany
Dimethyl sulfoxide (DMSO)	Sigma-Aldrich, Germany
DTT	Sigma-Aldrich, Germany
Ethanol (EtOH)	Sigma-Aldrich, Germany
FITC mouse anti-human CD24 antibody	Becton-Dickinson, USA
FlowCellect™ PI3K-mTOR signaling kit	Millipore, Germany
Formaldehyde (37% solution in H_2O)	Sigma-Aldrich, USA, MO
Formaldehyde-13C, d2 (20% solution in D_2O)	Sigma-Aldrich, USA, MO
Formic acid (FA)	Sigma-Aldrich, USA, MO
Fpg protein	Sigma-Aldrich, Germany

H_2DCFH-DA	Sigma-Aldrich, Germany
HBSS buffer	Invitrogen, Germany
Horseradish peroxidase	Sigma-Aldrich, Germany
Illumina® TotalPrep™ RNA Amplification Kit	Life Technologies, Germany
Indo-1	Invitrogen, Germany
Ionomycin	Sigma-Aldrich, Germany
JC-1	Biomol, Germany
M-PER Mammalian Protein Extraction Reagent	Thermo Scientific, Germany
MessageAmp™ II aRNA Amplification Kit	Life Technologies, Germany
Methanol	J. T. Baker, USA, NJ
Methyl methanethiosulfonate (MMTS)	Sigma-Aldrich, USA, MO
miRNA Complete Labeling and Hyb Kit	Agilent Technologies, Germany
miRNeasy Kit	Qiagen, Germany
MitoTracker Green FM	Invitrogen, Germany
Tetramethylethylenediamine (TEMED)	Sigma-Aldrich, USA, MO
PE mouse anti-human CD44 antibody	Becton-Dickinson, USA
Phenol red	Sigma-Aldrich, Germany
Polyethylenimine	Sigma-Aldrich, Germany
Propidium iodide (PI)	Sigma-Aldrich, Germany
Protease inhibitor cocktail	Roche, Switzerland
Resazurin	Sigma-Aldrich, Germany
RevertAid H Minus Reverse Transcriptase	Thermo Scientific, Germany
RNase A	Applichem Lifescience, Germany
Rneasy Kit	Qiagen, Germany
Small RNA Nano chip assay	Agilent Technologies, Germany
Sodium bicarbonate	Sigma-Aldrich, USA, MO
Sodium cyanoborohydride	Sigma-Aldrich, USA, MO
Sodium dodecyl sulfate (SDS)	J. T. Baker, USA, NJ
Sodium hydroxide (NaOH)	Sigma-Aldrich, Germany
SYBR Green	Biozol, Germany
Sytox® Red	Life Technologies, Germany
Taq-polymerase master mix	Roche, Switzerland
Total RNA Nano chip assay	Agilent Technologies, Germany
Total RNA Nano chip assay	Agilent Technologies, Germany
Triethylammonium bicarbonate (TEABC)	Sigma-Aldrich, USA, MO
Trifluoroacetic acid (TFA)	Sigma-Aldrich, USA, MO
Tris(2-carboxyethyl)phosphine (TCEP)	Sigma-Aldrich, USA, MO
Triton X-100	Sigma-Aldrich, USA, MO
Trypsin (modified, sequencing grade)	Promega, USA, WI
Vybrant DyeCycle^{TM} Violet Stain	Life Technologies, Germany

Technical equipment and special software

Table 13: Technical equipment and special software

Device	Producer
Adobe photoshop	Adobe Systems, USA
Agilent 2100 Bioanalyzer	Agilent Technologies GmbH, Germany
Agilent Feature Extraction Software	Agilent Technologies GmbH, Germany
Agilent Microarray Scanning system	Agilent Technologies GmbH, Germany
AutoDock 4.2 software	Molecular Graphics Laboratory, USA, CA
AutoDock Tools software	Molecular Graphics Laboratory, USA, CA
AutoDock Vina software	Molecular Graphics Laboratory, USA, CA
AutoGrid 4 software	Molecular Graphics Laboratory, USA, CA
Beckman Coulter Biomek 2000/SL robotic system	Beckman Coulter, USA
Centrifuge 5424	Eppendorf, Germany
CFX384™ Real-Time PCR Detection System	Bio-Rad, Germany
Chipster data analysis platform	CSC, Finland
Coulter Counter Z1	Beckman Coulter, Germany
FACS Calibur flow cytometer	Becton-Dickinson, USA
FlowJo software	Celeza, Switzerland
Fluorolog-2 spectrofluorometer	Horiba, Germany
GraphPad Prism 5.04 software	GraphPad Software, USA
Human miRNA microarray chips (8x60K)	Agilent Technologies GmbH, Germany
IKA RH basic 2 magnetic stirrer	IKA, Germany
Illumina Human Sentrix-HT12 Bead Chip arrays	Illumina, CA, USA
Illumina BeadStation	Illumina, CA, USA
Infinite M2000 Pro™ plate reader	Tecan, Germany
Ingenuity Pathway Analysis	Ingenuity Systems, USA
Labofuge 400R centrifuge	Thermo Scientific, Germany
LAS AF software	Leica, Germany
Leica TCS SP5 confocal microscope	Leica, Germany
LSR-Fortessa FACS analyzer	Becton-Dickinson, USA
Maxisafe 2020 laminar flow hood	Thermo Scientific, Germany
Milli-Q ultrapure water purification system	Millipore, Germany
Minicentrifuge	Labnet, Germany
NanoDrop 2000 UV-Vis spectrophotometer	Thermo Scientific, Germany
NanoDrop 2000 UV-Vis spectrophotometer	Thermo Scientific, Germany
Phase contrast microscope	Optika, Italy
PowerShot G5 digital camera	Canon, Japan
Reax 2000 vortexer	Heidolph, Germany
Steri-Cult 3310 CO_2-Incubator	Thermo Scientific, Germany
Sub Aqua 26 waterbath	Grant Scientific, Germany

Thermomixer comfort	Eppendorf, Germany
Tscratch software	CSE lab, ETH, Switzerland
Wallac MicroBeta scintillation counter	Perkin-Elmer, USA

6.2 Cell culture

All cell lines were maintained in a humidified environment at 37°C with 5% CO_2 and sub-cultured twice per week. Adherent cells were detached by the use of 0.25% trypsin/EDTA solution (Invitrogen). All experiments were performed on cells in the logarithmic growth phase.

6.2.1 Cancer cell lines

Leukemia cell lines

U937 cells were obtained from the German Cancer Research Center (DKFZ, Heidelberg, Germany). The original source of these cell lines is the American Type Culture Collection (ATCC, USA). The cells were maintained in complete RPMI 1640 medium with 2 mM L-glutamine (Invitrogen) supplemented with 10% FBS (Invitrogen) and 1% penicillin (100 U/ml)-streptomycin (100 µg/ml) (Invitrogen).

CCRF-CEM and CEM/ADR5000 cells were obtained from the University of Jena (Department of Pediatrics, Jena, Germany). Cells were cultured in complete RPMI 1640 medium with 10% FBS and 1% penicillin (100 U/ml)-streptomycin (100 µg/ml). To maintain the multidrug-resistance phenotype, the MDR1-expressing CEM/ADR5000 cells were treated with 5000 ng/ml doxorubicin. The multidrug resistance profile of these cell lines has been reported (172).

HL-60 and HL60/AR cells were obtained from the (University of Greifswald, Department of Pediatrics, Greifswald, Germany). Cells were cultured in complete RPMI 1640 medium with 10% FBS and 1% penicillin (100 U/ml)-streptomycin (100 µg/ml). To maintain the multidrug-resistance phenotype, the MRP1-expressing HL-60/AR subline was cultured in medium containing 100 nM daunorubicin. The multidrug resistance profile of these cell lines has been reported (100).

Breast cancer cell lines

MCF-7 and SK-BR-3 cell lines were obtained from the DKFZ (original source: ATCC). Both cell lines were maintained in complete DMEM culture medium with GlutaMAX™ (Invitrogen) supplemented with 10% FBS and 1% penicillin (100 U/ml)-streptomycin (100 µg/ml).

MDA MB 231 pcDNA3 and MDA MB 231 BCRP breast cancer cell lines transduced with control vector (MDA-MB-231-pcDNA3) or with cDNA for the breast cancer resistant protein BCRP (MDA-MB-231-BCRP clone 23) were obtained from the University of Maryland (Department of Medicine, Baltimore, Maryland). Both cell lines were continuously treated with 800 ng/ml geneticin (Sigma-Aldrich). The multidrug resistance profile of these cell lines has been reported (100).

Kidney cancer cell line

789-O cells were obtained from the DKFZ (original source: ATCC). Cells were maintained in complete RPMI 1640 medium with 2 mM L-glutamine supplemented with 10% FBS and 1% penicillin (100 U/ml)-streptomycin (100 µg/ml).

Colorectal carcinoma cell lines

SW1116, HCT-116, SW680, Capan1 and SUIT-2 cell lines were obtained from the DKFZ (original source: ATCC). All cell lines cells were maintained in complete DMEM culture medium with GlutaMAX™ supplemented with 10% FBS and 1% penicillin (100 U/ml)-streptomycin (100 µg/ml).

6.2.2 GFP-transfected cell lines

The human osteosarcoma cell line U2OS is stably transfected with a GFP fusion construct of α-tubulin. The cell line was obtained from the ETH Zurich (Light Microscopy Centre). Retinal pigment epithelial (RPE-1) cells stably expressing GFP-EB3 were also obtained from the ETH Zurich (115). U2OS-GFP-αTubulin and RPE-1-GFP-EB3 cells were maintained in DMEM medium containing 10% FBS and 1% penicillin (100 U/ml)-streptomycin (100 µg/ml) and were continuously treated with 250 µg/ml and 500 µg/ml geneticin, respectively.

6.2.3 ABCB5 transfected cell lines

HEK293 cells are human embryonic kidney cells transformed by DNA from human adenovirus type 5 (173). HEK293 cells and HEK293 cells transfected with the pCAL-MycABCB5-IRES-Zeo plasmid were obtained from the Keio University (Faculty of Pharmacy, Tokyo, Japan). The transfection protocol for the ABCB5 plasmid was published by Kawanobe *et al.* (132). Both cell lines were maintained in DMEM medium containing 10% FBS and 1% penicillin (100 U/ml)-streptomycin (100 µg/ml). The transfected HEK293 cells were continuously treated with 50 µg/ml zeocin (Invivogen).

6.2.4 Mammosphere formation

To form MCF-7 mammospheres, cells were plated in 25 cm^2 culture flasks coated with 20 mg/ml polyHEMA (Sigma) at a density of $2x10^5$ cells/ml in DMEM/F12 medium supplemented with fibroblast growth factor (10 ng/mL), epidermal growth factor (10 ng/mL), B27 supplement (100 units/mL), penicillin (100 units/mL), and streptomycin (100 µg/mL) (all from Invitrogen). After culturing for one week, spheres were visible by inverted phase-contrast microscopy, and these spheres were defined as mammospheres in passage 1 (MS P1). Prolonged mammosphere culture was achieved using weekly trypsinization and dissociation with a cell strainer followed by reseeding in mammosphere medium into polyHEMA treated culture flasks. Each generation was named after the week of culture (MS P1, MS P2, etc.). After five weeks mammospheres were dissociated by trypsinization and returned to standard adherent culture conditions in serum-supplemented DMEM medium. The CD44/CD24 phenotype of different mammosphere generations was measured by staining with PE mouse anti-human CD44 antibody and FITC mouse anti-human CD24 antibody (both BD Pharmingen) and subsequent FACS analysis.

6.3 Cell based assays

6.3.1 Resazurin reduction assay

Resazurin reduction assay (174) was performed to assess cytotoxicity of shikonin and other cytostatic compounds towards various sensitive and resistant cancer cell lines. The assay is based on reduction of the indicator dye, resazurin, to the highly fluorescent resorufin by

viable cells. Non-viable cells rapidly lose the metabolic capacity to reduce resazurin and thus produce no fluorescent signal. Briefly, adherent cells were detached by treatment with 0.25% trypsin/EDTA and an aliquot of $1x10^4$ cells was placed in each well of a 96-well cell culture plate in a total volume of 200 µl. Cells were allowed to attach overnight and then were treated with different concentrations of the compound of interest. For suspension cells, aliquots of 2×10^4 cells per well were seeded in 96-well-plates in a total volume of 100 µl. Compounds were immediately added in varying concentrations in an additional 100 µl of culture medium to obtain a total volume of 200 µl/well. After 24 h or 48 h, 20 µl resazurin (Sigma-Aldrich) 0.01% w/v in *dd*H_2O was added to each well and the plates were incubated at 37 °C for 4 h. Fluorescence was measured on an Infinite M2000 Pro^{TM} plate reader (Tecan) using an excitation wavelength of 544 nm and an emission wavelength of 590 nm. Each assay was done at least two times, with six replicates each. The viability was evaluated based on a comparison with untreated cells. IC50 values represent the test compound concentrations required to inhibit 50% of cell proliferation and were calculated from a calibration curve by linear regression using Microsoft Excel.

6.3.2 DNA damage detection and quantification by alkaline elution assay

The alkaline elution assay was originally described by Kohn *et al.* (175) and modified by Epe *et al.* (176). In this study, the assay was used to quantify different types of DNA modifications generated in U937 cells after shikonin treatment. Briefly, 10^6 cells were treated with 0.3 µM shikonin (IC50) for 3 h and 6 h or DMSO (solvent control). After incubation, cells were lysed on a polycarbonate filter (2 mm pore size) by pumping a lysis solution (100 mM glycine, 20 mM Na_2EDTA, 2% SDS, 500 mg/l proteinase K, pH 10.0) through the filter for 90 min at 25 °C. After washing, the DNA remaining on the filter was incubated with the repair endonuclease Fpg protein (1 µg/ml) for 30 min at 37 °C to detect DNA modifications sensitive to oxidative stress. To quantify DNA single-strand breaks, the incubation was also carried out without endonuclease. After Fpg endonuclease incubation the DNA was eluted with an alkaline solution at 25 °C and its elution rate determined. The slopes of elution curves obtained with γ-irradiated cells were used for calibration (6 Gγ = 1 single-strand break/10^6bp).

6.3.3 Caspase-Glo 3/7 and Caspase-Glo 9 assay

The influence of shikonin on caspase 3/7 and caspase 9 activity in U937 leukemia cells was detected using Caspase-Glo® 3/7 and Caspase-Glo® 9 Assay kits (Promega). Cells cultured in RPMI 1640 medium were seeded in 96-well plates and treated with different concentrations of shikonin or DMSO (solvent control). After 6 h of treatment, cellular caspase 3/7 or caspase 9 activity was determined according to the manufacturer`s protocol. Luminescence was measured using the Infinite M2000 Pro™ plate reader (Tecan). Caspase activity was expressed as percentage of the untreated control.

6.3.4 Scratch migration assay

The scratch migration assay is a well-developed method to investigate drug effects on cell migration *in vitro* (177). Briefly, 1×10^6 SKBR3 cells were seeded in each well of a 6-well plate and allowed to form a confluent monolayer. The cell monolayer was carefully scraped with a sterile p200 pipette tip to create a scratch. Subsequently, cells were washed with PBS and treated with DMEM culture medium containing different sub-toxic concentrations of shikonin or DMSO (solvent control). Images of the scratches were taken every 3 h using a phase contrast microscope (Optika, Italy) at 10x magnification. Data analysis was performed with Tscratch software (178).

6.4 Flow cytometry

6.4.1 Cellular uptake assays

Measuring quantitatively inherent fluorescent drug uptake in live cells

U937 cell suspension was transferred to a 50 ml centrifuge tube (Sarstedt) and centrifuged at 1200 rpm for 5 min. The supernatant was discarded and the cell pellet was resuspended in RPMI 1640 medium with 2 mM L-glutamine containing no phenol red (Invitrogen) to reach a final cell concentration of 5 x 10^5 cells/ml. 2 ml of the cell suspension was then transferred into 5 ml FACS tubes (Becton-Dickinson). For cellular shikonin uptake analysis, cells were measured on a LSR-Fortessa FACS analyzer (Becton-Dickinson) with 640 nm excitation (40 mW) and detected using a 730/45 nm bandpass filter. For drug uptake studies on other chemotherapeutics, cells were measured with excitation and emission parameters as shown in

Table 10. The background fluorescence of the cells was measured for 2 min and adjusted to be 10 x above the electronic noise of the analyzer to ensure precise measurements even with large cellular based coefficient of variation (CV). Dead cells were excluded either by staining with 2 µM Hoechst (Merck) or by FSC/SSC gating which in most cases was sufficient. After 2 min the FACS tube was removed from the flow cytometer without stopping the recording and the appropriate drug was added immediately in the desired concentration. The cell suspension containing the drug was gently but thoroughly mixed and reinserted into the flow cytometer within 30 sec after removing it from the machine. The measurements continued up to 20 min total time at a flow rate of 50-70 cells per second while recording the area signal of all respective channels. The experimental layout is displayed in Figure 46. Cytographs were analyzed using FlowJo software (Celeza).

Correlating direct fluorescence with supernatant fluorescence reduction for direct quantification of drug uptake

In order to correlate FACS-measured fluorescence with physical drug uptake a standard curve of cellular uptake of doxorubicin into U937 cells was ascertained fluorometrically based on the residual amounts of doxorubicin fluorescence in the supernatant of the measured cultures. In detail, 1 x 10^6 U937 cells in RPMI 1640 medium without phenol red indicator were transferred into a FACS tube in a total volume of 2 ml. Doxorubicin was added in various concentration (0.3, 0.6, 1.2, 2.4, and 4.8 µM) and the cells were incubated for 20 min. After incubation, the cells were transferred to a 15 ml centrifuge tube (Sarstedt) and centrifuged at 1200 rpm for 5 min. 100 µl of the supernatant was transferred into each of three wells of a white 96-well plate (Thermo Scientific). The residual fluorescence in the supernatant was measured at an excitation wavelength of 485 nm and an emission wavelength of 590 nm using the Infinite M2000 Pro™ plate reader (Tecan). Controls included FACS tubes with 2 ml of conditioned RPMI 1640 medium without cells that had been incubated with appropriate concentrations of doxorubicin. The percentage of cellular drug uptake relative to reference solutions was calculated and used to calculate the µM doxorubicin taken into the cells.

The drug uptake measured from the different supernatants was correlated with the background fluorescence increase (GeoMean Gate 3 – GeoMean Gate2) of the corresponding samples measured by FACS. The amount of internalized doxorubicin of each sample was converted to ng and divided by the background subtracted fluorescence increase of the corresponding sample, resulting in case of doxorubicin in a very exact correlation of ~0.5 ng doxorubicin per

fluorescence intensity unit (FIU). This correlation was plotted using Excel and is presented in Figure 48.

Multiplexing of drug uptake and further endpoint measurements

The uptake of doxorubicin was coupled with live functional assays for ROS detection, cell cycle analysis, and evaluation of live/dead cell ration. A precise protocol for the quantification of ROS can be found in a separate chapter (6.4.3). For multiplexing several endpoint measurements, 2 x 106 U937 cells were transferred into a 15 ml centrifuge tube (Sarstedt) and washed with 2 ml PBS (Invitrogen) by centrifugation at 1200 rpm for 5 min. Subsequently, cells were suspended in 2 ml PBS containing 2 µM H_2DCFH-DA and incubated for 20 min in darkness. After incubation, cells were washed with 2 ml of PBS by centrifugation at 1200 rpm for 5 min and suspended in 2 ml phenol red-free RPMI 1640 medium containing 4.8 µM doxorubicin. In other cases, the cells were incubated with doxorubicin for 16 h in clear media prior to staining with H_2DCFH-DA. H_2DCFH-DA loaded cells in culture medium without doxorubicin were used as untreated control. After 3 h incubation with doxorubicin, cells were washed with 2 ml PBS by centrifugation at 1200 rpm for 5 min and suspended in 2 ml phenol red-free RPMI 1640 medium. In the case of multi-parametric analysis being performed, the cells were incubated for 16 h with doxorubicin and additionally incubated with 1µl Vybrant DyeCycle reagent and 1µl SytoxRed (both Life Technologies) per ml of 1 x 10^6 cells/ml cell suspension for 30 min at 37 °C. Subsequently cells were measured in a LSR-Fortessa flow cytometer. Doxorubicin was measured with 561 nm excitation (150 mW) and detected using a 610/20 nm band width filter; dichlorofluorescein (DCF) was measured with 488 nm excitation (100 mW) and detected using a 530/30 nm band width filter; SytoxRed was measured with 640 nm excitation (40 mW) and detected using a 670/30 nm band width filter; Vybrant DyeCycle DNA dye was measured with 405 nm or 355 nm excitation (100 mW / 20 mW), in both cases using a 450/50 nm band width filter. All parameters were plotted on a logarithmic scale except for the Vybrant DyeCycle, as it was used for cell cycle analysis and henceforth was plotted linearly. All cells for live multi-parametric assays were gated exclusively on the criteria of being single cells using area vs width scattering of the side-scatter and no further gating on the FSC vs SSC characteristics. A neutral density filter 1.0 was used for the FSC photodiode to reduce the light so that the cells in the FSC channel could be visualized without reducing the sensor voltage below recommended values.

6.4.2 Analysis of the mitochondrial membrane potential

The effects of shikonin on the mitochondrial membrane potential were analyzed by JC-1 (Biomol) staining. JC-1 is a dye that can selectively enter into mitochondria and exhibits an intense red fluorescence in healthy mitochondria with normal membrane potentials. In cells with reduced mitochondrial membrane potential, the red fluorescence disappears. Briefly, 1×10^6 U937 cells were incubated with JC-1 staining solution according to the manufacturer`s protocol for 30 min. Stained cells were treated with different concentrations of shikonin or DMSO (solvent control) for 6 h. Subsequently, cells were measured in a LSR-Fortessa FACS analyzer (Becton-Dickinson). For each sample, 1×10^4 cells were counted. The JC-1 signal was measured with 561 nm excitation (150mW) and detected using a 586/15 nm bandpass filter. The shikonin signal was analyzed with 640 nm excitation (40mW) and detected using a 730/45 nm bandpass filter. All parameters were plotted on a logarithmic scale. Cytographs were analyzed using FlowJo software (Celeza). All experiments were performed at least in triplicate.

6.4.3 Measurement of reactive oxygen species

2´,7´-Dichlorodihydrofluorescein diacetate (H_2DCFH-DA) (Sigma-Aldrich) is a probe used for the highly sensitive and quantifiable detection of reactive oxygen species (ROS). The non-fluorescent H_2DCFH-DA diffuses into the cells and is cleaved by cytoplasmic esterases into 2´,7´-dichlorodihydrofluorescein (H_2DCF) which is unable to diffuse back out of the cells. In the presence of hydrogen peroxide, H_2DCF is oxidized to the fluorescent molecule dichlorofluorescein (DCF) by peroxidases. The fluorescent signal emanating from DCF can be measured and quantified by flow cytometry, thus providing an indication of intracellular ROS concentration (179, 180). Briefly, 2×10^6 U937 cells were resuspended in PBS and incubated with 2 µM H_2DCFH-DA for 20 min in the dark. Subsequently, cells were washed with PBS and resuspended in RPMI 1640 culture medium containing different concentrations of shikonin or DMSO (solvent control). After 1 h of incubation, cells were washed and suspended in PBS. Subsequently, cells were measured in a FACS Calibur flow cytometer (Becton-Dickinson). For each sample 1 x 10^4 cells were counted. DCF was measured at 488 nm excitation (25mW) and detected using a 530/30 nm bandpass filter. All parameters were plotted on a logarithmic scale. Cytographs were analyzed using FlowJo software (Celeza). All experiments were performed at least in triplicate.

For the measurement of real-time kinetics of ROS induction, U937 cells were stained with H_2DCFH-DA as described above. The cells were measured on a LSR-Fortessa FACS analyzer (Becton-Dickinson) with 488 nm excitation (100mW) for DCF and 649 nm excitation for shikonin. DCF and shikonin fluorescence were detected using a 530/30 nm and a 730/45 nm bandpass filter, respectively. After 2 min of recording, 0.6 µM shikonin was added to the cell suspension and the tube was immediately reinserted into the flow cytometer. The measurement continued for up to 1 h total time at a flow rate of 50-70 cells per second. Cytographs were analyzed using FlowJo software (Celeza).

6.4.4 Calcium signaling

For analysis of intracellular calcium signaling after shikonin treatment, the chemical calcium indicator indo-1 (Invitrogen) was used. The dye can be excited in the UV range at ~350 nm and peak emission occurs at ~405 nm and ~485 nm in the Ca^{2+} bound and free states, respectively (181). In this way, a relatively accurate measurement of the intracellular Ca^{2+} concentration by a fluorometric ratio technique is possible. Briefly, 2×10^6 U937 cells in 2 ml 1640 RPMI culture medium without phenol red indicator were incubated with 1 µM indo-1 for 30 min at 37°C in the dark. Following incubation, cells were centrifuged and resuspended in fresh culture medium. Subsequently, cells were measured on a LSR-Fortessa FACS analyzer (Becton-Dickinson) with 355 nm excitation (20mW) and detected using 405/20 nm and 530/30 nm bandpass filters. The ratio of both signals (405/20 nm / 530/30 nm) was used as an index for intracellular calcium concentration. After 2 min, the FACS tube was removed from the flow cytometer without stopping the recording and shikonin was added immediately in the desired concentration. The cell suspension containing the drug was mixed and reinserted into the flow cytometer within 30 sec after being removed. The measurements continued for up to 60 min total time at a flow rate of 100-150 cells per second while recording the area signal of all significant channels. Cytographs were analyzed using FlowJo software (Celeza). The Ca^{2+} exchanger ionomycin (Sigma-Aldrich) raises intracellular calcium levels and served as positive control at a final concentration of 0.4 µM. Cells treated with DMSO served as a solvent control.

6.4.5 Cell cycle

For cell-cycle analysis, $1x10^6$ U937 cells were treated with different concentrations of shikonin for 24 h. Following incubation, cells were washed in PBS and fixed in ice-cold 95% ethanol (Sigma-Aldrich). After washing in PBS, cells were incubated with 10 µg/ml RNase A (Applichem Lifescience) and 50 µg/ml propidium iodide (PI, Sigma-Aldrich) in PBS for 1 h in the dark. Cells were measured on a LSR-Fortessa FACS analyzer (Becton-Dickinson). 1×10^4 cells were counted for each sample. PI was measured with 488 nm excitation (100mW) and detected using a 610/20 nm bandpass filter. Cytographs were analyzed using FlowJo software (Celeza). All experiments were performed at least in triplicate.

6.4.6 FlowCellect^{TM} PI3K-mTOR signaling cascade assay

The FlowCellect^{TM} PI3K-mTOR signaling cascade assay kit (Millipore) was used to analyze the effect of shikonin on mTOR signaling. The assay is based on two directly conjugated 94ioinfor-specific signaling antibodies against phosphorylated Akt and phosphorylated riboS6, which are both important signaling nodes of the mTOR cascade. The phosphorylation of Akt is indicative of the upstream PI3K signaling, marking the cells' initiation into proliferation or cell survival. Phosphorylated riboS6 is indicative of downstream mTOR and p70S6K signaling leading to protein translation. The assay was performed according to the manufacturer protocol. Briefly, 1.5 x 10^6 U937 cells were treated with 0.3 µM shikonin or DMSO solvent control and incubated for 24 h. Subsequently, cells were fixed on ice for 20 min using the supplied fixation buffer. After fixation, cells were washed twice and treated with permeabilization buffer on ice for 20 min. After two further washing steps, cells were resuspended in a final volume of 90 µl assay buffer and incubated with 5 µl 20x Anti-phospho-Ribosomal Protein S6 (Ser235) PerCP conjugated monoclonal antibody and 5 µl 20x Anti-phospho-Akt1/PKBα (Ser473) Alexa Fluor 488 conjugated monoclonal antibody in the dark on ice for one hour. After antibody incubation, cells were centrifuged and resuspended in 500 µl assay buffer. Subsequently, cells were measured in a LSR-Fortessa FACS analyzer (Becton-Dickinson). For each sample, 1×10^4 cells were counted. The PerCP signal was measured with 488 nm excitation and detected using a 670/30 nm bandpass filter. The Alexa Fluor 488 signal was analyzed with 488 nm excitation and detected using a 530/30 nm bandpass filter. All parameters were plotted on a logarithmic scale. Cytographs were analyzed using FlowJo software (Celeza). All experiments were performed at least in triplicate.

6.4.7 Analysis of the CD44/CD24 phenotype

Briefly, MCF-7 cells or MCF-7 mammospheres were treated with 0.25% trypsin/EDTA solution to obtain a single cell suspension. Subsequently, cells were washed twice with staining buffer (DPBS + 5% FBS) and cell number was adjusted to 1×10^7 cells /ml. 20 µl of PE mouse anti-human CD44 antibody and FITC mouse anti-human CD24 antibody (both BD Pharmingen) were added to 100 µl of cell suspension (1×10^6 cells) and incubated in the dark on ice for 20 min. After antibody incubation cells were washed twice with staining buffer and finally resuspended in 500µl staining buffer. Subsequently, cells were measured in a LSR-Fortessa FACS analyzer (Becton-Dickinson). For each sample, 1×10^4 cells were counted. The PE signal was measured with 561 nm excitation and detected using a 586/15 nm bandpass filter. The FITC signal was analyzed with 488 nm excitation and detected using a 530/30 nm bandpass filter. All parameters were plotted on a logarithmic scale. Cytographs were analyzed using FlowJo software (Celeza). All experiments were performed at least in triplicate.

6.5 Confocal microscopy

6.5.1 Cellular localization of shikonin

For intracellular localization studies of shikonin, cells were stained with MitoTracker Green FM (Invitrogen). This fluorescent dye passively diffuses across the plasma membrane and accumulates in active mitochondria. Briefly, 4×10^4 U937 cells were placed in each well of a sterile ibiTreat µ-slide (ibidi) pretreated with polyethylenimine (Sigma-Aldrich) for sufficient cell adhesion or 2×10^4 SKBR3 cells were seeded in untreated ibiTreat µ-slides and allowed to attach overnight. According to the manufacturer's protocol, cells were incubated with 100 nM MitoTracker Green FM for 45 min at 37 °C in the dark. After incubation, the staining solution was removed and the cells were resuspended in fresh medium containing 25 µM shikonin. Live cell imaging was performed on a Leica TCS SP5 confocal microscope with a 40×/1.30 oil objective (Leica). The microscope was controlled by LAS AF software (Leica). A 561 nm laser was used for excitation of shikonin, and the emitted signal was detected at 680-780 nm. MitoTracker Green FM was excited with a 488 nm laser and detected at 500-549 nm. Analysis and averaging of images was performed with LAS AF software; further image processing was carried out with Adobe Photoshop.

6.5.2 Imaging of the structure and dynamics of the microtubule cytoskeleton

Live cell imaging was performed on a Leica TCS SP5 confocal microscope with a 40×/1.30 oil objective. The microscope was controlled by LAS AF software. A488 nm laser was used for excitation of GFP, and the emitted signal was detected at 500-549 nm. Shikonin was excited with a 561 nm laser and the emitted fluorescence was detected at 680-780 nm. Analysis and averaging of images was performed with LAS AF software, further image processing was carried out with Adobe Photoshop.

2×10^4 U2OS-GFP-αTubulin or RPE-1-GFP-EB3 cells were seeded in each well of a sterile ibiTreat µ-slide (ibidi) and cells were allowed to attach overnight. Cells were treated with 25 µM shikonin and subsequently analyzed by confocal microscopy. Each experiment was repeated at least three times and representative images and videos were selected.

6.6 *Omics* assays: transcriptomics and proteomics

6.6.1 mRNA Microarray and validation by real-time reverse transcription-PCR

mRNA microarrays were performed at the Genomics and Proteomics Core Facility of the DKFZ. Experiments were done in duplicates for treated and untreated samples.

RNA isolation

Total RNA from U937 cells after 24 h of treatment with shikonin at IC50 concentration or DMSO solvent control was isolated using the Rneasy Kit (Qiagen) according to the manufacturer's instruction. The quality of total RNA was checked by gel analysis using the total RNA Nano chip assay on an Agilent 2100 Bioanalyzer (both Agilent Technologies). Only samples with RNA index values greater than 9.3 were selected for expression profiling.

Probe labeling and hybridization

Biotin-labeled cRNA samples were prepared according to Illumina's recommended sample labeling procedure based on the modified Eberwine protocol (182). Briefly, 500 ng RNA were used for cDNA synthesis followed by an amplification/labeling step (*in vitro* transcription) to produce biotin-labeled cRNA using the MessageAmp II aRNA Amplification kit (Life Technologies) and Biotin-16-UTP (Roche). The cRNA was column purified with the Illumina® TotalPrep™ RNA Amplification Kit (Life Technologies) and quantified with a

NanoDrop 2000 UV-Vis spectrophotometer (Thermo Scientific). Quality of labeled RNA was controlled using the RNA Nano Chip Assay on an Agilent 2100 Bioanalyzer (both Agilent Technologies). Hybridization was performed on Illumina Human Sentrix-HT12 Bead Chip arrays (Illumina) according the manufacturer´s recommendations.

Scanning and data analysis

Microarray scanning was done using an Illumina® BeadStation array scanner (Illumina). Images were analyzed and data were extracted, background subtracted and normalized using the standard procedures of Illumina's Extraction Software. The expression data obtained was filtered with Chipster data analysis platform (http://chipster.csc.fi). Filtered genes were analyzed through the use of ingenuity pathway analysis (IPA; Ingenuity® Systems, CA, USA; www.ingenuity.com). The 97ioinformatics evaluation is explained in detail in 6.6.4.

Real-time reverse transcription-PCR

The same RNA samples used in the mRNA microarray experiments were also used for RT-PCR experiments. Total RNA samples were converted to cDNA by RevertAid H minus reverse transcriptase (Fermentas) with random hexamer primers. Quantification of cDNA was performed by real-time PCR using a Taq-polymerase master mix (Roche) containing the fluorescent dye SYBR Green (Biozol) and the CFX384^{TM} Real-Time PCR Detection System (Bio-Rad). The efficiency of all primer pairs used for real-time PCR expression was better than 90%. PCR was performed with an initial denaturation at 95 °C for 5 min followed by 50 cycles consisting of strand separation at 95 °C for 30 s and annealing and extension at 60 °C for 40 s. After PCR product amplification, melting curves were computed. Expression levels were normalized to the transcription level of G6PD. All samples were run in triplicates.

6.6.2 miRNA Microarray

miRNA microarrays were performed at the Genomics Core Facility of the Institute for Molecular Biology (IMB, Mainz, Germany). Experiments were done in duplicates for treated and untreated samples.

RNA isolation

miRNA from U937 cells after 24 h of treatment with shikonin at IC50 concentration was isolated using the miRNeasy Kit (Qiagen) according to the manufacturer's instruction. The

quality of miRNA was checked by gel analysis using the Small RNA Nano chip assay on an Agilent 2100 Bioanalyzer (both Agilent Technologies).

Probe labeling and hybridization

Probe labeling and hybridization were carried out following the miRNA complete labeling and hyb kit protocol form Agilent Technologies. Briefly, extracted RNA was treated with phosphatase and dephosphorylated RNA was fluorescently labeled by ligation of Cyanine 3-pCp molecules to the 3' end of RNA molecules using Agilent's miRNA Complete Labeling and Hyb Kit. The labeled RNA was desalted and hybridized to human miRNA microarray chips (8x60K) for 20 hours at 55°C and 20 rpm.

Scanning and data analysis

Microarray slides were scanned with Agilent Microarray Scanning system. Images were analyzed and data was extracted, background subtracted and normalized using the standard procedures of Agilent Feature Extraction Software. The expression data obtained was filtered with Chipster data analysis platform (http://chipster.csc.fi). Filtered miRNAs were analyzed through the use of ingenuity pathway analysis (IPA; Ingenuity® Systems, CA, USA; www.ingenuity.com). Furthermore, the Ingenuity microRNA Target filter tool was used to associate deregulated miRNAs from the miRNA microarray with experimentally observed and predicted mRNA targets. The 98ioinformatics evaluation is explained in detail in 6.6.4.

6.6.3 Proteomics analysis using dimethyl labeling

To examine quantitative changes in the proteome of U937 leukemia cells after shikonin treatment stable-isotope dimethyl labeling was performed. Briefly, 5 x 10^6 U937 cells were seeded in 10 ml RPMI 1640 medium in a 25 cm^2 culture flask. Subsequently, cells were treated with 0.3 µM shikonin (IC50) or DMSO as solvent control for 24 h. After incubation cells were washed with PBS and protein extraction was performed using the M-PER Mammalian Protein Extraction Reagent (Thermo Scientific) containing a protease inhibitor cocktail (Roche). Cells were incubated with the extraction reagent for 40 min at 4 °C. After incubation cellular debris was removed by centrifugation at 14000 x g for 15 min. Supernatants were transferred into new tubes and an acetone precipitation of the proteins was performed. After precipitation, the acetone was removed and the protein pellet in each of the tube was further diluted to 1 µg/µl with 50 mM TEABC, and reduced with 5 mM TCEP for

1 h at 37°C, followed by alkylation using 2 mM MMTS for 45 min at room temperature. For the proteolytic digestion, the modified tube-gel digestion protocol was applied and the detergent residue was checked using a previously described method (183). Two 200 µg proteolytic protein mixtures from DMSO and shikonin treated cells were first dissolved in 200 µl of 100 mM TEABC (pH 8.5) and respectively mixed with 20 µl of formaldehyde and formaldehyde-13C, d2 (4%, diluted with H_2O). After vortexing (5 min) and centrifugation, each of the sample solutions was mixed with 20 µl of 600 mM sodium cyanoborohydride solution. The sample solutions were vortexed (10 min) and centrifuged again, and then allowed to react for 30 min at 25°C. To quench the reaction, ammonium hydroxide (7% in water, 10 µl) was added to each sample solution. Finally, 16 µl of formic acid was added to acidify each of the sample solutions and two samples were further combined for strong cation exchange (SCX) fractionation.

For SCX fractionation, the buffer SCX-A (5 mM KH_2PO_4 in 25% ACN at pH 3) and SCX-B (5 mM KH_2PO_4 and 350 mM KCl in 25% ACN at pH 3) were used as the mobile phase. The peptide mixtures were reconstituted in buffer SCX-A and then loaded into a PolySOLFOETHYL A column (200 × 2.1 mm, 5 µm, 300 Å, PolyLC, Columbia, MD) for 10 min at the flow rate of 0.2 ml/min. Peptides were fractionated using a 75 min gradient from 0 to 100% of buffer SCX-B. Fractions were collected every three minutes from the retention time of 10 to 55 min using a fraction collector (BioFrac Fraction Collector, BioRad Laboratories, Hercules, CA). The peptide mixture in each of the fraction was further analyzed by the LC-MS/MS.

LC-MS/MS analysis was performed with a nanoUHPLC system (nanoACQUITY UPLC, Waters, Millford, MA) coupled online to the nanoelectrospray source of a hybrid quadrupole time-of-flight mass spectrometer (Q-TOF-MS) (SYNAPT HDMS G2, Waters, Manchester, UK). For LC-MS/MS analysis, water with 0.1% FA and ACN with 0.1% FA were used as the mobile phase. The sample was injected into a trap column (Symmetry C18, 5 µm, 180 µm × 20 mm, Waters, Milford, MA), and separated online with a reverse phase column (BEH C18, 1.7 µm, 75 µm × 250 mm, Waters, Milford, MA) at the flow rate of 300 nl/min using either a 95 min gradient with 5-90% ACN/water ratio. The mass spectrometry instruments were all operated in the positive ion mode and data dependent acquisition methods were applied for all experiments. The acquisition settings were set to one full MS scan (350-1600 m/z) with a scan time of 1 second and switched to six product ion scans (50-1900 m/z) with 0.4 second scan time when a precursor ion charge was 2+, 3+ or 4+, and the intensity was higher than 200

counts. The data files generated from LC-MS/MS were processed by UniQua and further analyzed by the MASCOT and Trans Proteomics Pipeline (TPP) 1 version 4.4 rev. 1, the details and criteria of data processing were described in a protocol of Chang *et al*. (184). All identified proteins were detected with a minimum of two unique peptides.

6.6.4 Bioinformatic evaluation

Chipster analysis

Chipster is an analysis software for high-throughput data (http://chipster.csc.fi). The expression data sets obtained in mRNA and miRNA microarrays were filtered with Chipster data analysis platform. These steps include filtering of genes by two times standard deviation of deregulated molecules and a subsequent assessment of significance using empirical Bayes t-test ($p < 0.01$).

Ingenuity pathway analysis

Omics datasets were analyzed through the use of ingenuity pathway analysis (IPA; Ingenuity® Systems, CA, USA; www.ingenuity.com). This software integrates the experimental results to known biological relationships, mechanisms and functions using the regularly updated Ingenuity Knowledge Base, a giant database of biological findings and relations gathered from literature. Only molecules from the *omics* datasets that met the expression fold change cutoff of $\geq \pm 1.2$ were used for analysis with IPA. Briefly, filtered molecules were fed into Ingenuity Pathway Analysis software and a separate core analysis was performed for each of the three *omics* assays to assign the deregulated mRNA, miRNA and proteins to cellular networks, functions, and pathways. Furthermore, the Ingenuity microRNA Target filter tool was used to associate deregulated miRNAs from the miRNA microarray with experimentally observed and predicted mRNA targets. The results of the core analysis were further studied in a comparison analysis to identify cellular functions affected in all three assays. Finally, the results of the *omics* assays were merged in one dataset that was screened for overlapping cellular signaling pathways using the core analysis tool. For molecules, that showed a non consistent deregulation of mRNA and protein expression (36 cases), the stronger deregulated expression values were considered for analysis.

6.7 Fluorescence scan

Shikonin was solved in aqueous buffer at a final concentration of 50 µM. A 2d excitation (200-600 nm) vs. emission (300-700 nm) scan was performed on a Fluorolog-2 spectrofluorometer (Horiba).

6.8 Redox cycling

The H_2O_2 generation assay was performed according to a modified high-throughput assay protocol (109). The assay is based on the ability of horseradish peroxidase to catalyze the oxidation of phenol red by H_2O_2, producing a change in its absorbance at 610 nm after the assay reaction has been terminated and adjusted to alkaline pH by addition of 1N NaOH. The assay was performed in 96-well flat-bottomed clear polystyrene microtiter plates (Thermo Scientific). Shikonin and H_2O_2 were diluted to the required concentrations in HBSS buffer (Invitrogen). Phenol red and horseradish peroxidase were solved in HBSS and mixed to a detection reagent (300 µg/ml phenol red and 180 µg/ml horseradish peroxidase). 30 µl of shikonin, H_2O_2 or buffer control were mixed with 30 µl DTT (2 mM) and incubated for 30 min in the dark. Subsequently 30 µl detection reagent were added. After 45 min incubation the reaction was terminated by addition of 15 µl of 1 N NaOH. The absorbance of the oxidized phenol red was measured at 610 nM using an Infinite M2000 Pro^{TM} plate reader (Tecan). A reaction scheme for the interaction of shikonin and DTT to generate H_2O_2 is displayed in Figure 22.

6.9 Virtual Docking experiments

Virtual docking experiments represent an approach to identify possible binding interactions and binding sites between ligands and proteins. If there is no prior knowledge of binding sites of ligand and protein, the entire surface of the protein target has to be scanned in a so-called blind docking experiment. Since shikonin deregulates the PI3K-Akt-mTOR signaling cascade, a virtual screening approach was used to identify proteins of this pathway, which are most likely targeted by shinonin, and to calculate their corresponding binding energies. Therefore, blind docking was performed using AutoDock Vina with the graphical user interface AutoDock Tools (123). X-ray structures of proteins involved in the signaling cascade were downloaded from the “Protein Data Bank” (www.pdb.org). The three

dimensional structure of shikonin was downloaded from the PubChem compound library (http://pubchem.ncbi.nlm.nih.gov). The virtual screening and further wet lab validation studies identified IGF1R as target of shikonin. Thus, in a second docking experiment possible binding sites of shikonin and IGF1R were calculated using AutoGrid 4 and AutoDock 4.2 with the graphical user interface AutoDock Tools. An X-ray structure of IGF1-R was again downloaded from the PDB (PDB ID: 2OJ9).

6.10 IGF1R kinase inhibition assay

The kinase inhibition assay was performed by ProQinase GmbH (Freiburg, Germany). Shikonin was provided as 1.85 x 10^{-3} M stock solution in DMSO. In the process, shikonin was serially diluted in semi-log steps with 100% DMSO in a 96-well microtiter plate. Directly before use shikonin was further diluted 1:10 with water. Shikonin was tested at 10 final assay concentrations in the range from 1.85×10^{-5} M to 5.55×10^{-10} M. The final DMSO concentration in the reaction cocktails was 1% in all cases. A radiometric protein kinase assay (^{33}PanQinase® Activity Assay) was used for measuring the kinase activity of IGF1R. All kinase assays were performed in 96-well FlashPlates™ (Perkin Elmer) in a 50 µl reaction volume. The reaction cocktail was pipetted in 4 steps in the following order: 10 µl of non-radioactive ATP solution (in H_2O), 25 µl of assay buffer/[γ-^{33}P]-ATP mixture, 5 µl shikonin in 10% DMSO, 10 µl of IGF1R / Poly(Glu,Tyr)-4:1-mixture. The reaction cocktails were incubated at 30 °C for 60 minutes. The reaction was stopped with 50 µl of 2% (v/v) H3PO4, plates were aspirated and washed two times with 200 µl 0.9% (w/v) NaCl. Incorporation of $^{33}P_i$ (counting of "cpm") was determined with a Wallac MicroBeta® scintillation counter (Perkin Elmer). All assays were performed with a Beckman Coulter Biomek 2000/SL robotic system. Kinase activity was evaluated based on a comparison with experiments containing the complete reaction cocktail, but no shikonin. A complete reaction cocktail without kinase served as control for unspecific binding of radioactivity to the plate in the absence of protein kinase but in the presence of shikonin. IC50 values were calculated by nonlinear regression using Prism 5.04 (Graphpad).

7 References

1. Ferlay J, Shin HR, Bray F, Forman D, Mathers C, Parkin DM. Estimates of worldwide burden of cancer in 2008: GLOBOCAN 2008. Int J Cancer. 2010 Dec 15;127(12):2893-917.
2. Hanahan D, Weinberg RA. The hallmarks of cancer. Cell. 2000 Jan 7;100(1):57-70.
3. Hanahan D, Weinberg RA. Hallmarks of cancer: the next generation. Cell. 2011 Mar 4;144(5):646-74.
4. Croce CM. Oncogenes and cancer. N Engl J Med. 2008 Jan 31;358(5):502-11.
5. Anand P, Kunnumakkara AB, Sundaram C, Harikumar KB, Tharakan ST, Lai OS, et al. Cancer is a preventable disease that requires major lifestyle changes. Pharm Res. 2008 Sep;25(9):2097-116.
6. Balis FM. The Goal of Cancer Treatment. Oncologist. 1998;3(4):V.
7. Efferth T. Molekulare Pharmakologie und Toxikologie: Biologische Grundlagen von Arzneimitteln und Giften: Springer; 2006.
8. Mutschler E, Geisslinger G, Kroemer H, Ruth P, Schäfer-Korting M. Mutschler Arzneimittelwirkungen: Lehrbuch der Pharmakologie und Toxikologie: Wissenschaftliche Verlagsgesellschaft; 2008.
9. Gottesman MM, Fojo T, Bates SE. Multidrug resistance in cancer: role of ATP-dependent transporters. Nat Rev Cancer. 2002 Jan;2(1):48-58.
10. Talmadge JE, Fidler IJ. AACR centennial series: the biology of cancer metastasis: historical perspective. Cancer Research. 2010 Jul 15;70(14):5649-69.
11. Redmond KM, Wilson TR, Johnston PG, Longley DB. Resistance mechanisms to cancer chemotherapy. Front Biosci. 2008;13:5138-54.
12. Szakacs G, Paterson JK, Ludwig JA, Booth-Genthe C, Gottesman MM. Targeting multidrug resistance in cancer. Nat Rev Drug Discov. 2006 Mar;5(3):219-34.
13. Jones PM, George AM. The ABC transporter structure and mechanism: perspectives on recent research. Cell Mol Life Sci. 2004 Mar;61(6):682-99.
14. Higgins CF. Multiple molecular mechanisms for multidrug resistance transporters. Nature. 2007 Apr 12;446(7137):749-57.
15. Raguz S, Yague E. Resistance to chemotherapy: new treatments and novel insights into an old problem. British Journal of Cancer. 2008 Aug 5;99(3):387-91.
16. Newman DJ, Cragg GM. Natural products as sources of new drugs over the 30 years from 1981 to 2010. Journal of Natural Products. 2012 Mar 23;75(3):311-35.
17. Efferth T, Li PC, Konkimalla VS, Kaina B. From traditional Chinese medicine to rational cancer therapy. Trends Mol Med. 2007 Aug;13(8):353-61.
18. Efferth T, Kahl S, Paulus K, Adams M, Rauh R, Boechzelt H, et al. Phytochemistry and pharmacogenomics of natural products derived from traditional Chinese medicine and Chinese materia medica with activity against tumor cells. Mol Cancer Ther. 2008 Jan;7(1):152-61.
19. Abelson PH. Medicine from plants. Science. 1990 Feb 2;247(4942):513.
20. WHO fact sheet No 134. 2008.
21. Chen X, Yang L, Oppenheim JJ, Howard MZ. Cellular pharmacology studies of shikonin derivatives. Phytother Res. 2002 May;16(3):199-209.
22. Sankawa U, Ebizuka Y, Miyazaki T, Isomura Y, Otsuka H. Antitumor activity of shikonin and its derivatives. Chem Pharm Bull (Tokyo). 1977 Sep;25(9):2392-5.
23. Guo XP, Zhang XY, Zhang SD. [Clinical trial on the effects of shikonin mixture on later stage lung cancer]. Zhong Xi Yi Jie He Za Zhi. 1991 Oct;11(10):598-9, 80.
24. Chang IC, Huang YJ, Chiang TI, Yeh CW, Hsu LS. Shikonin induces apoptosis through reactive oxygen species/extracellular signal-regulated kinase pathway in osteosarcoma cells. Biol Pharm Bull. 2010;33(5):816-24.

25. Han W, Li L, Qiu S, Lu Q, Pan Q, Gu Y, et al. Shikonin circumvents cancer drug resistance by induction of a necroptotic death. Mol Cancer Ther. 2007 May;6(5):1641-9.
26. Fujii N, Yamashita Y, Arima Y, Nagashima M, Nakano H. Induction of topoisomerase II-mediated DNA cleavage by the plant naphthoquinones plumbagin and shikonin. Antimicrob Agents Chemother. 1992 Dec;36(12):2589-94.
27. Cheng YW, Chang CY, Lin KL, Hu CM, Lin CH, Kang JJ. Shikonin derivatives inhibited LPS-induced NOS in RAW 264.7 cells via downregulation of MAPK/NF-kappaB signaling. J Ethnopharmacol. 2008 Nov 20;120(2):264-71.
28. Wu Z, Wu L, Li L, Tashiro S, Onodera S, Ikejima T. p53-mediated cell cycle arrest and apoptosis induced by shikonin via a caspase-9-dependent mechanism in human malignant melanoma A375-S2 cells. J Pharmacol Sci. 2004 Feb;94(2):166-76.
29. Yang H, Zhou P, Huang H, Chen D, Ma N, Cui QC, et al. Shikonin exerts antitumor activity via proteasome inhibition and cell death induction in vitro and in vivo. Int J Cancer. 2009 May 15;124(10):2450-9.
30. Chiu SC, Yang NS. Inhibition of tumor necrosis factor-alpha through selective blockade of Pre-mRNA splicing by shikonin. Mol Pharmacol. 2007 Jun;71(6):1640-5.
31. Chen J, Xie J, Jiang Z, Wang B, Wang Y, Hu X. Shikonin and its analogs inhibit cancer cell glycolysis by targeting tumor pyruvate kinase-M2. Oncogene. [Research Support, Non-U.S. Gov't]. 2011 Oct 20;30(42):4297-306.
32. Sawyers C. Targeted cancer therapy. Nature. 2004 Nov 18;432(7015):294-7.
33. Druker BJ, Tamura S, Buchdunger E, Ohno S, Segal GM, Fanning S, et al. Effects of a selective inhibitor of the Abl tyrosine kinase on the growth of Bcr-Abl positive cells. Nat Med. 1996 May;2(5):561-6.
34. Kurzrock R, Kantarjian HM, Druker BJ, Talpaz M. Philadelphia chromosome-positive leukemias: from basic mechanisms to molecular therapeutics. Ann Intern Med. 2003 May 20;138(10):819-30.
35. Druker BJ, Guilhot F, O'Brien SG, Gathmann I, Kantarjian H, Gattermann N, et al. Five-year follow-up of patients receiving imatinib for chronic myeloid leukemia. N Engl J Med. 2006 Dec 7;355(23):2408-17.
36. Gerber DE. Targeted therapies: a new generation of cancer treatments. Am Fam Physician. 2008 Feb 1;77(3):311-9.
37. Hudis CA. Trastuzumab--mechanism of action and use in clinical practice. N Engl J Med. 2007 Jul 5;357(1):39-51.
38. Kalia M. Personalized oncology: recent advances and future challenges. Metabolism. 2013 Jan;62 Suppl 1:S11-4.
39. Nahta R, Yu D, Hung MC, Hortobagyi GN, Esteva FJ. Mechanisms of disease: understanding resistance to HER2-targeted therapy in human breast cancer. Nat Clin Pract Oncol. 2006 May;3(5):269-80.
40. Pfisterer PH, Wolber G, Efferth T, Rollinger JM, Stuppner H. Natural products in structure-assisted design of molecular cancer therapeutics. Curr Pharm Des. 2010 May;16(15):1718-41.
41. Fulda S, Debatin KM. Extrinsic versus intrinsic apoptosis pathways in anticancer chemotherapy. Oncogene. 2006 Aug 7;25(34):4798-811.
42. Li P, Nijhawan D, Budihardjo I, Srinivasula SM, Ahmad M, Alnemri ES, et al. Cytochrome c and dATP-dependent formation of Apaf-1/caspase-9 complex initiates an apoptotic protease cascade. Cell. 1997 Nov 14;91(4):479-89.
43. Fulda S, Galluzzi L, Kroemer G. Targeting mitochondria for cancer therapy. Nat Rev Drug Discov. 2010 Jun;9(6):447-64.
44. Brookes PS, Yoon Y, Robotham JL, Anders MW, Sheu SS. Calcium, ATP, and ROS: a

mitochondrial love-hate triangle. Am J Physiol Cell Physiol. 2004 Oct;287(4):C817-33.
45. Modica-Napolitano JS, Singh KK. Mitochondrial dysfunction in cancer. Mitochondrion. 2004 Sep;4(5-6):755-62.
46. Gogvadze V, Orrenius S, Zhivotovsky B. Mitochondria in cancer cells: what is so special about them? Trends Cell Biol. 2008 Apr;18(4):165-73.
47. Chen G, Wang F, Trachootham D, Huang P. Preferential killing of cancer cells with mitochondrial dysfunction by natural compounds. Mitochondrion. 2010 Nov;10(6):614-25.
48. Kroemer G, Pouyssegur J. Tumor cell metabolism: cancer's Achilles' heel. Cancer Cell. 2008 Jun;13(6):472-82.
49. Brandon M, Baldi P, Wallace DC. Mitochondrial mutations in cancer. Oncogene. 2006 Aug 7;25(34):4647-62.
50. Guizzunti G, Theodorakis EA, Yu AL, Zurzolo C, Batova A. Cluvenone induces apoptosis via a direct target in mitochondria: a possible mechanism to circumvent chemo-resistance? Invest New Drugs. 2011 Sep 7.
51. Petros JA, Baumann AK, Ruiz-Pesini E, Amin MB, Sun CQ, Hall J, et al. mtDNA mutations increase tumorigenicity in prostate cancer. Proc Natl Acad Sci U S A. 2005 Jan 18;102(3):719-24.
52. Canter JA, Kallianpur AR, Parl FF, Millikan RC. Mitochondrial DNA G10398A polymorphism and invasive breast cancer in African-American women. Cancer Research. 2005 Sep 1;65(17):8028-33.
53. Wang F, Ogasawara MA, Huang P. Small mitochondria-targeting molecules as anti-cancer agents. Mol Aspects Med. 2010 Feb;31(1):75-92.
54. Plescia J, Salz W, Xia F, Pennati M, Zaffaroni N, Daidone MG, et al. Rational design of shepherdin, a novel anticancer agent. Cancer Cell. 2005 May;7(5):457-68.
55. Sarin SK, Kumar M, Garg S, Hissar S, Pandey C, Sharma BC. High dose vitamin K3 infusion in advanced hepatocellular carcinoma. J Gastroenterol Hepatol. 2006 Sep;21(9):1478-82.
56. Wenner CE. Targeting mitochondria as a therapeutic target in cancer. J Cell Physiol. 2012 Feb;227(2):450-6.
57. Meric-Bernstam F, Gonzalez-Angulo AM. Targeting the mTOR signaling network for cancer therapy. J Clin Oncol. 2009 May 1;27(13):2278-87.
58. Chiang GG, Abraham RT. Targeting the mTOR signaling network in cancer. Trends Mol Med. 2007 Oct;13(10):433-42.
59. Proud CG. mTORC1 signalling and mRNA translation. Biochem Soc Trans. 2009 Feb;37(Pt 1):227-31.
60. Hsieh AC, Liu Y, Edlind MP, Ingolia NT, Janes MR, Sher A, et al. The translational landscape of mTOR signalling steers cancer initiation and metastasis. Nature. 2012 May 3;485(7396):55-61.
61. Chapuis N, Tamburini J, Green AS, Willems L, Bardet V, Park S, et al. Perspectives on inhibiting mTOR as a future treatment strategy for hematological malignancies. Leukemia. 2010 Oct;24(10):1686-99.
62. Chabner B, Longo D. Cancer Chemotherapy and Biotherapy: Principles and Practice. 5th edition ed: Lippincott Williams&Wilki.
63. Tee AR, Manning BD, Roux PP, Cantley LC, Blenis J. Tuberous sclerosis complex gene products, Tuberin and Hamartin, control mTOR signaling by acting as a GTPase-activating protein complex toward Rheb. Curr Biol. 2003 Aug 5;13(15):1259-68.
64. Laplante M, Sabatini DM. mTOR signaling in growth control and disease. Cell. 2012 Apr 13;149(2):274-93.
65. Brown EJ, Albers MW, Shin TB, Ichikawa K, Keith CT, Lane WS, et al. A mammalian

protein targeted by G1-arresting rapamycin-receptor complex. Nature. 1994 Jun 30;369(6483):756-8.
66. Vignot S, Faivre S, Aguirre D, Raymond E. mTOR-targeted therapy of cancer with rapamycin derivatives. Ann Oncol. 2005 Apr;16(4):525-37.
67. O'Reilly KE, Rojo F, She QB, Solit D, Mills GB, Smith D, et al. mTOR inhibition induces upstream receptor tyrosine kinase signaling and activates Akt. Cancer Research. 2006 Feb 1;66(3):1500-8.
68. Tamburini J, Chapuis N, Bardet V, Park S, Sujobert P, Willems L, et al. Mammalian target of rapamycin (mTOR) inhibition activates phosphatidylinositol 3-kinase/Akt by up-regulating insulin-like growth factor-1 receptor signaling in acute myeloid leukemia: rationale for therapeutic inhibition of both pathways. Blood. 2008 Jan 1;111(1):379-82.
69. Wan X, Harkavy B, Shen N, Grohar P, Helman LJ. Rapamycin induces feedback activation of Akt signaling through an IGF-1R-dependent mechanism. Oncogene. 2007 Mar 22;26(13):1932-40.
70. Al-Hajj M, Wicha MS, Benito-Hernandez A, Morrison SJ, Clarke MF. Prospective identification of tumorigenic breast cancer cells. Proc Natl Acad Sci U S A. 2003 Apr 1;100(7):3983-8.
71. Li C, Heidt DG, Dalerba P, Burant CF, Zhang L, Adsay V, et al. Identification of pancreatic cancer stem cells. Cancer Research. 2007 Feb 1;67(3):1030-7.
72. Hemmati HD, Nakano I, Lazareff JA, Masterman-Smith M, Geschwind DH, Bronner-Fraser M, et al. Cancerous stem cells can arise from pediatric brain tumors. Proc Natl Acad Sci U S A. 2003 Dec 9;100(25):15178-83.
73. Collins AT, Berry PA, Hyde C, Stower MJ, Maitland NJ. Prospective identification of tumorigenic prostate cancer stem cells. Cancer Research. 2005 Dec 1;65(23):10946-51.
74. Wang Y, Krivtsov AV, Sinha AU, North TE, Goessling W, Feng Z, et al. The Wnt/beta-catenin pathway is required for the development of leukemia stem cells in AML. Science. 2010 Mar 26;327(5973):1650-3.
75. Greve B, Kelsch R, Spaniol K, Eich HT, Gotte M. Flow cytometry in cancer stem cell analysis and separation. Cytometry A. 2012 Apr;81(4):284-93.
76. Hatina J. The dynamics of cancer stem cells. Neoplasma. 2012;59(6):700-7.
77. Clarke MF, Dick JE, Dirks PB, Eaves CJ, Jamieson CH, Jones DL, et al. Cancer stem cells--perspectives on current status and future directions: AACR Workshop on cancer stem cells. Cancer Research. 2006 Oct 1;66(19):9339-44.
78. Borovski T, De Sousa EMF, Vermeulen L, Medema JP. Cancer stem cell niche: the place to be. Cancer Research. 2011 Feb 1;71(3):634-9.
79. Bjerkvig R, Tysnes BB, Aboody KS, Najbauer J, Terzis AJ. Opinion: the origin of the cancer stem cell: current controversies and new insights. Nat Rev Cancer. 2005 Nov;5(11):899-904.
80. Ratajczak MZ. Cancer stem cells--normal stem cells "Jedi" that went over to the "dark side". Folia Histochem Cytobiol. 2005;43(4):175-81.
81. Baccelli I, Trumpp A. The evolving concept of cancer and metastasis stem cells. J Cell Biol. 2012 Aug 6;198(3):281-93.
82. Soltanian S, Matin MM. Cancer stem cells and cancer therapy. Tumour Biol. 2011 Jun;32(3):425-40.
83. Zhao Y, Bao Q, Renner A, Camaj P, Eichhorn M, Ischenko I, et al. Cancer stem cells and angiogenesis. Int J Dev Biol. 2011;55(4-5):477-82.
84. Filatova A, Acker T, Garvalov BK. The cancer stem cell niche(s): the crosstalk between glioma stem cells and their microenvironment. Biochim Biophys Acta. 2013 Feb;1830(2):2496-508.

85. Alison MR, Lim SM, Nicholson LJ. Cancer stem cells: problems for therapy? J Pathol. 2011 Jan;223(2):147-61.
86. Baumann M, Krause M, Hill R. Exploring the role of cancer stem cells in radioresistance. Nat Rev Cancer. 2008 Jul;8(7):545-54.
87. Patel P, Chen EI. Cancer stem cells, tumor dormancy, and metastasis. Front Endocrinol (Lausanne). 2012;3:125.
88. Calabrese C, Poppleton H, Kocak M, Hogg TL, Fuller C, Hamner B, et al. A perivascular niche for brain tumor stem cells. Cancer Cell. 2007 Jan;11(1):69-82.
89. Moitra K, Lou H, Dean M. Multidrug efflux pumps and cancer stem cells: insights into multidrug resistance and therapeutic development. Clin Pharmacol Ther. 2011 Apr;89(4):491-502.
90. Alison MR, Lin WR, Lim SM, Nicholson LJ. Cancer stem cells: in the line of fire. Cancer Treat Rev. 2012 Oct;38(6):589-98.
91. Reya T, Morrison SJ, Clarke MF, Weissman IL. Stem cells, cancer, and cancer stem cells. Nature. 2001 Nov 1;414(6859):105-11.
92. Efferth T. Stem cells, cancer stem-like cells, and natural products. Planta Med. 2012 Jun;78(10):935-42.
93. Torchilin VP. Recent approaches to intracellular delivery of drugs and DNA and organelle targeting. Annual Review of Biomedical Engineering. 2006;8:343-75.
94. Shen F, Chu S, Bence AK, Bailey B, Xue X, Erickson PA, et al. Quantitation of doxorubicin uptake, efflux, and modulation of multidrug resistance (MDR) in MDR human cancer cells. J Pharmacol Exp Ther. 2008 Jan;324(1):95-102.
95. Egorin MJ, Hildebrand RC, Cimino EF, Bachur NR. Cytofluorescence localization of adriamycin and daunorubicin. Cancer Research. 1974 Sep;34(9):2243-5.
96. Gryczynski I, Gryczynski Z, Lakowicz JR, Yang D, Burke TG. Fluorescence spectral properties of the anticancer drug topotecan by steady-state and frequency domain fluorometry with one-photon and multi-photon excitation. Photochemistry and Photobiology. 1999 Apr;69(4):421-8.
97. Schuurhuis GJ, van Heijningen TH, Cervantes A, Pinedo HM, de Lange JH, Keizer HG, et al. Changes in subcellular doxorubicin distribution and cellular accumulation alone can largely account for doxorubicin resistance in SW-1573 lung cancer and MCF-7 breast cancer multidrug resistant tumour cells. British Journal of Cancer. 1993 Nov;68(5):898-908.
98. Effenberger-Neidnicht K, Breyer S, Mahal K, Sasse F, Schobert R. Modification of uptake and subcellular distribution of doxorubicin by N-acylhydrazone residues as visualised by intrinsic fluorescence. Cancer Chemother Pharmacol. 2011 May 24.
99. Blumenthal RD, Goldenberg DM. Methods and goals for the use of in vitro and in vivo chemosensitivity testing. Mol Biotechnol. 2007 Feb;35(2):185-97.
100. Efferth T, Sauerbrey A, Olbrich A, Gebhart E, Rauch P, Weber HO, et al. Molecular modes of action of artesunate in tumor cell lines. Mol Pharmacol. 2003 Aug;64(2):382-94.
101. He SM, Li R, Kanwar JR, Zhou SF. Structural and functional properties of human multidrug resistance protein 1 (MRP1/ABCC1). Curr Med Chem. 2011;18(3):439-81.
102. Ejendal KF, Hrycyna CA. Multidrug resistance and cancer: the role of the human ABC transporter ABCG2. Curr Protein Pept Sci. 2002 Oct;3(5):503-11.
103. Bours V, Bentires-Alj M, Hellin AC, Viatour P, Robe P, Delhalle S, et al. Nuclear factor-kappa B, cancer, and apoptosis. Biochem Pharmacol. 2000 Oct 15;60(8):1085-9.
104. Vassilev LT, Vu BT, Graves B, Carvajal D, Podlaski F, Filipovic Z, et al. In vivo

activation of the p53 pathway by small-molecule antagonists of MDM2. Science. 2004 Feb 6;303(5659):844-8.
105. Chen K, Rajewsky N. The evolution of gene regulation by transcription factors and microRNAs. Nat Rev Genet. 2007 Feb;8(2):93-103.
106. Henry TR, Wallace KB. Differential mechanisms of induction of the mitochondrial permeability transition by quinones of varying chemical reactivities. Toxicol Appl Pharmacol. 1995 Oct;134(2):195-203.
107. Kowaltowski AJ, de Souza-Pinto NC, Castilho RF, Vercesi AE. Mitochondria and reactive oxygen species. Free Radic Biol Med. 2009 Aug 15;47(4):333-43.
108. Gong K, Li W. Shikonin, a Chinese plant-derived naphthoquinone, induces apoptosis in hepatocellular carcinoma cells through reactive oxygen species: A potential new treatment for hepatocellular carcinoma. Free Radic Biol Med. 2011 Dec 15;51(12):2259-71.
109. Johnston PA, Soares KM, Shinde SN, Foster CA, Shun TY, Takyi HK, et al. Development of a 384-well colorimetric assay to quantify hydrogen peroxide generated by the redox cycling of compounds in the presence of reducing agents. Assay Drug Dev Technol. 2008 Aug;6(4):505-18.
110. Eiberger W, Volkmer B, Amouroux R, Dherin C, Radicella JP, Epe B. Oxidative stress impairs the repair of oxidative DNA base modifications in human skin fibroblasts and melanoma cells. DNA Repair (Amst). 2008 Jun 1;7(6):912-21.
111. Oltra AM, Carbonell F, Tormos C, Iradi A, Saez GT. Antioxidant enzyme activities and the production of MDA and 8-oxo-dG in chronic lymphocytic leukemia. Free Radic Biol Med. 2001 Jun 1;30(11):1286-92.
112. Darzynkiewicz Z, Bruno S, Del Bino G, Gorczyca W, Hotz MA, Lassota P, et al. Features of apoptotic cells measured by flow cytometry. Cytometry. 1992;13(8):795-808.
113. Taylor RC, Cullen SP, Martin SJ. Apoptosis: controlled demolition at the cellular level. Nat Rev Mol Cell Biol. 2008 Mar;9(3):231-41.
114. Watanabe T, Noritake J, Kaibuchi K. Regulation of microtubules in cell migration. Trends Cell Biol. 2005 Feb;15(2):76-83.
115. Thoma CR, Matov A, Gutbrodt KL, Hoerner CR, Smole Z, Krek W, et al. Quantitative image analysis identifies pVHL as a key regulator of microtubule dynamic instability. J Cell Biol. 2010 Sep 20;190(6):991-1003.
116. Stepanova T, Slemmer J, Hoogenraad CC, Lansbergen G, Dortland B, De Zeeuw CI, et al. Visualization of microtubule growth in cultured neurons via the use of EB3-GFP (end-binding protein 3-green fluorescent protein). J Neurosci. 2003 Apr 1;23(7):2655-64.
117. Diehl MR, Zhang K, Lee HJ, Tirrell DA. Engineering cooperativity in biomotor-protein assemblies. Science. 2006 Mar 10;311(5766):1468-71.
118. O'Brien ET, Salmon ED, Erickson HP. How calcium causes microtubule depolymerization. Cell Motil Cytoskeleton. 1997;36(2):125-35.
119. Hsu JL, Huang SY, Chow NH, Chen SH. Stable-isotope dimethyl labeling for quantitative proteomics. Anal Chem. 2003 Dec 15;75(24):6843-52.
120. Boersema PJ, Raijmakers R, Lemeer S, Mohammed S, Heck AJ. Multiplex peptide stable isotope dimethyl labeling for quantitative proteomics. Nat Protoc. 2009;4(4):484-94.
121. Kleno TG, Kiehr B, Baunsgaard D, Sidelmann UG. Combination of 'omics' data to investigate the mechanism(s) of hydrazine-induced hepatotoxicity in rats and to identify potential biomarkers. Biomarkers. 2004 Mar-Apr;9(2):116-38.
122. Rix U, Superti-Furga G. Target profiling of small molecules by chemical proteomics. Nat Chem Biol. 2009 Sep;5(9):616-24.

123. Trott O, Olson AJ. AutoDock Vina: improving the speed and accuracy of docking with a new scoring function, efficient optimization, and multithreading. J Comput Chem. 2010 Jan 30;31(2):455-61.
124. Singh F, Gao D, Lebwohl MG, Wei H. Shikonin modulates cell proliferation by inhibiting epidermal growth factor receptor signaling in human epidermoid carcinoma cells. Cancer letters. 2003 Oct 28;200(2):115-21.
125. Dontu G, Abdallah WM, Foley JM, Jackson KW, Clarke MF, Kawamura MJ, et al. In vitro propagation and transcriptional profiling of human mammary stem/progenitor cells. Genes Dev. 2003 May 15;17(10):1253-70.
126. Ponti D, Costa A, Zaffaroni N, Pratesi G, Petrangolini G, Coradini D, et al. Isolation and in vitro propagation of tumorigenic breast cancer cells with stem/progenitor cell properties. Cancer Research. 2005 Jul 1;65(13):5506-11.
127. Cioce M, Gherardi S, Viglietto G, Strano S, Blandino G, Muti P, et al. Mammosphere-forming cells from breast cancer cell lines as a tool for the identification of CSC-like- and early progenitor-targeting drugs. Cell Cycle. 2010 Jul 15;9(14):2878-87.
128. Guttilla IK, Phoenix KN, Hong X, Tirnauer JS, Claffey KP, White BA. Prolonged mammosphere culture of MCF-7 cells induces an EMT and repression of the estrogen receptor by microRNAs. Breast Cancer Res Treat. 2012 Feb;132(1):75-85.
129. Calcagno AM, Salcido CD, Gillet JP, Wu CP, Fostel JM, Mumau MD, et al. Prolonged drug selection of breast cancer cells and enrichment of cancer stem cell characteristics. J Natl Cancer Inst. 2010 Nov 3;102(21):1637-52.
130. Grimm M, Krimmel M, Polligkeit J, Alexander D, Munz A, Kluba S, et al. ABCB5 expression and cancer stem cell hypothesis in oral squamous cell carcinoma. Eur J Cancer. 2012 Nov;48(17):3186-97.
131. Chartrain M, Riond J, Stennevin A, Vandenberghe I, Gomes B, Lamant L, et al. Melanoma chemotherapy leads to the selection of ABCB5-expressing cells. PLoS One. 2012;7(5):e36762.
132. Kawanobe T, Kogure S, Nakamura S, Sato M, Katayama K, Mitsuhashi J, et al. Expression of human ABCB5 confers resistance to taxanes and anthracyclines. Biochem Biophys Res Commun. 2012 Feb 24;418(4):736-41.
133. Zhao Y, McLaughlin D, Robinson E, Harvey AP, Hookham MB, Shah AM, et al. Nox2 NADPH oxidase promotes pathologic cardiac remodeling associated with Doxorubicin chemotherapy. Cancer Research. 2010 Nov 15;70(22):9287-97.
134. Brown I, Ward HW. The comparative toxicity and therapeutic efficacy of adriamycin and the adriamycin-DNA complex in the chemotherapy of C3H mice with transplanted mammary adenocarcinoma. Cancer letters. 1977 Mar;2(4-5):227-32.
135. Ubezio P, Civoli F. Flow cytometric detection of hydrogen peroxide production induced by doxorubicin in cancer cells. Free Radic Biol Med. 1994 Apr;16(4):509-16.
136. Barlogie B, Drewinko B, Johnston DA, Freireich EJ. The effect of adriamycin on the cell cycle traverse of a human lymphoid cell line. Cancer Research. 1976 Jun;36(6):1975-9.
137. Levine AJ. p53, the cellular gatekeeper for growth and division. Cell. 1997 Feb 7;88(3):323-31.
138. Gilmore TD. Introduction to NF-kappaB: players, pathways, perspectives. Oncogene. 2006 Oct 30;25(51):6680-4.
139. Buzzai M, Bauer DE, Jones RG, Deberardinis RJ, Hatzivassiliou G, Elstrom RL, et al. The glucose dependence of Akt-transformed cells can be reversed by pharmacologic activation of fatty acid beta-oxidation. Oncogene. 2005 Jun 16;24(26):4165-73.
140. Yang C, Sudderth J, Dang T, Bachoo RM, McDonald JG, DeBerardinis RJ. Glioblastoma cells require glutamate dehydrogenase to survive impairments of glucose metabolism or Akt signaling. Cancer Research. 2009 Oct 15;69(20):7986-93.

141. Ralph SJ, Neuzil J. Mitochondria as targets for cancer therapy. Mol Nutr Food Res. 2009 Jan;53(1):9-28.
142. Iyanagi T, Yamazaki I. One-electron-transfer reactions in biochemical systems. V. Difference in the mechanism of quinone reduction by the NADH dehydrogenase and the NAD(P)H dehydrogenase (DT-diaphorase). Biochim Biophys Acta. 1970 Sep 1;216(2):282-94.
143. Criddle DN, Gillies S, Baumgartner-Wilson HK, Jaffar M, Chinje EC, Passmore S, et al. Menadione-induced reactive oxygen species generation via redox cycling promotes apoptosis of murine pancreatic acinar cells. J Biol Chem. 2006 Dec 29;281(52):40485-92.
144. Gutierrez PL. The metabolism of quinone-containing alkylating agents: free radical production and measurement. Front Biosci. 2000 Jul 1;5:D629-38.
145. Jackson SP, Bartek J. The DNA-damage response in human biology and disease. Nature. 2009 Oct 22;461(7267):1071-8.
146. Kroemer G, Galluzzi L, Brenner C. Mitochondrial membrane permeabilization in cell death. Physiol Rev. 2007 Jan;87(1):99-163.
147. Park S, Chapuis N, Saint Marcoux F, Recher C, Prebet T, Chevallier P, et al. A phase Ib GOELAMS study of the mTOR inhibitor RAD001 in association with chemotherapy for AML patients in first relapse. Leukemia. 2013 Jan 16.
148. Martelli AM, Tazzari PL, Evangelisti C, Chiarini F, Blalock WL, Billi AM, et al. Targeting the phosphatidylinositol 3-kinase/Akt/mammalian target of rapamycin module for acute myelogenous leukemia therapy: from bench to bedside. Curr Med Chem. 2007;14(19):2009-23.
149. Barrett D, Brown VI, Grupp SA, Teachey DT. Targeting the PI3K/AKT/mTOR signaling axis in children with hematologic malignancies. Paediatr Drugs. 2012 Oct 1;14(5):299-316.
150. Amadori S, Stasi R, Martelli AM, Venditti A, Meloni G, Pane F, et al. Temsirolimus, an mTOR inhibitor, in combination with lower-dose clofarabine as salvage therapy for older patients with acute myeloid leukaemia: results of a phase II GIMEMA study (AML-1107). Br J Haematol. 2012 Jan;156(2):205-12.
151. Li B, Gao S, Wei F, Bellail AC, Hao C, Liu T. Simultaneous targeting of EGFR and mTOR inhibits the growth of colorectal carcinoma cells. Oncol Rep. 2012 Jul;28(1):15-20.
152. Sanchez Y, Simon GP, Calvino E, de Blas E, Aller P. Curcumin stimulates reactive oxygen species production and potentiates apoptosis induction by the antitumor drugs arsenic trioxide and lonidamine in human myeloid leukemia cell lines. J Pharmacol Exp Ther. 2010 Oct;335(1):114-23.
153. Dave B, Chang J. Treatment resistance in stem cells and breast cancer. J Mammary Gland Biol Neoplasia. 2009 Mar;14(1):79-82.
154. Lyseng-Williamson KA, Fenton C. Docetaxel: a review of its use in metastatic breast cancer. Drugs. 2005;65(17):2513-31.
155. Li X, Lewis MT, Huang J, Gutierrez C, Osborne CK, Wu MF, et al. Intrinsic resistance of tumorigenic breast cancer cells to chemotherapy. J Natl Cancer Inst. 2008 May 7;100(9):672-9.
156. Schatton T, Murphy GF, Frank NY, Yamaura K, Waaga-Gasser AM, Gasser M, et al. Identification of cells initiating human melanomas. Nature. 2008 Jan 17;451(7176):345-9.
157. Visvader JE, Lindeman GJ. Cancer stem cells in solid tumours: accumulating evidence and unresolved questions. Nat Rev Cancer. 2008 Oct;8(10):755-68.
158. Yang JY, Ha SA, Yang YS, Kim JW. p-Glycoprotein ABCB5 and YB-1 expression

plays a role in increased heterogeneity of breast cancer cells: correlations with cell fusion and doxorubicin resistance. BMC Cancer. 2010;10:388.
159. Zhou J, Wulfkuhle J, Zhang H, Gu P, Yang Y, Deng J, et al. Activation of the PTEN/mTOR/STAT3 pathway in breast cancer stem-like cells is required for viability and maintenance. Proc Natl Acad Sci U S A. 2007 Oct 9;104(41):16158-63.
160. Mueller MT, Hermann PC, Witthauer J, Rubio-Viqueira B, Leicht SF, Huber S, et al. Combined targeted treatment to eliminate tumorigenic cancer stem cells in human pancreatic cancer. Gastroenterology. 2009 Sep;137(3):1102-13.
161. Khan JA, Kudgus RA, Szabolcs A, Dutta S, Wang E, Cao S, et al. Designing nanoconjugates to effectively target pancreatic cancer cells in vitro and in vivo. PLoS One. 2011;6(6):e20347.
162. Sato M, Umezawa Y. FRET-based reporters for intracellular enzyme activity. Encyclopedia of Genetics, Genomics, Proteomics and Bioinformatics. 2005.
163. Billinton N, Barker MG, Michel CE, Knight AW, Heyer WD, Goddard NJ, et al. Development of a green fluorescent protein reporter for a yeast genotoxicity biosensor. Biosens Bioelectron. 1998 Oct 1;13(7-8):831-8.
164. Ichikawa K, Eki T. A novel yeast-based reporter assay system for the sensitive detection of genotoxic agents mediated by a DNA damage-inducible LexA-GAL4 protein. J Biochem. 2006 Jan;139(1):105-12.
165. Nicholls SB, Chu J, Abbruzzese G, Tremblay KD, Hardy JA. Mechanism of a Genetically Encoded Dark-to-Bright Reporter for Caspase Activity. J Biol Chem. 2011 Jul 15;286(28):24977-86.
166. Di L, Whitney-Pickett C, Umland JP, Zhang H, Zhang X, Gebhard DF, et al. Development of a new permeability assay using low-efflux MDCKII cells. J Pharm Sci. 2011 Nov;100(11):4974-85.
167. Cars O, Hedin A, Heddini A. The global need for effective antibiotics-moving towards concerted action. Drug Resist Updat. 2011 Apr;14(2):68-9.
168. Indran IR, Tufo G, Pervaiz S, Brenner C. Recent advances in apoptosis, mitochondria and drug resistance in cancer cells. Biochim Biophys Acta. 2011 Jun;1807(6):735-45.
169. Wu CP, Hsieh CH, Wu YS. The Emergence of Drug Transporter-Mediated Multidrug Resistance to Cancer Chemotherapy. Mol Pharm. 2011 Jul 26.
170. Kern W, Haferlach C, Schnittger S, Haferlach T. Clinical utility of multiparameter flow cytometry in the diagnosis of 1013 patients with suspected myelodysplastic syndrome: correlation to cytomorphology, cytogenetics, and clinical data. Cancer. 2010 Oct 1;116(19):4549-63.
171. Tiyanont K, Doan T, Lazarus MB, Fang X, Rudner DZ, Walker S. Imaging peptidoglycan biosynthesis in Bacillus subtilis with fluorescent antibiotics. Proc Natl Acad Sci U S A. 2006 Jul 18;103(29):11033-8.
172. Gillet JP, Efferth T, Steinbach D, Hamels J, de Longueville F, Bertholet V, et al. Microarray-based detection of multidrug resistance in human tumor cells by expression profiling of ATP-binding cassette transporter genes. Cancer Research. 2004 Dec 15;64(24):8987-93.
173. Graham FL, Smiley J, Russell WC, Nairn R. Characteristics of a human cell line transformed by DNA from human adenovirus type 5. J Gen Virol. 1977 Jul;36(1):59-74.
174. O'Brien J, Wilson I, Orton T, Pognan F. Investigation of the Alamar Blue (resazurin) fluorescent dye for the assessment of mammalian cell cytotoxicity. Eur J Biochem. 2000 Sep;267(17):5421-6.
175. Kohn KW, Erickson LC, Ewig RA, Friedman CA. Fractionation of DNA from mammalian cells by alkaline elution. Biochemistry. 1976 Oct 19;15(21):4629-37.

176. Epe B, Pflaum M, Boiteux S. DNA damage induced by photosensitizers in cellular and cell-free systems. Mutat Res. 1993 May;299(3-4):135-45.
177. Liang CC, Park AY, Guan JL. In vitro scratch assay: a convenient and inexpensive method for analysis of cell migration in vitro. Nat Protoc. 2007;2(2):329-33.
178. Geback T, Schulz MM, Koumoutsakos P, Detmar M. TScratch: a novel and simple software tool for automated analysis of monolayer wound healing assays. Biotechniques. 2009 Apr;46(4):265-74.
179. Bass DA, Parce JW, Dechatelet LR, Szejda P, Seeds MC, Thomas M. Flow cytometric studies of oxidative product formation by neutrophils: a graded response to membrane stimulation. J Immunol. 1983 Apr;130(4):1910-7.
180. Cossarizza A, Ferraresi R, Troiano L, Roat E, Gibellini L, Bertoncelli L, et al. Simultaneous analysis of reactive oxygen species and reduced glutathione content in living cells by polychromatic flow cytometry. Nat Protoc. 2009;4(12):1790-7.
181. Paredes RM, Etzler JC, Watts LT, Zheng W, Lechleiter JD. Chemical calcium indicators. Methods. 2008 Nov;46(3):143-51.
182. Eberwine J, Yeh H, Miyashiro K, Cao Y, Nair S, Finnell R, et al. Analysis of gene expression in single live neurons. Proc Natl Acad Sci U S A. 1992 Apr 1;89(7):3010-4.
183. Chen CJ, Tseng MC, Lin HJ, Lin TW, Chen YR. Visual indicator for surfactant abundance in MS-based membrane and general proteomics applications. Anal Chem. 2010 Oct 1;82(19):8283-90.
184. Chang WH, Lee CY, Lin CY, Chen WY, Chen MC, Tzou WS, et al. UniQua: a universal signal processor for MS-based qualitative and quantitative proteomics applications. Anal Chem. 2013 Jan 15;85(2):890-7.

8 Appendix

8.1 Abbreviations

Table 14: Abbreviations

Abbreviation	Connotation
4E-BP1	4E-binding protein 1
8-oxoG	7,8-dihydro-8-oxoguanine
ABC-transporter	ATP-binding cassette transporter
ABCB1	Multidrug resistance protein 1 / p-glycoprotein
ABCB5	ATP-binding cassette sub-family B member 5
ABCC1	Multidrug resistance-associated protein 1
ABCG2	Breast cancer resistance protein
Abl1	Abelson tyrosine protein kinase 1
ACN	Acetonitrile
APS	Ammonium persulfate
ATCC	American Type Culture Collection
BCR	Breakpoint cluster region
BCRP	Breast cancer resistance protein
BCSC	Breast cancer stem cell
BSA	Bovine serum albumin
CML	Chronic myelogenous leukemia
CSC	Cancer stem cell
DCF	Dichlorofluorescein
DKFZ	German Cancer Research Center
DMSO	Dimethyl sulfoxide
DTT	Dithiothreitol
EB3	End binding protein-3
EGF	Epidermal growth factor
EGFR	Epidermal growth factor receptor
eIF2	Eukaryotic initiation factor-2
eIF4	Eukaryotic initiation factor-4
FACS	Fluorescence-activated cell sorting
FDA	US Food and Drug Administration
Fpg	Formamidopyrimidine DNA glycosylase
GFP	Green fluorescent protein
H_2DCFH-DA	Dichlorodihydrofluorescein diacetate
HEPES	4-(2-hydroxyethyl)-1-piperazineethanesulfonic acid
HER2/neu	Human epidermal growth factor receptor type 2
HMOX1	Heme oxygenase 1
HRP	Horse radish peroxidase

IGF	Insulin-like growth factor
IGF1R	Insulin-like growth factor 1 receptor
IMB	Institute for Molecular Biology
LC-MS	Liquid chromatography – mass spectrometry
MDR	Multidrug resistance
mLST8	Mammalian lethal with sec-13 protein 8
MMP	Mitochondrial membrane potential
MMTS	Methyl methanethiosulfonate
MRP1	Multidrug resistance-associated protein 1
MS	Mass spectrometry
mTOR	Mammalian target of rapamycin
mTORC1/2	Mammalian target of rapamycin complex 1 and 2
n.d.	Not detected
NFκB	Nuclear factor kappa-light-chain-enhancer of activated B cells
PI3K	Phosphoinositide 3-kinase
pRiboS6	p-ribosomal protein S6
Q-TOF-MS	Quadrupole time-of-flight mass spectrometer
Raptor	Regulatory-associated protein of mTOR
Rheb	Ras homolog enriched in brain
Rictor	Rapamycin-insensitive companion of mTOR
ROS	Reactive oxygen species
RTK	Receptor tyrosine kinase
S6K1	S6 kinase 1
SCX	Strong cation exchange
SD	Standard deviation
SDS	Sodium dodecyl sulfate
SEM	Standard error of the mean
SGK1	Serine/threonine-protein kinase Sgk1
SSB	DNA single-strand break
TCEP	Tris(2-carboxyethyl)phosphine
TCM	Traditional Chinese Medicin
TEABC	Triethylammonium bicarbonate
TEMED	Tetramethylethylenediamine
TFA	Trifluoroacetic acid
TGFα	Transforming growth factor alpha
TPP	Trans proteomics pipeline
TSC1/2	Tuberous sclerosis proteins 1 and 2
TX-100	Triton X-100
WHO	World Health Organization

8.2 Publications

Original publications as lead author

- Wiench B, Chen YR, Paulsen M, Hamm R, Schroeder S, Yang NS, Efferth T, "Integration of different *omics* technologies identifies inhibition of the IGF1R-Akt-mTOR signaling cascade involved in the cytotoxic effect of shikonin against leukemia cells", submitted at *Evidence-based complementary and alternative medicine (eCAM*), Accepted 7 May 2013
- Wiench B, Eichhorn T, Paulsen M, Efferth T, "Shikonin directly targets mitochondria and causes mitochondrial dysfunction in cancer cells", *Evidence-based complementary and alternative medicine (eCAM*), 2012: 726025, 2012
- Wiench B, Eichhorn T, Korn B, Paulsen M, Efferth T, "Utilizing inherent fluorescence of therapeutics to analyze real-time uptake and multi-parametric effector kinetics", *Methods*, 57(3): 376-82, 2012

Original publications as co-author

- Kuete V, Eichhorn T, Wiench B, Krusche B, Efferth T, "Cytotoxicity, anti-angiogenic, apoptotic effects and transcript profiling of a naturally occurring naphthyl butenone, guieranone A", *Cell division*, 7: 16, 2012
- Kuete V, Wiench B, Hegazy ME, Mohamed TA, Fankam AG, Shahat AA, Efferth T, "Antibacterial activity and cytotoxicity of selected Egyptian medicinal plants", *Planta medica*, 78: 193-199, 2012
- Kuete V, Wabo HK, Eyong KO, Feussi MT, Wiench B, Krusche B, Tane P, Folefoc GN, Efferth T, "Anticancer activities of six selected natural compounds of some Cameroonian medicinal plants", *PloS one*, 6: e21762, 2011
- Kuete V, Ngameni B, Wiench B, Krusche B, Horwedel C, Ngadjui BT, Efferth T, "Cytotoxicity and mode of action of four naturally occuring flavonoids from the genus Dorstenia: gancaonin Q, 4-hydroxylonchocarpin, 6-prenylapigenin, and 6,8-diprenyleriodictyol", *Planta medica*, 77: 1984-1989, 2011
- Bauch C, Kolle SN, Fabian E, Pachel C, Ramirez T, Wiench B, Wruck CJ, van Ravenzwaay B, "Intralaboratory validation of four in vitro assays for the prediction of the skin sensitizing potential of chemicals", *Toxicology in vitro*, 25: 1162-1168, 2011

Submitted manuscripts

- Kuete V, Sandjo LP, Wiench B, Efferth T, "Cytotoxicity and modes of action of four Cameroonian dietary spices ethnomedically used to treat cancers: *Echinops giganteus*, *Xylopia aethiopica*, *Imperata cylindrical* and Piper *capense*", submitted at *Evidence-based complementary and alternative medicine (eCAM*), 2013
- Kuete V, Wiench B, Alsaid MS, Alyahya MA, Frankam G, Shahat AA, Efferth T, "Cytotoxicity, mode of action and antibacterial activities of selected Saudi Arabian medicinal plants", submitted at *BMC Complementary and Alternative Medicine*, 2013

Posters and abstracts

- Wiench B, Eichhorn T, Paulsen M, Efferth T, "Shikonin causes cancer cell death by inducing mitochondrial dysfunction" [Poster], *AACR Annual Meeting*, Chicago, 2012
- Wiench B, Eichhorn T, Paulsen M, Efferth T, "Shikonin causes cancer cell death by inducing mitochondrial dysfunction" [Abstract], *AACR Proceedings*, 53, 1130, 2012

8.3 Grants and scholarships

- Full PhD scholarship from the Stipendienstiftung Rheinland-Pfalz
- DAAD travel grant containing financial support for visiting the AACR Annual Meeting 2012 in Chicago

8.4 Curriculum vitae

Ein Lebenslauf ist in der elektronischen Fassung der Dissertation nicht enthalten.